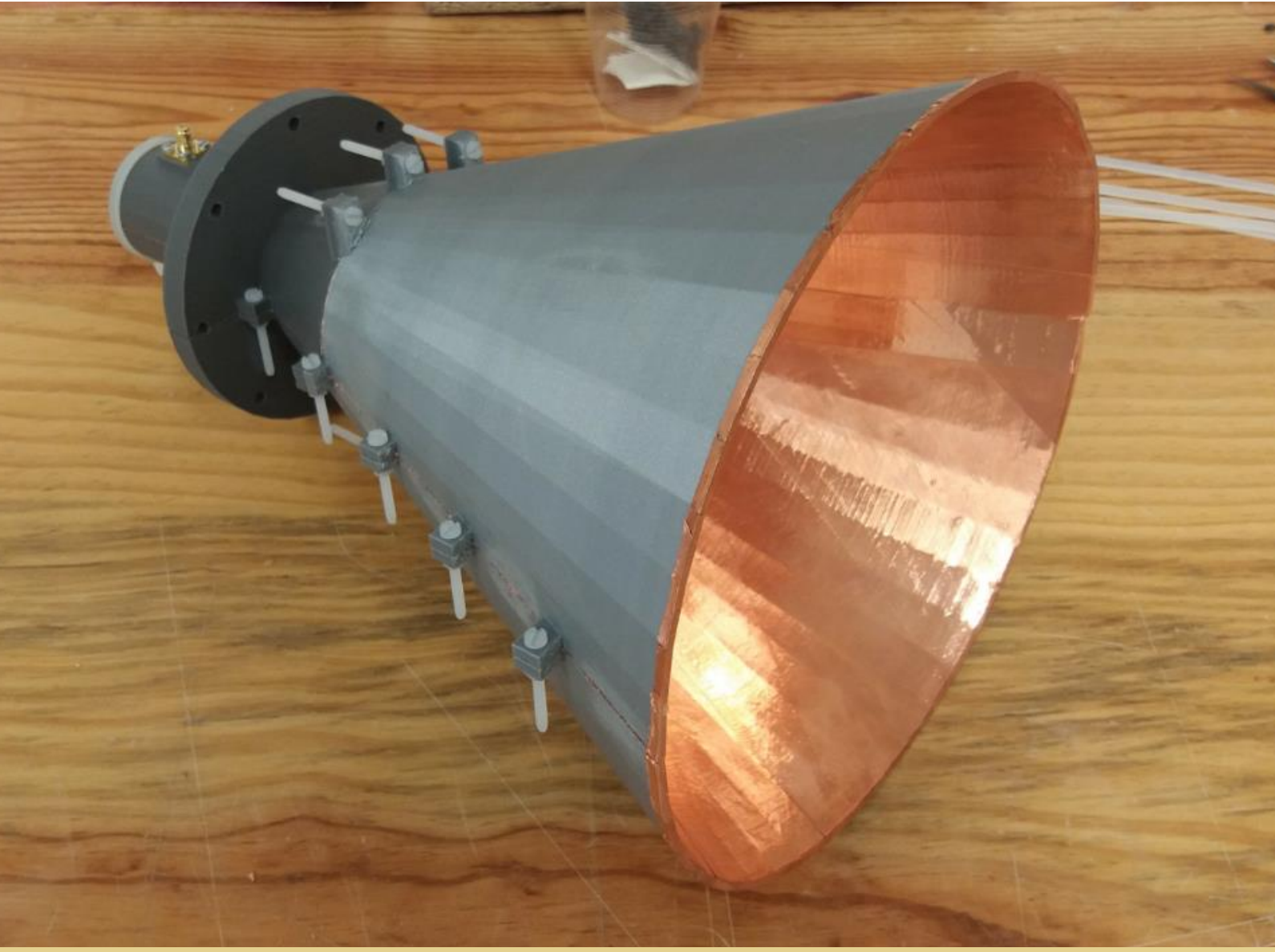

Ricardo André Mendes Pereira

Gaussian Beam Microwave Antennas in Quasi-Optical Systems for Wireless Power Transfer

Dissertation submitted for the
degree of Master in Physics Engineering

September, 2017

· U C ·

UNIVERSIDADE DE COIMBRA

• U C •

FCTUC FACULDADE DE CIÊNCIAS
E TECNOLOGIA
UNIVERSIDADE DE COIMBRA

Gaussian Beam Microwave Antennas in Quasi-optical Systems for Wireless Power Transfer

Dissertation submitted to the University of Coimbra in partial fulfilment of the requirements for the Master's degree in Physics Engineering, specialisation in Instrumentation.

Supervisors:

- Prof. Nuno Borges Carvalho
  Institute of Telecommunications, University of Aveiro, Portugal
- Prof. José Pinto da Cunha
  Physics Department, University of Coimbra, Portugal

Ricardo André Mendes Pereira

Coimbra, September 2017

Work done in collaboration with:

FCTUC FACULDADE DE CIÊNCIAS
E TECNOLOGIA
UNIVERSIDADE DE COIMBRA

instituto de
telecomunicações

Agradecimentos

Depois de estes longos e calorosos anos na Universidade de Coimbra, é chegada a altura da despedida, possível apenas graças àqueles que me rodeiam. Houve momentos altos e baixos, mas o que importa é que tudo passou e ficam memórias de tempos espetaculares. No entanto, o fim desta etapa marca muito mais do que o fim da vida de estudante universitário. Aproveito, portanto, para fazer chegar uma palavra de carinho aos meus mais queridos.

Em primeiro lugar, a todos os meus professores, um grande abraço e beijinho. Foi graças a todos, sem exceção, que cheguei a este ponto.

Nany, devo-te um agradecimento muito especial! Foste a primeira pessoa a sugerir, muito sabiamente, que eu seguisse para a área de Física. Marcaste a minha relação com a matemática e não poderia estar mais agradecido. Beijão enorme!

Em especial para esta dissertação, não podia deixar de realçar os meus orientadores: Prof. Nuno Borges Carvalho, pela disponibilidade em acolher e confiar em mim para este projeto. Prof. José Pinto da Cunha não sabe como apreciei as tardes (e por vezes noites) passadas a discutir física e a sua orientação na melhoria dos documentos.

Agradeço ainda ao pessoal do IT Aveiro pela ajuda que todos prestaram: aos técnicos Paulo Gonçalves e Nuno Silva, que tanto me facilitarem o acesso às ferramentas necessárias para avançar cada etapa mas em especial um agradecimento ao Hugo Mostardinha pela fulcral ajuda e acompanhamento em todas as etapas da parte experimental, mesmo em alturas de aflição, e pelo contacto com a empresa Famaval. Por outro lado, queria agradecer ao Daniel Belo por me ajudar a integrar no IT, desde o CST aos almoços. Mais recentemente, foi graças à ajuda do Daniel e do Ricardo Correia que foi possível obter os melhores resultados na experiência final, ao alinharem as antenas segurando-as à mão. Grande abraço aos dois!

A todos os meus amigos, não me vou alongar, um enorme abraço! Obrigado por me ajudarem a descomprimir nas alturas mais complicadas!

Ao Dr. Joaquim Mira, um abraço especial por me incutir o valor do trabalho desde a tenra idade.

Por último mas não menos importante:

Tânia e D. Alice, obrigado por toda a ajuda e por simplificarem o meu dia-a-dia, por serem sempre umas queridas.

Meus pais e irmãos, obrigado por todo o amor, apoio e dedicação que sempre demonstraram, por me trazerem à terra e simplesmente estarem sempre lá. Mais do que ninguém é a vocês que devo o maior agradecimento.

Finalmente, Patrícia. Sempre me apoiaste incondicionalmente com a tua maneira tão doce e querida de ser. Por isso agradeço-te do fundo do meu coração. Obrigado por tudo. Beijão enorme meu amor!

Resumo

Através de ferramentas quasi-óticas, a análise de um sistema composto por dois refletores parabólicos foi feita com o objetivo de transferir energia sem fios, usando micro-ondas (à frequência de 5.8 GHz).

Primeiramente desenvolveram-se scripts com duas principais finalidades: visualizar a frente de onda dos feixes gaussianos para diferentes modos de propagação, tanto em coordenadas retangulares como em cilíndricas e a propagação de feixes gaussianos através de um sistema (composto por refletores ou lentes).

Depois de este estudo, recorreu-se a uma análise teórica com o intuito de permitir a prototipagem do sistema usando o mínimo parâmetros possível. Foi possível simplificar a análise através da utilização do princípio da reciprocidade, ao igualar os dois espelhos e as antenas (emissora e recetora). Conseguiu-se chegar a um conjunto de equações que cumprem o objetivo.

De seguida concretizou-se o sistema com base nos resultados anteriores por forma a efetuar experiências laboratoriais, com vista na validação da teoria. A antena escolhida para emissor e recetor de radiação são do tipo corneta circular de superfície plana, uma vez que estas oferecem uma maior aproximação da radiação emitida a um feixe gaussiano, juntamente com uma relativa facilidade de construção. Após o desenho e simulação da antena, juntamente com o guia de ondas e o conetor SMA que a alimenta, utilizando um software CAD, CST Studio Suite, prosseguiu-se à sua construção. Tal foi efetuado numa impressora 3D, seguindo-se a colagem de fita de cobre como material condutor da antena. Foi necessário encomendar conetores SMA específicos, procedendo-se de seguida à medição dos parâmetros principais da antena. Tendo concluindo que os resultados foram positivos, procedeu-se à construção da segunda antena. Por outro lado, foi possível obter dois espelhos parabólicos, juntamente com os suportes necessários, através da empresa Famaval.

Finalmente, utilizando um gerador de sinal e um analisador de espetro, efetuou-se uma experiência preliminar de transferência de energia de uma antena para a outra. Os resultados foram positivos mas não satisfatórios pelo que existe necessidade de efetuar um varrimento dos parâmetros mais completo. A dificuldade de alinhamento dos diferentes componentes do sistema é apontado como o principal fator pela principal perda de eficiência.

Este estudo apresenta métodos de análise que possibilitam rapidamente prototipar sistemas de transferência de energia por microondas, compostos por dois componentes que permitem a aplicação do princípio da reciprocidade.

Abstract

Using the quasi-optical formalism a double parabolic reflector system was analysed in order to achieve Wireless Power Transfer, using Microwaves (at the frequency of 5.8 GHz).

Firstly, scripts were developed with two main goals: the visualisation of the gaussian beam wave fronts for different modes of propagation, in both rectangular and cylindrical coordinates, and the propagation of gaussian beams throughout a system (composed of either mirrors or lenses).

After this analysis a theoretical approach is made to arrive at a way to quickly prototype the system, using the minimum parameters possible. The use of the reciprocity principle to simplify this analysis can be done by simply making both reflectors and antennas (emitting and receiving) equal. A set of equations were derived, which serve this purpose.

A system set-up based on the results obtained was made with the objective of setting up a lab experiment, so as to validate the theory. The chosen antenna for the emitter and receiver was a smooth surface conical antenna for having the radiation pattern best approximated to that of a gaussian beam while remaining relatively easy to build. After designing and simulating the antenna, as well as the waveguide and the SMA connector which feed it, in a CAD software, CST Studio Suite, the antenna was built. It was done on a 3D printer, followed by the gluing of copper tape as the antenna's conducting material. It was necessary to order the specific SMA connectors for this antenna. After their arrival, the main parameters of the antenna were measured with positive results. Because of it, the second antenna was built and measured in the same way. On the other hand, it was possible to obtained the parabolic reflectors, along with the necessary supports, from the company Famaval.

Finally, using a signal generator and a spectrum analyser, a preliminary experiment of power transfer from one antenna to other was performed. The results were not satisfactory, for which a more thorough parameter sweep is necessary. The difficulty in aligning the different system's components is pointed as the main factor for the major efficiency loss.

In this study one can find analysis tools that allow for fast prototyping of systems for power transfer through microwaves, made up of two components that respect the reciprocity principle.

Contents

List of Figures

List of Tables

Listings

Chapter 1

Introduction

1.1 Background and Motivation

For the majority of history even though the origins of physics phenomena were not fully understood their effects were observed, studied and, more often than not, used to improve the overall quality of human life.

Such was the case with electricity. The observation of electrical effects can be traced back to the ancient world. A famous example is the "Thunderer of the Nile", the electric fish which the Ancient Egyptians considered to be the "protector" of all other fish. Speculation on the origin and nature of the electric and magnetic phenomena prompted the realization of various experiments throughout the ages. However, it was only recently in the history of mankind that the electric and magnetic phenomena were linked, with the ripening of the electromagnetic theory in the 19th century. It was the culmination of the work of many, resulting in the essential description of electromagnetism in the form of the Maxwell's Equations.

The evolution of this theory greatly affected common people's lives ever since light bulbs revolutionized lighting. It was only a matter of time before electrical appliances swirled through the front door of our homes and infrastructure to best manage the generation, storage and distribution of electric power became a pillar of modern civilization.

Nevertheless, there is always room for improvement. What if we could transfer electric power without wires? Nikola Tesla's work is simply inescapable for numerous reasons, among which his contribution to Wireless Power Transfer (WPT). The potential applications are immense, ranging from our everyday lives to the space industry.

It was the author's fascination for electromagnetism which prompted the choice of researching in this field, with WPT assuming the role of an obviously related, greatly potential, interesting and useful subject to study.

1.2 History and State-of-the-art

Microwave's high directionality along with a high transmission efficiency in the atmosphere made this type of radiation interesting for long distance transmissions.

These features made the millimetre and sub-mm waves also convenient for power transmission in the air [1]. However, the divergence effects are significant and have to be considered. The common theory of optics has then been adapted to contexts with high diffraction (such as microwave propagation), being referred to as "quasi-optics" [2, 3]. There is vast literature on this subject with comprehensive treatment, both on electromagnetics [4] and optics [5], which dedicate sections to the diffraction effect.

WPT using Radio Frequencies (RF) can be traced back to the 19th century, with the work of Heinrich Hertz [6]. His experiments demonstrated the propagation of electromagnetic waves and their reflection on parabolic mirrors at the receiver and transmitter ends. Later on, Nikola Tesla pioneered a different concept of WPT by using low frequency standing waves along the surface of the Earth which would power strategically located antennas. There was no focusing and the radiation would propagate in every direction [7, 8].

Since then, many efforts and important contributions have been done. For a summary of the state-of-the-art on WPT refer to [9, 10]. WPT has immense potential for numerous applications, ranging from distances of a few centimetres (with inductive and capacitive fields) all the way to kilometres using microwaves [11]. Long distance WPT remains a field of interest since there is still much to be done in order to improve the overall efficiency.

A review of the general applications for RF and, specifically, microwave power transfer can be found in [12]. Microwaves have been used to power drones [6, 13] by using rectennas (rectifying antennas) as receivers [14, 15]. The use of microwaves and rectennas form the basis of a Space Solar System for power harvesting where the Sun energy would be converted to electricity in space via solar panels, and transferred to Earth by microwaves [16, 17].

In general, emitting antennas can have any form but the use of planar arrays is very interesting in various situations due to their relatively small size and low manufacturing costs. Their use in WPT has been contemplated [18] and interesting studies developed, namely on the maximization of the power transfer efficiency [19] or the possibility of focusing multiple targets [20].

That brings us to another important aspect in electromagnetic waves which is the focusing of the radiation. It is common to use reflectors or lenses to create systems that focus the beam, thus reducing the spillover losses. On one hand parabolic reflectors are advantageous to avoid spherical aberration and are common in the industry [21, 22].

Off-set parabolic reflectors are crucial to avoid blockage from the feed [23] at the price of some undesired beam aberrations [24]. On the other hand, depending on the application, lenses can eventually be more advantageous [25, 26] with dielectric lenses receiving a lot of attention [27, 28], due to their simplicity. Fresnel Zone Plate Lens [29, 30] and electronically reconfigurable Luneburg lenses [31] are also worth mentioning. Several studies make use of both reflectors and lenses [32, 33].

An interesting application of the quasi-optical theory applied to WPT that considers a metasurface aperture to dynamically focus a radiation beam to specific points is discussed in [34].

The present study applies the quasi-optical theory in the study of a double-reflector WPT system, using the reciprocity principle to simplify the analysis.

1.3 Structure

The main body of this dissertation is separated into four parts.

Firstly, in the introduction is presented the author's motivation for studying WPT, as well as a historical overview along with the state-of-the-art.

This is followed by an overview of the necessary theoretical concepts, starting at the electromagnetic theory. The principles of the quasi-optics theory are then discussed.

The original work beings with the development of scripts for representing the beam, followed by a theoretical analysis of a proposed quasi-optical system.

Finally, the necessary components are discussed in order to be able to set-up a preliminary experiment.

A final note on the navigation of the this document, it includes links to various points of interests. They are simply hidden for aesthetic purposes.

Chapter 2

Electromagnetism

As David J. Griffiths eloquently elaborated on *Introduction to Electrodynamics*: "it is scarcely and exaggeration to say that we live in an electromagnetic world - for virtually every force we experience in everyday life, with the exception of gravity, is electromagnetic in origin".

This statement hints us of the vast and crucial role of electromagnetism in the universe, even more so when acknowledging that the electromagnetic force is one of the four known fundamental forces. There are immense applications and WPT is no exception, but let us start with the most basic electromagnetic concept.

2.1 Particles and Electric Charges

All matter is composed of atoms which are in turn generally made up of protons and neutrons (in the nucleus) and electrons (in the electron cloud). Protons and electrons are some of the most fundamental particles in the universe having respectively $+e$ and $-e$ of charge, the smallest discovered on free particles. The electric charge of every object in nature is always a multiple of the *elementary charge*, $e = 1.602 \times 10^{-19}$C.

But we can go even deeper. According to the Standard Model of particle physics, fermions are particles that respect the Fermi-Dirac statistics, having half-integer spin (1/2). The elementary fermions are leptons and quarks, with a huge difference between them being that the former can exist on their own. Such is the case of the electron. On the other hand, quarks, charged with either 2/3 or 1/3 e, combine in different ways, making up various particles. For example, protons are made up of two up quarks ($+2/3\,e$) and one down quark ($-1/3\,e$), resulting in $+1\,e$ of charge.

At the time of writing, there is still debate on the origin of electric charge[1]. Regardless of this fact, its effects are widely known and form the basis of electromagnetism: in a very rudimentary summary one can state that stationary charges create constant electric fields, whereas moving charges (currents) with constant velocity form constant magnetic fields. Accelerating charges produce varying magnetic fields which result in the emission of radiation through space. This is the phenomena which most interests us.

However, in order to create electromagnetic radiation, one must make charges move. Conductors are materials which easily allow the flow of electric charges and generators, which create Direct or Alternating Currents (DC, AC), are common in every laboratory. Natural conductors can be found in most metals, whose outer electrons are loosely bound, with silver being the best conducting one, followed by copper and gold. Copper is the most used for economic reasons but sometimes gold is required for its higher corrosion resistance.

We have cleared the basis for electromagnetism and now more complex analysis are in order. Most uniquely, all of the electromagnetic theory can be summarised in a small set of equations.

2.2 Maxwell's Equations

Firstly some notation clarification. Arbitrarily time-varying vector fields, functions of (x, y, z, t), are symbolised by script letters. For the most part, the electromagnetic laws will be introduce in a chronological order.

2.2.1 Gauss's Electric Law

Electric charges are "the ultimate source of the electromagnetic field" [43], first and foremost because they create electric fields,

$$\nabla \cdot \vec{\mathcal{E}} = \frac{\rho}{\epsilon_0}. \tag{2.1}$$

ρ is the *charge density* and this equation is known as *Gauss's Law* (or *Gauss's Flux Theorem*), presented here for the case of the analysis in a vacuum. When that is not the case, the effect of the electric field on the medium (or on a dielectric material) must be taken into account: the medium's internal dipole moments will align resulting in an overall dipole moment, commonly denominated *Polarisation*, $\vec{\mathcal{P}} = \epsilon_0 \chi_e \vec{\mathcal{E}}$. This overall dipole moment creates an electric field, contributing (constructively or not) to the original one. χ_e is the *electric susceptibility*, a constant[2] that indicates how polarisable

[1] although there are hypothesis linking it to spin []

[2] for linear and homogeneous medium.

the medium is. To differentiate between these two electric field sources, $\mathcal{D}$, the *Electric Displacement* (or electric flux density) is introduced and the charges are separated into *free* (ρ_f) and *bound* (ρ_b), respectively associated with the original electric field and with the polarisation. The electric displacement is then given by,

$$\vec{\mathcal{D}} = \epsilon_0 \vec{\mathcal{E}} + \vec{\mathcal{P}}, \qquad \vec{\mathcal{D}} = \epsilon \vec{\mathcal{E}}, \tag{2.2}$$

where $\epsilon = \epsilon_0(1 + \chi_e)$ is the *absolute permittivity* of the medium. The ratio of the medium permittivity to that of the *vacuum permittivity* (the also called *electric constant*, $\epsilon_0 = 8.854 \times 10^{-12}\mathrm{F/m}$) is the *relative permittivity* of the medium, $\epsilon_r = \frac{\epsilon}{\epsilon_0} = 1 + \chi_e$.

Gauss's law can now be rewritten using $\mathcal{D}$ as $\nabla \cdot \vec{\mathcal{D}} = \rho_f$. In the integral form it becomes

$$\oint_S \vec{\mathcal{D}} \cdot d\vec{s} = \int_V \rho_f \cdot dv = \mathcal{Q}, \tag{2.3}$$

where $\mathcal{Q}$ is the free electric charge contained in the volume V.

We now know how electric charges create electric fields, but what happens if we move them?

2.2.2 Ampère's Law and Maxwell's Correction

Great improvements on electromagnetism happened in the 19th century, beginning in 1820, when Oersted first connected electricity and magnetism by noting that an electrical current deflects nearby compass needles. Ampère, after acknowledging this fact, elaborated several experiments in order to study electrical currents, the magnetic field originating from them and the way two wires with currents affect each other. *Ampère's Law*, states that steady electric currents create steady magnetic fields,

$$\nabla \times \vec{\mathcal{B}} = \mu_0 \vec{\mathcal{J}}, \tag{2.4}$$

where $\mathcal{J}$ is the *electric current density*.

In a similar fashion to the electric field, the *Magnetisation* (*magnetic polarisation*) is the account of the internal magnetic dipole moments, enabling the study of how the material reacts to an external magnetic field. The reaction can be very different, enabling the categorization of the materials into ferromagnetic, paramagnetic and diamagnetic. In some materials, $\vec{\mathcal{M}} = \chi_m \vec{\mathcal{H}}$, where χ_m is the *magnetic susceptibility*. Similarly we have $H = \frac{B}{\mu}$, the *magnetic field intensity*,

$$\vec{\mathcal{B}} = \mu_0 \vec{\mathcal{H}} + \vec{\mathcal{M}}, \qquad \vec{\mathcal{B}} = \mu \vec{\mathcal{H}}, \tag{2.5}$$

where μ, $\mu_0 = 4\pi \times 10^{-7}\mathrm{N/A^2}$ (the *magnetic constant*) and $\mu_r = \frac{\mu}{\mu_0} = 1 + \chi_m$ are respectively the *absolute*, *vacuum* and *relative* permeability.

There is still a term which is missing from the equation below. The creation of a magnetic field is not only due to electric currents, but can also originate from a varying electric field. Maxwell later proceeds to introduce the extra term, $\mu_0\vec{\mathcal{J}}_d$, where $\vec{\mathcal{J}}_d = \epsilon_0\frac{\partial\vec{\mathcal{E}}}{\partial t}$ is the *displacement current*. The corrected form of the Ampère's Law is,

$$\nabla \times \vec{\mathcal{B}} = \mu_0\vec{\mathcal{J}} + \mu_0\epsilon_0\frac{\partial\vec{\mathcal{E}}}{\partial t}, \tag{2.6}$$

or we can write it in integral form, also using (2.5),

$$\oint_C \vec{\mathcal{H}} \cdot d\vec{l} = \int_S \vec{\mathcal{J}} \cdot d\vec{s} + \frac{\partial}{\partial t}\int_S \vec{\mathcal{D}} \cdot d\vec{s} = \mathcal{I} + \frac{\partial}{\partial t}\int_S \vec{\mathcal{D}} \cdot d\vec{s}, \tag{2.7}$$

where $\mathcal{I} = \int_S \vec{\mathcal{J}} \cdot \vec{s}$ is simply the *total electric current flow through a surface S*.

2.2.3 Faraday's Law

Following this discovery several experiments were set-up. Francesco Zantedeschi preceded Faraday in noting the electrical induction effect due to the motion of a nearby magnet, but it was Faraday and his experiments that led to the statement that a changing magnetic field induces an electric field. In a closed circuit, it is evident as the *electromotive force* (*EMF*) which arises with the variation of the *magnetic flux*, Φ_B,

$$EMF = -\frac{d\Phi_B}{dt} \tag{2.8}$$

In a differential form the equation becomes,

$$\nabla \times \vec{\mathcal{E}} = -\frac{\partial\vec{\mathcal{B}}}{\partial t}. \tag{2.9}$$

There is an extra term which can be useful in some cases, but completely fictitious. By introducing the *magnetic current*, $\mathcal{J}_m$, as a mathematical convenience, the equation becomes,

$$\nabla \times \vec{\mathcal{E}} = -\frac{\partial\vec{\mathcal{B}}}{\partial t} - \vec{\mathcal{J}}_m. \tag{2.10}$$

We mention it is a fictitious because magnetic charges do not exist[3], therefore their movement is purely hypothetical. The effect of magnetic currents, however, are real and that is why we mathematically use it. The origin can be loops of electric currents or magnetic dipoles [43]. In integral form, and using (2.5),

$$\oint_C \vec{\mathcal{E}} \cdot d\vec{l} = -\frac{\partial}{\partial t}\int_S \vec{\mathcal{B}} \cdot d\vec{s} - \int_S \vec{\mathcal{J}}_m \cdot d\vec{s} \tag{2.11}$$

The lack of magnetic charges leads to the final Maxwell equation.

[3]There is still no evidence for its existence

2.2.4 Gauss's Magnetic Law

Magnetic monopoles have not been found, hence,

$$\nabla \cdot \vec{\mathcal{B}} = 0, \tag{2.12}$$

or in the integral form, using (2.5),

$$\oint_S \vec{\mathcal{B}} \cdot d\vec{s} = 0. \tag{2.13}$$

2.2.5 Continuity Equation and Lorentz Force Law

Before finishing this section it is important to refer two other equations, fundamental for the understanding of electromagnetism.

The *continuity equation* can be obtained from the divergence of (2.6) and it states that charge is conserved or the current continuous,

$$\nabla \cdot \vec{\mathcal{J}} + \frac{\partial \rho}{\partial t} = 0, \tag{2.14}$$

Finally, *Lorentz Force Law* is

$$F = Q[\vec{\mathcal{E}} + (\vec{v} \times \vec{\mathcal{B}})] \tag{2.15}$$

and it describes the force that a particle with charge Q suffers when travelling in an electric and magnetic field.

We have concluded the basic electromagnetic laws.

2.2.6 Summary

Now that all of Maxwell's Equations have been introduced, we can summarise them in the differential form,

$$\nabla \times \vec{\mathcal{E}} = -\frac{\partial \vec{\mathcal{B}}}{\partial t} - \vec{\mathcal{J}}_m, \tag{2.16a}$$

$$\nabla \times \vec{\mathcal{H}} = \vec{\mathcal{J}} + \frac{\partial \vec{\mathcal{D}}}{\partial t}, \tag{2.16b}$$

$$\nabla \cdot \vec{\mathcal{D}} = \rho, \tag{2.16c}$$

$$\nabla \cdot \vec{\mathcal{H}} = 0, \tag{2.16d}$$

or as integrals,

$$\oint_C \vec{\mathcal{E}} \cdot d\vec{l} = -\frac{\partial}{\partial t} \int_S \vec{\mathcal{B}} \cdot d\vec{s} - \int_S \vec{\mathcal{J}}_m \cdot d\vec{s}, \tag{2.17a}$$

$$\oint_C \vec{\mathcal{H}} \cdot d\vec{l} = \int_S \vec{\mathcal{J}} \cdot d\vec{s} + \frac{\partial}{\partial t} \int_S \vec{\mathcal{D}} \cdot d\vec{s} = \mathcal{I} + \frac{\partial}{\partial t} \int_S \vec{\mathcal{D}} \cdot d\vec{s}, \tag{2.17b}$$

$$\oint_S \vec{\mathcal{D}} \cdot d\vec{s} = \int_V \rho \cdot dv = \mathcal{Q}, \tag{2.17c}$$

$$\oint_S \vec{\mathcal{B}} \cdot d\vec{s} = 0, \tag{2.17d}$$

where,

Table 2.1: Common electromagnetic quantities, their symbols and SI units.

Symbol	Terminology	SI units
$\vec{\mathcal{E}}$	Electric Field	V/m
$\vec{\mathcal{H}}$	Magnetic Field	A/m
$\vec{\mathcal{D}}$	Electric Flux Density	C/m^2
$\vec{\mathcal{B}}$	Magnetic Flux Density	Wb/m^2
$\vec{\mathcal{J}}_m$	(Fictitious) Magnetic Current Density	V/m^2
$\vec{\mathcal{J}}$	Electric Current Density	A/m^2
$\vec{\mathcal{P}}$	Electric Polarisation	C/m^2
$\vec{\mathcal{M}}$	Magnetisation	A/m
ρ	Electric Charge Density	C/m^3

and,

$$\vec{\mathcal{D}} = \epsilon \vec{\mathcal{E}}, \qquad \epsilon = \epsilon_0(1 + \chi_e), \tag{2.18}$$

$$\vec{\mathcal{H}} = \frac{\vec{\mathcal{B}}}{\mu}, \qquad \mu = \mu_0(1 + \chi_m). \tag{2.19}$$

We have reached a point where we can introduce the phenomena that most interests us, electromagnetic waves.

2.3 Electromagnetic Radiation

In the absence of charges, Maxwell's equations inside a medium are,

$$\begin{aligned} \nabla \cdot \vec{\mathcal{D}} &= 0, & \nabla \times \vec{\mathcal{E}} &= -\frac{\partial \vec{\mathcal{B}}}{\partial t}, \\ \nabla \cdot \vec{\mathcal{B}} &= 0, & \nabla \times \vec{\mathcal{H}} &= \frac{\partial \vec{\mathcal{D}}}{\partial t}. \end{aligned}$$

Furthermore, if the medium is linear and homogeneous,

$$\begin{aligned} \nabla \cdot \vec{\mathcal{E}} &= 0, & \nabla \times \vec{\mathcal{E}} &= -\frac{\partial \vec{\mathcal{B}}}{\partial t}, \\ \nabla \cdot \vec{\mathcal{B}} &= 0, & \nabla \times \vec{\mathcal{B}} &= \mu\epsilon \frac{\partial \vec{\mathcal{E}}}{\partial t}. \end{aligned} \tag{2.20}$$

After applying the curl operation to the right sided equations the electric and magnetic field vectors become decoupled,

$$\nabla^2 \vec{\mathcal{E}} = \mu\epsilon \frac{\partial^2 \vec{\mathcal{E}}}{\partial t^2}, \qquad \nabla^2 \vec{B} = \mu\epsilon \frac{\partial^2 \vec{B}}{\partial t^2}. \tag{2.21}$$

These satisfy the 3D wave equation,

$$\nabla^2 f = \frac{1}{v^2} \frac{\partial^2 f}{\partial t^2}, \tag{2.22}$$

thus enabling us to conclude that $v = 1/\sqrt{\mu\epsilon} = c/n$, where $n = \sqrt{\epsilon\mu/\epsilon_0\mu_0}$ is the *index of refraction*. In the air, $n \approx 1$, and thus the results are very similar, and in most applications equivalent, to that of electromagnetic waves propagating in vacuum. In that case $v = 1/\sqrt{\mu_0\epsilon_0} = c = 3 \times 10^8$ m/s, the *speed of light in a vacuum*, evidence that light is electromagnetic in nature.

2.3.1 Electromagnetic Spectrum and Why Microwaves

Just like light, there are a lot of different types of radiation, defined according to their uses and effects. The electromagnetic waves can then be characterized by the frequency of the electric/magnetic field variation because this quantity is independent of the propagation medium. On the photon level, the Planck's equation (2.23) dictates that a photon with a higher frequency has a higher energy,

$$E = h\nu. \tag{2.23}$$

The eight classifications are, in increasing order of energy, radio waves, microwaves, terahertz radiation, infrared radiation, light, ultraviolet radiation, X-rays and gamma rays.

From all the possibilities, microwaves are used for long distance transmissions because of their relative high directivity, allowing point-to-point transmission, along with a low interaction with the air particles. This is evident in Fig. 2.1, where the microwave transmittance in the air is $\approx 100\%$ for the smaller frequencies, including the frequency of operation, $\nu = 5.8\,\text{GHz}$. This frequency was chosen because it has gained ground on the WPT Standards and Regulations as being one of the most used frequency for far field applications, along with 2.45 GHz [42]. Between the two, the former was chosen because it has a smaller wavelength, useful for longer distances.

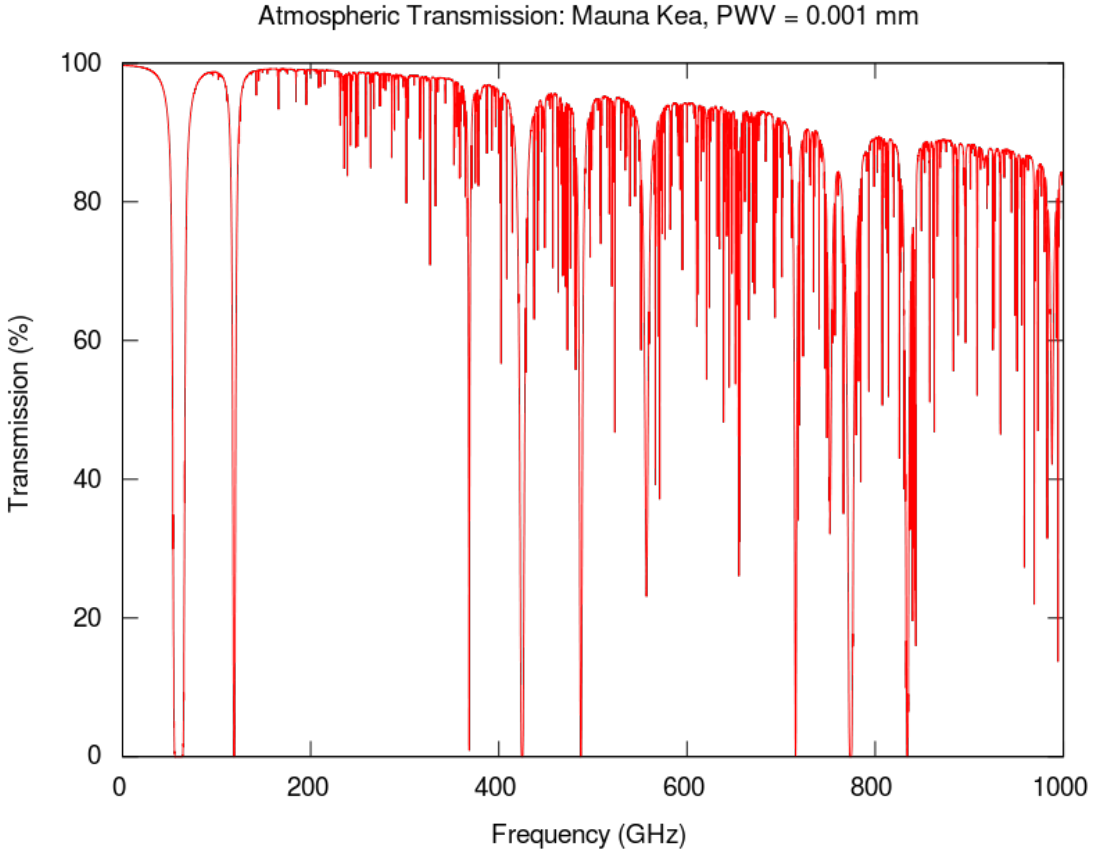

FIGURE 2.1: Microwave transmittance through the air. Plot obtained from the CSO Atmospheric Transmission Interactive Plotter[4].

Microwaves typically cover the radiation from the electromagnetic spectrum between the interval of frequencies of [3 - 300] GHz, which corresponds to wavelengths of [100 - 1] (mm). They are usually represented in the spectrum along RF as in Fig. 2.2.

[4]By Westeros91 (Own work) [CC0], via Wikimedia Commons

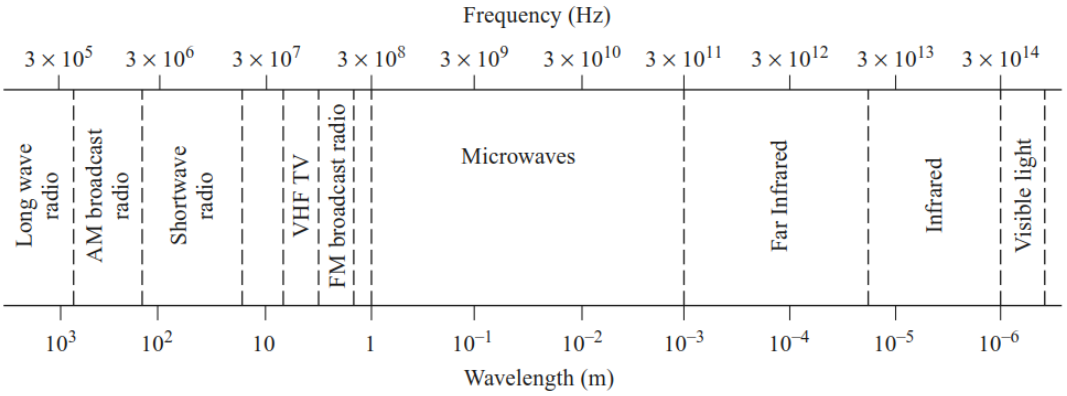

FIGURE 2.2: Electromagnetic spectrum centred at the microwave band. [43]

The introduction of the theoretical foundation necessary for our study has been finished. In a sense, the remaining theoretical sections will elaborate on the electromagnetic results obtained, in order to reduce the level of abstractness to specific applications.

Chapter 3

Quasi-Optics

The electromagnetic waves introduced in the previous chapter were a consequence of advances in 19th century physics. However, experiments on light have been performed millennia before their derivation, yet again in the Ancient World, possibly with the development of the first lenses. The theory of *Geometrical Optics* was first presented by Euclid, the Greek mathematician.

These facts hugely validate the theory of optics because its results and conclusions have been tested and proven throughout the centuries, until this very day. Therefore, it would be hugely advantageous if its formalism could be applied to other types of electromagnetic waves. Fortunately, under certain circumstances, that is the case. It is only necessary to make some adjustments.

Quasi-optics is the field of optics that deals with cases where the wavelength is comparable to the size of the system's components, making the diffraction[1] effects not negligible [2]. Consequently, the electromagnetic front wave approximation is no longer valid being necessary to resort to *Gaussian Beams*. Examples of real cases are light in micrometre scale systems (lasers) and microwaves propagating through the air.

3.1 Gaussian Beam Formalism

In most cases, the study of the electromagnetic fields assume a harmonic time variation[2] which can be written in phasor notation, $e^{i\omega t}$, with $\omega = 2\pi\nu$ being the *angular frequency*. By doing so, the *wave number*, $k = 2\pi/\lambda$, can be written as $k = \omega(\epsilon_r\mu_r)^{1/2}/c$. This notation allows us to keep the time dependence on a separate term, which will always be suppressed.

[1] The alteration of the radiation distribution with the distance from the source of radiation.
[2] Harmonic time varying fields are denoted with roman letters.

We can start by stating that the beam propagates in the $\hat{z}$ direction, with z_0 being the point at which the power is most concentrated and the diffraction less evident - the beam wave front can correctly be approximated by a plane wave at the surroundings of this point. For now, we will define $z_0 = 0$. As z increases (i.e. as the beam propagates), the beam spreads and the wave front[3], assumes a curved shape.

Then, the plane wave approximation is no longer valid and the electric field can be is generally defined as $E(x, y, z, t) = u(x, y, z)e^{-ikz}$, where u is the "function that defines the non-plane wave part of the beam" [2]. The major variation assumed is in the direction of propagation allowing us to continue assuming that the electric and magnetic fields are perpendicular to each other and to the direction of propagation.

If we introduce this form of the electric field in the *Helmholtz Wave Equation*,

$$(\nabla^2 + k^2)\,\Psi = 0, \tag{3.1}$$

where Ψ is any component of $\vec{E}$ or $\vec{H}$, we arrive at the *reduced wave equation*,

$$\frac{\partial^2 u}{\partial x^2} + \frac{\partial^2 u}{\partial y^2} + \frac{\partial^2 u}{\partial z^2} - 2ik\frac{\partial u}{\partial z} = 0. \tag{3.2}$$

3.1.1 Paraxial Approximation

The assumption that the vector rays which characterise a beam's wave front have a small divergence angle[4], θ, throughout the system ($\theta \lesssim 10\ ^\circ$), is called the paraxial approximation. This allows us to neglect the third term in (3.2), thus arriving at the *paraxial equation* for rectangular coordinates,

$$\frac{\partial^2 u}{\partial x^2} + \frac{\partial^2 u}{\partial y^2} - 2ik\frac{\partial u}{\partial z} = 0. \tag{3.3}$$

Cylindrical coordinates may be more advantageous for our analysis due to the symmetry along the optical axis. In that case the paraxial equation becomes

$$\frac{\partial^2 u}{\partial r^2} + \frac{1}{r}\frac{\partial u}{\partial r} + \frac{1}{r}\frac{\partial^2 u}{\partial \varphi^2} - 2ik\frac{\partial u}{\partial z} = 0, \tag{3.4}$$

In either case, the solutions to the paraxial equation are the gaussian beam modes. The electric field of a gaussian beam propagating freely in the fundamental mode is axially symmetric; its value depends only on the *distance from the axis of propagation (radius)*, r, and the *position along the axis*, z. In cylindrical coordinates, normalised so that

[3] The surface of equal phase of the electric field.

[4] The angle is measured between the ray and the *optical axis*, the axis of propagation (in this analysis z).

$\int_0^\infty |E|^2 \cdot 2\pi\, r\, \mathrm{d}r = 1$, the distribution is

$$E(r,z) = \sqrt{\frac{2}{\pi\varpi^2}} \exp\left(-\frac{r^2}{\varpi^2} - ikz - \frac{i\pi r^2}{\lambda R} + i\phi_0\right), \tag{3.5}$$

This field distribution is represented in Fig. 3.1. Several important parameters have been introduced: ϖ is the *beam radius*, R is the *radius of curvature* of the wave front, $\phi_\mathbf{0}$ is the *phase shift* and λ is the *wavelength*.

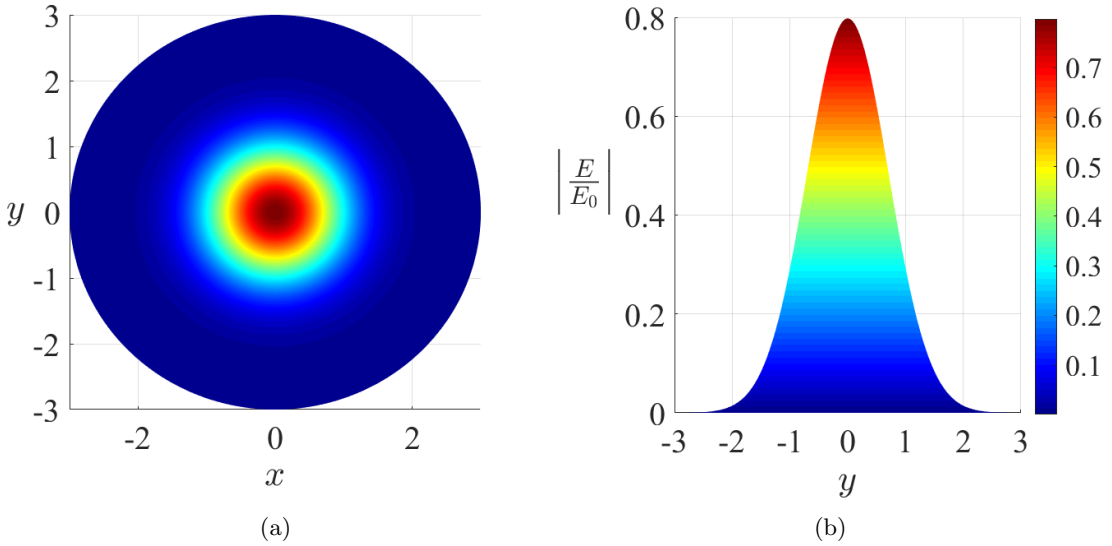

(a) (b)

FIGURE 3.1: Normalized electric field distribution of a gaussian beam in the fundamental mode ($\varpi_0 = 1\,\mathrm{m}$): (a) front view and (b) transverse view.

These parameters will now be explained.

3.1.2 Beam Parameters

Gaussian Beams are mainly described by three parameters, ϖ, R and ϕ_0:

- The ***Beam Radius***, $\varpi(z)$, is the distance to the axis at which the field drops to $1/e$ of its on-axis value and is generally a function of the position along the propagation direction (Fig. 3.2). Its minimum value, which is characteristic of the beam, is called the *Beam Waist Radius* (ϖ_0) and it is located at the *Beam Waist* point, z_0, which is defined according to a reference point (e.g. the aperture of a horn antenna). As stated before, it is assumed that $z_0 = 0$. It can be shown that [2],

$$\varpi = \varpi_0 \sqrt{1 + \left(\frac{z}{z_c}\right)^2}, \tag{3.6}$$

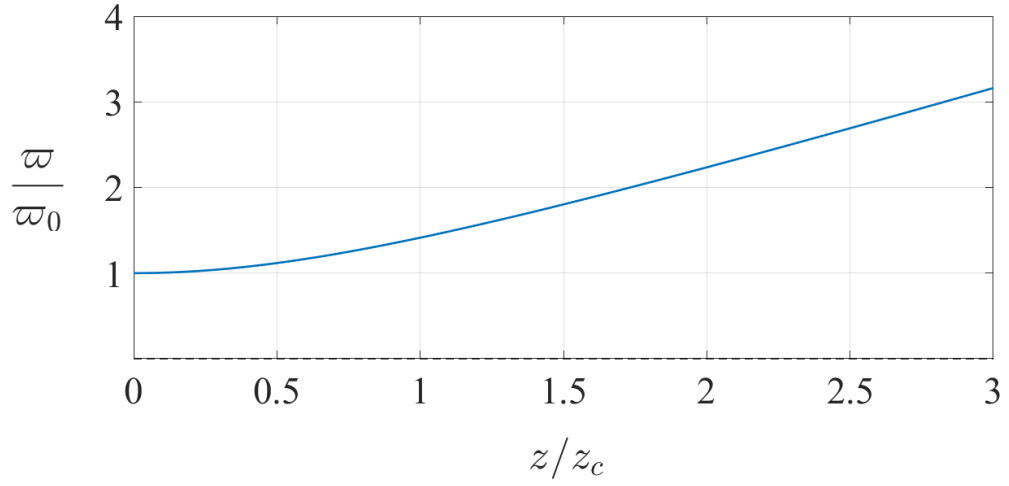

FIGURE 3.2: The normalized beam radius is plotted as a function of the propagation axis, z.

where $z_c = (\pi\varpi_0^2)/\lambda$ is the confocal distance, an important quantity which will be defined below.

- The ***Radius of Curvature***, $R(z)$, is the radius of curvature of a wave front at z (Fig. 3.3), if the wave was plane at $z = 0$,

$$R = z + \frac{z_c^2}{z}. \tag{3.7}$$

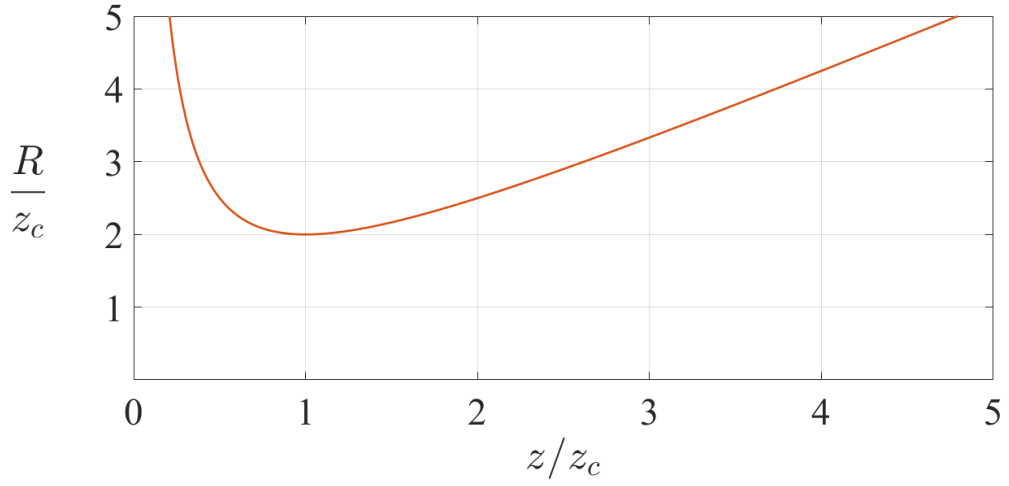

FIGURE 3.3: The radius of curvature of the wave front along z.

Naturally, at the beam waist $z = z_0 = 0$ and $R \to \infty$, typical of a plane surface.

- The ***Beam Phase Shift***, ϕ_0, (sometimes called the *Guoy Phase Shift*) is the difference between the on-axis wave front phase and that of a corresponding plane

wave. It generally changes along z (Fig. 3.4), being

$$\phi_0 = \arctan\left(\frac{z}{z_c}\right). \tag{3.8}$$

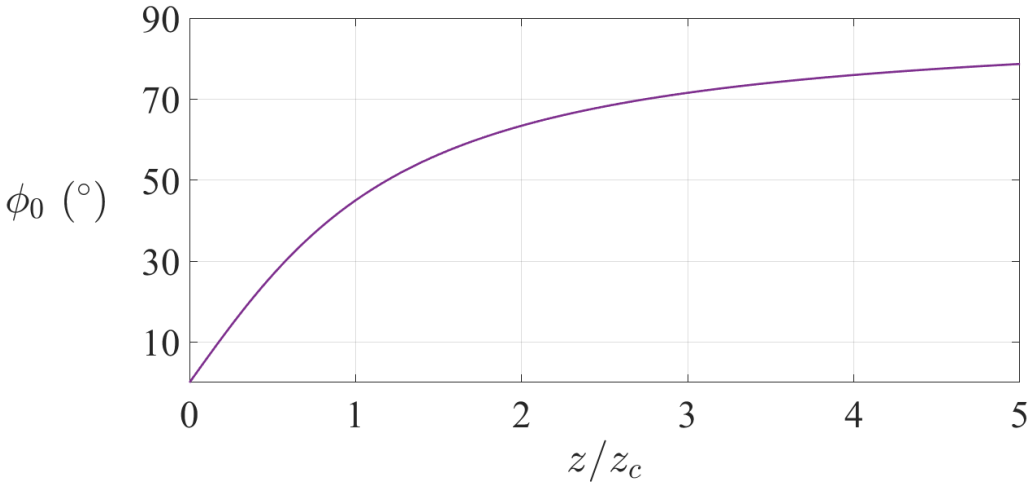

FIGURE 3.4: Phase shift along z.

- When studying beam transformations it is particularly convenient to define the so called ***Gaussian Beam Parameter***, q,

$$\frac{1}{q} = \frac{1}{R} - i\frac{\lambda}{\pi\varpi^2} \tag{3.9}$$

or (as a function of ϖ_0)

$$q = z + iz_c. \tag{3.10}$$

- The crucial quantity after which all the other parameters are written is the ***Confocal Distance*** (or *Rayleigh Range*),

$$z_c = \frac{\pi\varpi_0^2}{\lambda}. \tag{3.11}$$

This parameter sets the scale at which a gaussian beam remains collimated (i.e. the beam's rays remain parallel, with minimum divergence). Therefore, z_c parameterizes the transition between the near-field region, $z \ll z_c$, and the far-field, $z \gg z_c$.

It is important to differentiate between the definition of the field regions of gaussian beams from that of antennas'. The antenna's near-field is the region where non-radiative fields dominate while the far-field is associated with the emission of radiation. On the other hand, since gaussian beams are a representation of electromagnetic waves the field regions are always related to the beam of radiation

and the way it behaves and propagates. The diffraction is the major differentiator between the near and far-field of gaussian beams with z_c being the transition region.

3.1.3 Near and Far Field Regions

The Gaussian Beam mode solutions offer a way of describing the behaviour of the beam parameters at all distances from the beam waist. However, in analogy to other calculations it is still natural to divide the beam into Near and Far Field. As stated previously, this approach can be easily done in terms of the *Confocal Distance* (3.11).

One can summarise a beam propagating, as a function of the distance from the beam waist, as follows.

At the Beam Waist

At this point the beam can be correctly approximated by a plane wave ($R \to \infty$ and $\phi_0 = 0$) meaning that the diffraction effects are negligible. The beam radius assumes its minimum value $\varpi = \varpi_0$, which is the same to say that the electric field and power density have their maximum on-axis value.

As z increases, ϖ grows hyperbolically (Fig. 3.2).

In the Near Field ($z << z_c$)

Firstly the beam radius increases very slowly, remaining relatively similar to the beam waist ($\varpi \leq \sqrt{2}\varpi_0$). While that is the case, the beam is said to be *collimated*.

At the confocal distance ($z = z_c$)

This point marks the transition of the near and far field regions, delimiting the end of the collimation, $\varpi = \sqrt{2}\varpi_0$. The radius of curvature has its minimum value, $R = 2z_c$, and $\phi_0 = \pi/4$.

From this point on, the beam greatly increases, entering the far field region.

In the Far Field ($z >> z_c$)

The beam assumes a linear growth where the *divergence angle*, θ_0, is $\theta_0 \cong \frac{\lambda}{\pi\varpi_0}$. Just as ϖ, the radius of curvature grows linearly, with the form $R \to z$. In 2D the phase shift has the asymptotic limit $\phi_0 = \pi/2$.

An important note is now in order.

In the paraxial limit the wave fronts are considered to propagate near the optical axis. These have wave vectors (rays) that are almost parallel to the optical axis at any point

(i.e. the divergence angle is $\theta_0 \lesssim 10$ °). In such an approximation,

$$\sin\theta_0 \approx \theta_0, \quad \tan\theta_0 \approx \theta_0 \quad \text{and} \quad \cos\theta_0 \approx 1.$$

The importance of this result is immense since it means that the beam transformations can be linearly analysed, allowing the use of matrices[5]. In quasi-optics the paraxial approximation is considered valid as long as,

$$\frac{\varpi_0}{\lambda} \gtrsim 0.9. \tag{3.12}$$

3.2 Higher Order Modes

Sometimes, the most common solutions are not enough to describe a certain beam and the fundamental mode derived above doesn't provide a good approximation to the radiation beam. More complex solutions can be achieved by deriving Higher Order Gaussian Beam Solutions. These have the same behaviour in terms of radius of curvature and beam radius but differ in phase shift.

3.2.1 Higher Order Modes in Cylindrical Coordinates

Higher order modes in cylindrical coordinates account for radiating systems with high axial symmetric but which are not perfectly described by the fundamental radiating pattern:

$$\begin{aligned} E_{pm}(r,\varphi,z) = & \sqrt{\frac{2p!}{\pi(p+m)!}}\,\frac{1}{\varpi(z)}\left[\frac{\sqrt{2}r}{\varpi(z)}\right]^m L_{pm}\left(\frac{2r^2}{\varpi^2(z)}\right) \\ & \cdot \exp\left[-\frac{r^2}{\varpi^2(z)} - ikz - \frac{i\pi r^2}{\lambda R(z)} - i(2p+m+1)\phi_0(z)\right] \\ & \cdot \exp\left(im\varphi\right). \end{aligned} \tag{3.13}$$

The higher order Gaussian Beam mode solutions are normalised so that each represent unit power flow and are related orthogonally:

$$\int\int r\,dr\,d\varphi\, E_{pm}(r,\varphi,z)\, E^*_{qn}(r,\varphi,z) = \delta_{pq}\delta_{mn}. \tag{3.14}$$

These modes are called the *pm Gaussian Beam* modes, *pm* modes, or *Gaussian-Laguerre* modes. **p** refers to radial variations while **m** is related with axial variations.

[5]This will be clearer in section 3.3.

The L_{pm} polynomials are solutions to Laguerre's differential equation,

$$u\frac{d^2L_{pm}}{du^2} + (m+1-u)\frac{dL_{pm}}{du} + pLpm = 0, \tag{3.15}$$

which can be obtained in direct series representations,

$$L_{pm}(u) = \sum_{l=0}^{l=p} \frac{(p+m)!\,(-u)^l}{(m+l)!\,(p-l)!\,l!}. \tag{3.16}$$

It is quite normal to take $m = 0$, assuming that there is axial symmetry, to describe radiating systems (axially symmetric horns, etc). Different beam can be observed in Fig. 3.5.

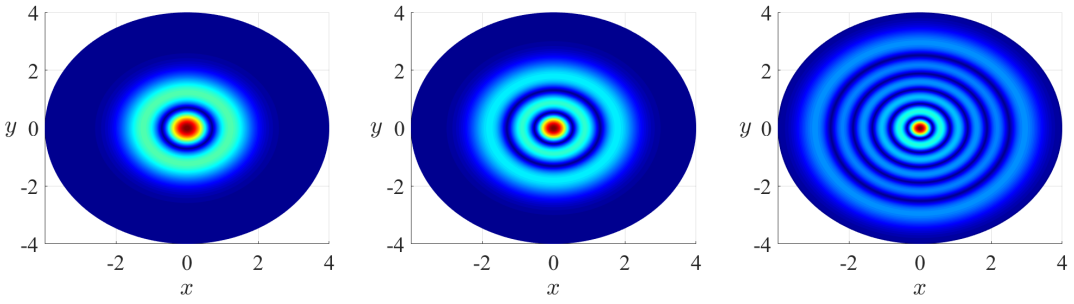

(a) (b) (c)

FIGURE 3.5: Different gaussian beam cylindrical modes assuming axial symmetry, $m = 0$: (a) $p = 1$ (b) $p = 2$ (c) $p = 5$.

3.2.2 Higher Order Modes in Rectangular Coordinates

The rectangular coordinate system may be useful to describe some systems, specifically if there is independent variation along two different directions. They are given by

$$\begin{aligned} E_{mn}(x,y,z) = &\sqrt{\frac{1}{\pi\,\varpi_x\,\varpi_y\,2^{m+n-1}\,m!\,n!}}\,H_m\left(\frac{\sqrt{2x}}{\varpi_x}\right)H_n\left(\frac{\sqrt{2y}}{\varpi_y}\right) \\ &\cdot\exp\left[-\frac{x^2}{\varpi_x^2} - \frac{y^2}{\varpi_y^2} - ikz - \frac{i\pi x^2}{\lambda R_x} - \frac{i\pi y^2}{\lambda R_y} + \frac{i(2m+1)\phi_{0_x}}{2} + \frac{i(2n+1)\phi_{0_y}}{2}\right]. \end{aligned} \tag{3.17}$$

These modes also obey the orthogonality relationship,

$$\int\int_{-\infty}^{\infty} E_{mn}(x,y,z)\,E^*_{pq}(x,y,z)dxdy = \delta_{mp}\delta_{nq}. \tag{3.18}$$

These solve the Hermite's differential equation,

$$\frac{d^2H(u)}{du^2} - 2u\frac{dH(u)}{du} + 2mH(u) = 0, \tag{3.19}$$

m being a positive integer. The polynomials in direct series are obtained from

$$H_{n+1}(u) = 2\,[uH_n(u) - nH_{n-1}(u)], \tag{3.20}$$

knowing that $H_0(u) = 1$ and $H_1(u) = 2u$.

The indexes **m** and **n** are related to the x and y electric field components as the number of roots. For example, $m = 1$ means that the electric field distribution has a null in the x component. A couple of rectangular modes are represented in Fig. 3.6.

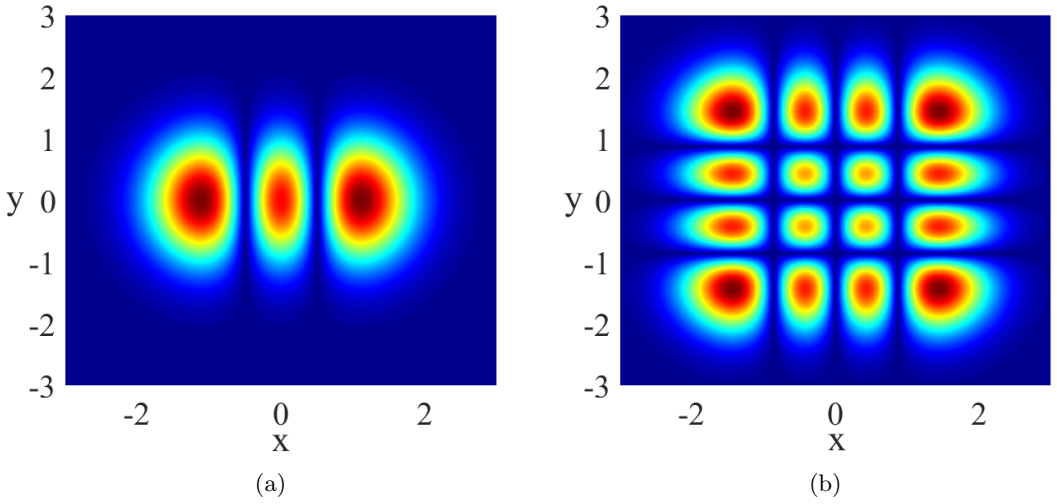

FIGURE 3.6: Different gaussian beam rectangular modes: (a) $m = 2$, $n = 0$ (b) $m = 3$, $n = 3$.

3.3 Beam Transformation

While in the previous section was introduced the way Gaussian beams propagate[6] now it will be shown how to perform beam transformations. Like in optical systems, lenses and mirrors are the base components.

The fundamental mode will be the focus of the discussion due to its simplicity and the fact that most of the radiating patterns can be well approximated by it.

A general quasi-optical system can is represented in Fig. 3.7:

[6] i.e. how the parameters vary with the distance.

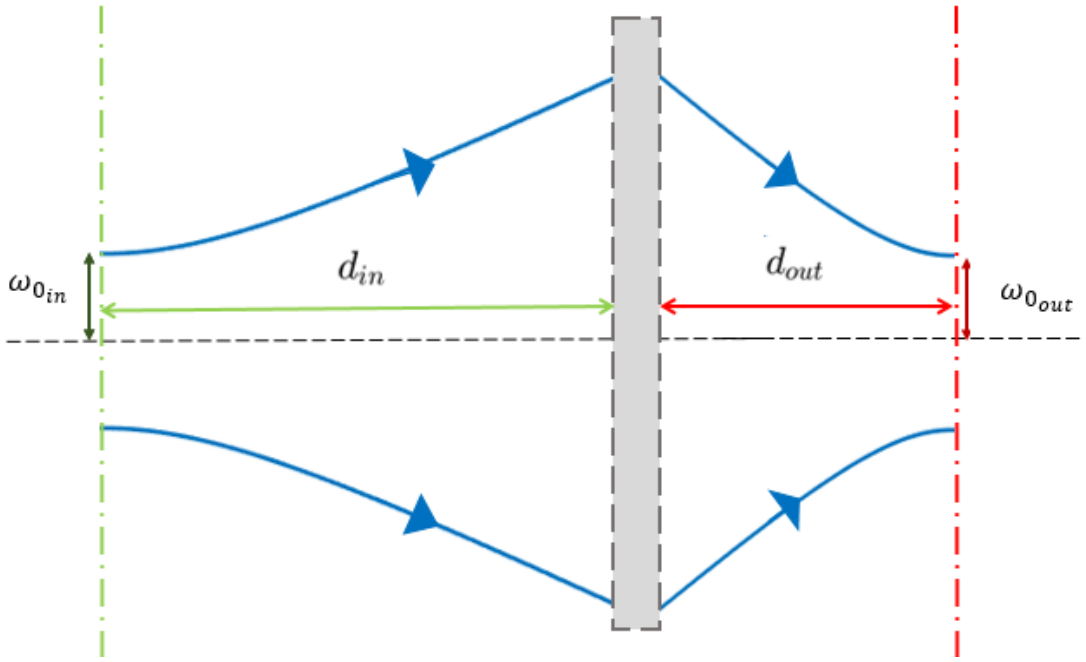

FIGURE 3.7: General quasi-optical system. d_{in} is the distance from the input beam waist to the first system's component whereas d_{out} is the distance from the final component to the output beam waist. The grey box illustrates the general system which can be composed of various components.

3.3.1 Rays, Matrices and the Complex Beam Parameter

Rays propagating freely in a homogeneous medium can be ascribed at each point to their distance (r) and slope (θ) to the optical axis. If a ray encounters a quasi-optical component it is formally transformed and an output ray will emerge. In the paraxial approximation these transformations are linear, hence the output ray is linearly related to the input one:

$$\begin{bmatrix} r_{out} \\ \theta_{out} \end{bmatrix} = \begin{bmatrix} A & B \\ C & D \end{bmatrix} \cdot \begin{bmatrix} r_{in} \\ \theta_{in} \end{bmatrix}.$$

The $ABCD$ elements form the so called *Ray Transfer Matrix* ($\mathbf{M}$), which is characteristic of the system with its components. It can be calculated by multiplying the matrices of each component that interacts with a ray in reverse order (e.g. if a ray enters a system and encounters the component A and then B, the overall matrix is $M = M_B \times M_A$).

The radius of curvature of the wave front of a beam is $R = r/\theta$ and therefore the gaussian beam parameter, q, can be related to the ray parameters. Defining q_{in} as the input gaussian beam parameter at the input beam waist we can arrive at the output gaussian beam parameter (at the output beam waist),

$$q_{out} = \frac{A \cdot q_{in} + B}{C \cdot q_{in} + D}. \tag{3.21}$$

By using (3.9) we can obtain the beam radius (ϖ) and the radius of curvature (R) of the output beam as a function of z.

A general system matrix, M_{sys}, can be written by taking the matrices representing the propagation of the incoming and outgoing rays together with the ray transfer matrix, M. It enables us to write the input and output parameters for any system configuration in simple terms:

$$\begin{aligned} M_{sys} &= \begin{bmatrix} 1 & d_{out} \\ 0 & 1 \end{bmatrix} \cdot \begin{bmatrix} A & B \\ C & D \end{bmatrix} \cdot \begin{bmatrix} 1 & d_{in} \\ 0 & 1 \end{bmatrix} \\ &= \begin{bmatrix} A + Cd_{out} & Ad_{in} + B + d_{out}(Cd_{in} + D) \\ C & Cd_{in} + D \end{bmatrix} \\ &= \begin{bmatrix} A' & B' \\ C' & D' \end{bmatrix} \end{aligned} \tag{3.22}$$

where d_{in}, the *input distance*, is the distance from the input beam waist to the first element of the system and d_{out} is the *output distance* from the last element of the system to the output beam waist (see Fig. 3.7).

Since the beam parameter (3.10) at the beam waist (where $z = 0$) is $q_{in} = iz_c$ then, by inserting $A'B'C'D'$ elements of the overall matrix, M_{sys}, in (3.21), the output beam parameter q_{out} becomes,

$$q_{out} = \frac{(A + Cd_{out})iz_c + [(A + Cd_{out})d_{in} + (B + Dd_{out})]}{Ciz_c + Cd_{in} + D}, \tag{3.23}$$

and, given that at the output beam waist, $z_{out} = 0$, q_{out} is imaginary, and

$$d_{out} = -\frac{(Ad_{in} + B)(Cd_{in} + D) + ACz_c^2}{(Cd_{in} + D)^2 + C^2 z_c^2} \tag{3.24}$$

and finally the output beam waist radius $\varpi_{0_{out}}$ (knowing that $\det M = 1$),

$$\varpi_{0_{out}} = \frac{\varpi_{0_{in}}}{\sqrt{(Cd_{in} + D)^2 + C^2 z_c^2}}. \tag{3.25}$$

This ends the quasi-optical formalism theory. In the next chapters a script developed to visualize the beam propagation and transformation (chapter 4) will be explained as well as theoretical results obtained when analysing the proposed double reflector system (chapter 5).

Chapter 4

Graphical Representation Scripts

In order to better understand the phenomena of gaussian beams, scripts were developed to help fulfil two major goals: firstly, the visualisation of the gaussian beam wave front, for different modes of propagation, in both rectangular and cylindrical coordinates; the other objective was to represent gaussian beam propagation and transformation in a system (which can be composed by reflectors or lenses), through the beam radius' value as a function of the position in the system, $\varpi(z)$. The propagation and transformation follow [2] (presented in section 3.3).

4.1 Initialisation

At first, it is necessary to define the physics constants and parameter values that will be used, done by `Gaussian_Beam.m`:

```
1 %%      Global Variables
2 global lambda k;          %   to be used in other .m files
3
4 %%      Constants
5 c = 3e8;                  %   Speed of light in vacuum (m/s)
6 freq = 5.8e9;             %   Frequency is 5.8 GHz
7 n = 1;                    %   Refraction index (n = c/v) of air n = 1.0003
8 lambda = c / (n * freq); %   Wavelength (lambda =~ 0.0517 (m)
9 k = 2*pi / lambda;        %   Wave Vector (1/m)
```

LISTING 4.1: `Gaussian_Beam.m` - The initialisation file.

It is necessary to run this script at the beginning of each session.

4.2 Wave Front

The wave front is a set of beam points which have the same phase. The location of the wave front is characterised by the distance from the beam waist, z, where the analysis is made. MATLAB functions[1] were used to describe and obtain the necessary quasi-optical quantity values and use them in the calculus of the electric field distribution.

As an example, the beam radius[2] function is presented in Listing 4.2:

```
function y = w_(z, w0)

    global lambda;
    y = w0 .* (1 + (lambda .* z ./ (pi .* (w0 .^ 2))) .^ 2) .^ (0.5);
end
```

LISTING 4.2: `w_.m` - Beam radius MATLAB function.

This function assumes two input arguments, z and ϖ_0 (the beam waist value, a constant parameter characteristic of the beam). For a certain wave front, the beam radius[3] is constant.

After defining the other necessary variables, the final electric field distribution function in cylindrical coordinates is given in Listing 4.3. It allows us to know the electric field values of a gaussian beam at any point[4] (r, φ, z). The gaussian beam can be propagating in any **pm** mode.

```
function y = pelec(r, z, w0, phi, p, m)

    global lambda k;

    y = ((2 .* factorial( p ) ./ (pi .* factorial(p + m))) .^ 0.5) .* (1
    ./ w_(z, w0)) .* ((sqrt(2 .* r) ./ w_(z, w0)) .^ m) .* Lag(((2 .* (r
    .^ 2)) ./ (w_(z, w0) .^ 2)), m, p) .* exp(-(r .^ 2) ./ (w_(z, w0) .^
    2) - 1i .* k .* z - (1i .* pi .* (r .^ 2)) ./ (lambda .* R_(z, w0)) -
    1i .* (2 .* p + m + 1) .* phi0_(z, w0)) .* exp(1i .* m .* phi);
end
```

LISTING 4.3: `pelec.m` - Higher order modes in cylindrical coordinates MATLAB function.

The Laguerre polynomials (3.16) are defined as another MATLAB function (Listing 4.4):

[1] To differentiate between variables and functions which have similar names, the latter's end with underscore, '_'.

[2] The symbol used for the beam radius in MALTAB is w for being easier to implement than ϖ.

[3] *lambda* is the global variable defined in the initialisation file, `Gaussian_Beam.m`.

[4] r, φ, z are the common cylindrical coordinates

```
function y = Lag(u, p, m)
    y = 0;
    for l = 0:p
        y = y + (factorial(p + m).*((- u).^l))./(factorial(m + l).*
    factorial(p - l).*factorial(l));
    end
end
```

LISTING 4.4: `Lag.m`, Laguerre polynomials in direct series representation.

Having obtained the wave front electric field distribution, it is only necessary to plot the function. Matlab allows the plotting of a surface with the `surf` command. By defining the surface basis as x and y with the `meshgrid` command, it is only necessary to obtain the z value (the value of electric field distribution at (x, y)).

The implementation was done by the use of another function (partially presented[5] in Listing 4.5) which immediately outputs a figure with the wave front plot. The use of a plotting function avoids having to change the script for different modes of propagation.

```
function cc(z, w0, p, m)                % Cylindrical Coordinates

    Nres = 1000;                                % Number of Points

    %%      Grid Definition for a Circular x and y Basis.

    theta = linspace(0, 360, Nres) .* pi ./ 180;          % Angle is 360
     degrees
    r     = linspace(0, 4.*(w_(z, w0)./w0), Nres);%  0 < r < 4*w0

    [th, rho] = meshgrid(theta, r);              % Meshgrid creation

    fun = @(r) abs(pelec(r, z, w0, 0, p, m));    % Function handle

    %%      Top View

    figure;
    surf(rho .* cos(th), rho .* sin(th), fun(rho), 'linestyle', 'none');
    view(2);
    grid on;
end
```

LISTING 4.5: `cc.m` - Wave front in cylindrical coordinates plotting function.

The function handle (`fun`) enables us to choose which variables will vary and the value of the ones that are constant. In this case, axial symmetry is assumed ($\varphi = const = 0$) and the electric field distribution becomes a function only of r. The electric field is a

[5] The MATLAB figure formatting was left out of the listing.

complex vector field but it is here represented as an electric field amplitude by the use of the `abs` command.

Finally, a similar approach was repeated for the rectangular coordinates beam modes. All the wave front graphical representations in this document have been obtained through these scripts.

Having finalised the wave front representation section, beam propagation and transformation will now be presented.

4.3 Beam Propagation and Transformation

In order to visualise the beam propagating through the system, several different steps must be made which will be presented in different sections. The main difference is that z is now a system variable. In fact, the beam propagation is considered to be one dimensional, happening only in the $\hat{z}$ axis.

Firstly, the functionality is condensed in a single script (called `test_final.m`) where it is possible to call the initialiser script `Gaussian_Beam.m`. We proceed by defining the beam waist radius, ϖ_0, which allows us to obtain the confocal distance, z_c.

4.3.1 Cell Array

This script makes use of several requests for user input to define the system[6], the first of which is for `N`, the number of elements in the system. It is important to emphasise that all information regarding the elements composing the system are stored in `zelem`, a $\mathtt{N} \times 3$ cell array[7].

```
1  Gaussian_Beam           %   Call for the initialising script.
2
3  w0 = 0.04902;
4  zc = pi * (w0 ^ 2) / lambda;
5
6  Nres = 1000;            %   Related to the graphic's resolution
7
8  %%      System Definition
9
10 zelem = {};             %   Cell array initialisation.
11 N = input('\n\nNumber of elements (integer) = ');       %   # of elements
12
13 i = 1;
14 while i < N + 1
```

[6] The input requests are only made for the parameters which are more likely to be changed.
[7] Cell arrays can contain any type of data, hence their usefulness.

```
    fprintf('\n\n       Element number %i\n', i);
    element = input('Element Type ("mirror" or "lens")\n   ', 's');
    if strcmp(element, 'mirror')
        f = input('\nFocal length of the element (f) = ');
        zelem{i, 1} = [1 0; -1/f 1];
        zelem{i, 2} = input('\nElement Position (in m) = ');
        zelem{i, 3} = -1;
        i = i + 1;
    elseif strcmp(element, 'lens')
        f = input('\nFocal length of the element (f) = ');
        zelem{i, 1} = [1 0; -1/f 1];
        zelem{i, 2} = input('Element Position (in m) = ');
        zelem{i, 3} = 1;
        i = i + 1;
    else
        fprintf('Invalid element type!\nPlease repeat.');
    end
end
```

LISTING 4.6: `test_final.m` - Part 1. System Definition.

The cell array `zelem` can be explained as follows:

- Each row contains information about one element;
- There are three columns for each row: the first is the ray transfer matrix M, characteristic of each element[8]; the second is the position along the $\hat{z}$ axis where the element is placed (in meters); finally the third cell has either the integer -1 or $+1$, respectively for when the element is reflective or not[9].

4.3.2 Arrays for Storing Quantity Values

The beam propagation starts at a position z_0 dictated by the user. Its value will be saved in an array, `z_array`, that serves as the independent variable when plotting the beam propagation. The other variable is the beam radius which starts with the beam waist value and will also be kept in an array, `w_array`.

The final user requested information is the initial s[10], the direction of propagation of the beam, with $+1$ and -1 being respectively the positive and negative direction of the $\hat{z}$ axis (right and left in the plot figure).

```
z0 = input('\nBeam starting position\n   ');
s  = input('\nDirection of propagation (-1 for negative diretion, 1 for
    positive)\n   ');
```

[8] As described in section 3.3.
[9] The reason for it will be explained further down in this section.
[10] The choice is only between $+1$ or -1.

```
3
4  z_array = [z0]; %   Saving values and initialising the arrays
5  w_array = [w_(z, w0)];
6
7  z0_last = z0;   %   Position of the beam waist after the transformation
8  w0_last = w0;   %   Beam waist value after the last transformation
```

LISTING 4.7: `test_final.m` - Part 2. Array initialisation.

A final note goes to the `w0_last` and `z0_last`. These variables are necessary to obtain the correct quantity values after each transformation[11]. These are used to keep track of the most recent quantity values.

4.3.3 Main Loop

The main code is a `while` loop, where each iteration coincides with a variation in the wave front position of s/N. The reason why s is defined with a ± 1 is now evident: it makes it easy to have the beam propagate in the positive or negative direction.

It it is now important to differentiate with the beam wave front position (the one that is being saved in z_array) and the z used to calculate quasi-optical quantities. As stated in the end of the previous section, new beam transformations are the same as terminating the beam interacting with the component and having another beam, with a new ϖ_0 at a certain z_0, start at exactly the component's position.

Since the d_{out} is defined as the distance between the component and the output beam waist, it equals to say that, at the component's position, the beam has $z = -d_{out}$. It will proceed to propagate and converge until $z = 0$ at the beam waist location (z_0 in the system reference frame). In the script it is presented as follows:

```
1  while size(z_array, 2) < 120 * N + 1
2
3      z = z + 1 / N;              %   Increase of z in every step.
4
5          %%      Saving the new values in the arrays
6
7      w_array(end + 1) = w_(z, w0_last);
8      z_array(end + 1) = z_array(end) + s / N;
```

LISTING 4.8: `test_final.m` - Part 3. Beam propagation.

After having propagated the extra step, s/N, the beam may interact with a system component. If so, the beam transformation formalism of section 3.3 is used to calculate

[11] After each transformation, the beam can be mathematical treated as a new beam with a certain beam waist located in a certain position.

the output beam waist and its location. Afterwards, the necessary updates to the variables are made and the beam continues to propagate.

As can be seen in line 23 of Listing 4.9, the third cell of `zelem` is used to control the beam direction of propagation through a multiplication between it and s.

```
1     %%      Check if the beam coincides with a system element
2     for i = 1:N
3         if abs(z_array(end) - zelem{i, 2}) < (1 / N)
4
5             %%      Transformation Matrix
6
7             A = zelem{i, 1}(1, 1);
8             B = zelem{i, 1}(1, 2);
9             C = zelem{i, 1}(2, 1);
10            D = zelem{i, 1}(2, 2);
11
12            din = s * (zelem{i, 2} - z0_);      %   din < 0 = virtual
    image, din > 0 = real image
13
14            zc = pi * (w0_last ^ 2) / lambda;
15
16            dout = -((A * abs(din) + B) * (C * abs(din) + D) + A * C * (
    zc ^ 2)) / ((C * abs(din) + D) ^ 2 + (C ^ 2) * (zc ^ 2));
17            z = - dout;
18
19            w0out = w0_last / ((((C * abs(din) + D) ^ 2) + (C ^ 2) * (zc
    ^ 2)) ^ 0.5);
20            w0_last = w0out;
21
22            s = s * zelem{i, 3};                %   Transformation of the
     direction of propagation
23
24            z0_ = zelem{i, 2} + s * dout;       %   sfinal (s - direction
     of propagation) after transformation
25        end
26    end
27 end
28
29 plot(z_array, w);
```

Listing 4.9: `test_final.m` - Part 4. Beam transformation.

With the `plot` function this chapter is finalised, having been possible to fulfil both proposed goals.

Chapter 5

Double Reflector Quasi-optical System Analysis and Results

After having the tools to analyse any general quasi-optical system, it is necessary to choose a system for further study. The proposed quasi-optical system is a double reflector configuration (represented in Fig. 5.1), somewhat inspired by the acoustic mirror. The idea is that:

1. A feed antenna radiates on the first reflector;
2. The mirror transforms the radiation in order for it to better propagate through space, directing the beam at the second mirror;
3. This last one will in turn transform the beam so that it can be better received in the final antenna.

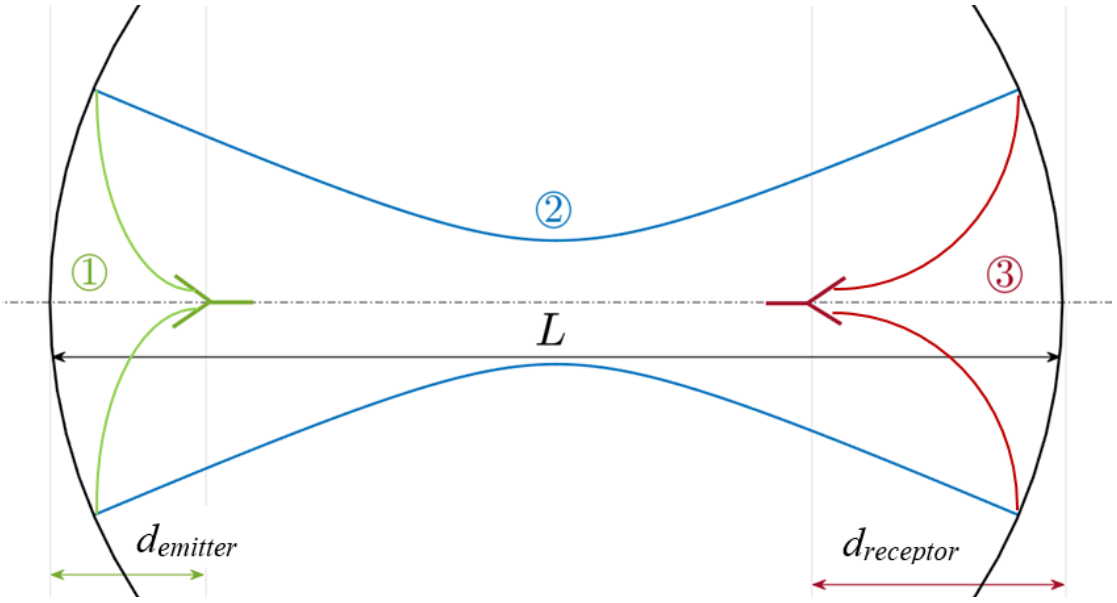

FIGURE 5.1: Double-Reflector configuration. $d_{emitter}$ is the distance from the input beam waist radiated by the emitter antenna to the first reflector, after which one can find a beam waist clearly located at $z = L/2$. $d_{receptor}$ is the distance from the final reflector to the output beam waist, at the reception antenna.

Although represented on-axis, an offset reflector should be mandatory since most energy flows in the centre of the axis. This set-up was chosen for being the most simple (reflectors are the only type of components used besides the mandatory feed antennas) which serves the purpose of theory validation and preparation for more advanced systems (e.g. adding lenses will enable increasingly complex and improved solutions). Parabolic reflectors were chosen in order to avoid spherical aberration.

The *separation between reflectors* (L) is the quantity that specially characterizes the system. Our final goal is to understand how to achieve the maximum power transmission efficiency, for the maximum L possible.

It is extremely necessary to make a note here. Every quasi-optical system analysis is made by considering an incident beam, with a certain beam waist radius $\varpi_{0_{in}}$ located at a distance d_{in} from the first component of the system, that suffers transformations by the system. The result is an output beam with a certain $\varpi_{0_{out}}$ that will be located at a distance d_{out} from the last component of the system. A representation of a general quasi-optical system is represented in Fig. 3.7.

For our double-reflector system, the quasi-optical system is composed by three components: the first reflector, the distance between reflectors and the final reflector, where $d'_{in} = d_{emitter}$, $d'_{out} = d_{receptor}$ (the inverted comas are used for quantities referring to the total double-reflector system).

However, we can begin our analysis by simplifying the double mirror set-up by making both mirrors and antennas equal: in optics and quasi-optics, rays respect the reciprocity principle, therefore the same laws apply to incoming or outgoing beams - the transformations are simply reversed. One can then analyse the mirrors' effect by studying only one of them.

By doing so, the quasi-optical system represents only one reflector and although $d_{in} = d_{emitter}$ remains exactly the same, the output beam waist will now be the beam after the first reflector. By observing Fig. 5.1, it is clear that $d_{out} = L/2$.

In that case, the ray transfer matrix is exactly that of a single mirror with a certain *focal length* (f),

$$\begin{bmatrix} 1 & 0 \\ -\frac{1}{f} & 1 \end{bmatrix}. \tag{5.1}$$

To clarify, the feed antenna originates a beam whose beam waist is at certain distance d_{in} from the reflector. This beam will diverge until it is transformed by the reflector. The output beam will converge until it reaches $L/2$ where the output beam waist is located by definition (i.e. $d_{out} = L/2$). That finalises the quasi-optical system analysis, but not the beam propagation, which proceeds until the receptor. Because of reciprocity, the beam is expected to diverge until it reaches L, the position where the second mirror is, with the same characteristics (parameters' values) it had in the first mirror. Then the beam will be transformed by the mirror and focused at the receiving antenna, which, reciprocally, is at a distance of d_{in} from the last reflector. In this case $d_{emitter} = d_{receptor} = d_{in}$.

In the end, the incoming beam at the receiving antenna should have the same characteristics of the outgoing beam at the transmitting antenna,

$$\varpi_{0_{final}} = \varpi_{0_{initial}}.$$

At this point the wave front is approximately a plane wave, which might be advantageous for conversion efficiency (at the receptor).

By substituting the parameters of (5.1): $A = 1,\ B = 0,\ C = -1/f$ and $D = 1$ into (3.23) and (3.24), and solving as a function of the mirror's focal length (f) we arrive at

$$af^2 + bf + c = 0, \tag{5.2}$$

with $a = \frac{L}{2} + d_{in},\ b = -\left(Ld_{in} + d_{in}^2 + z_c^2\right)$ and $c = \frac{L}{2}\left(d_{in}^2 + z_c^2\right)$. This is a quadratic polynomial equation, which has two solutions. In order for the focal length to be a real quantity

$$b^2 - 4ac \geq 0 \tag{5.3}$$

Therefore,

$$\left[-\left(Ld_{in} + d_{in}^2 + z_c^2\right) \right]^2 - 4\left[\frac{L}{2} + d_{in}\right]\left[\frac{L}{2}\left(d_{in}^2 + z_c^2\right)\right] \geq 0,$$

which can be solved for L, yielding the condition,

$$L \leq z_c + \frac{d_{in}^2}{z_c}. \tag{5.4}$$

5.1 Maximum Distance Between Mirrors

We have arrived at an interval of possible values for L, ranging from zero up to $L_{max}(d_{in}, z_c) = z_c + d_{in}^2/z_c$.

For the sake of simplicity, L will always refer to its maximum value.

In order to maximize the distance between mirrors it is necessary to optimize on z_c and d_{in}. Hence,

$$\begin{cases} \dfrac{\partial L}{\partial z_c} = 1 - \dfrac{d_{in}^2}{z_c^2} = 0 \quad \Rightarrow \quad z_c^2 = d_{in}^2 \quad \Rightarrow \quad z_c = \pm d_{in} \\ \dfrac{\partial L}{\partial d_{in}} = \dfrac{2d_{in}}{z_c} = 0 \quad \Rightarrow \quad d_{in} = 0 \end{cases}$$

The only critical point is therefore $z_c = d_{in} = 0$ which is obviously of no interest since we look forward to quantities that have positive non-zero values. Hence, it should be assumed that d_{in} is a controllable parameter and optimize for z_c.

In so doing we find that L is minimum at $z_c = d_{in}$, given that $\frac{d^2L}{dz_c^2} = \frac{2d_{in}^2}{z_c^3} = \frac{2}{z_{c_{crit}}} > 0$. The function $L(z_c)$ is represented in Fig. 5.2 for different values of d_{in}.

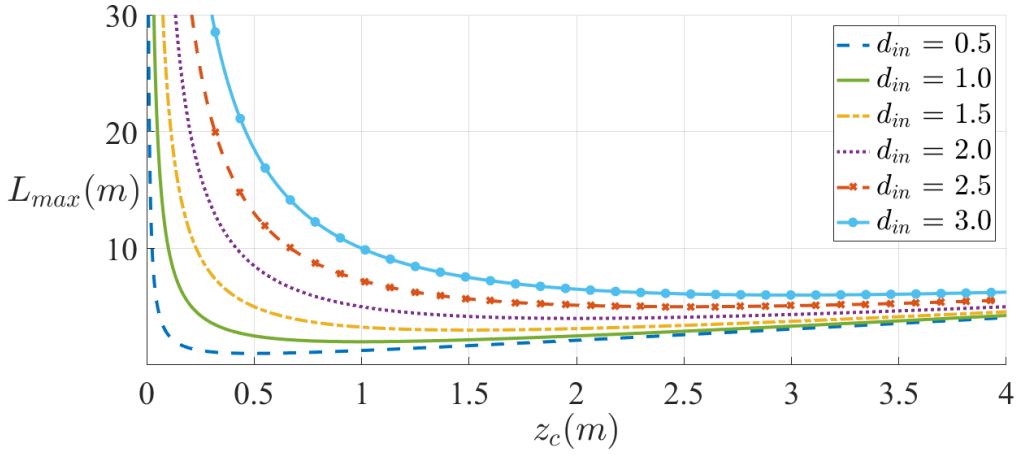

FIGURE 5.2: Distance between mirrors, L, for different values of d_{in}.

It is convenient to consider separately the regions below and above the minimum of L, $L_{min} = 2d_{in}$. For each of the regions an assumption can be made, which allows for a simplification of L. These regions correspond respectively to,

$$z_c \ll d_{in} \Rightarrow L \approx d_{in}^2/z_c \tag{5.5a}$$

and

$$z_c \gg d_{in} \Rightarrow L \approx z_c, \tag{5.5b}$$

which means that in the two regions the beam is propagating in the far and near-field, respectively. To avoid any possible ambiguity with near and far-field antennas, we shall call the above regions simply *region 1* and *2* or instead *small* and *big beam regions* because, as can be seen in Fig. 5.4, for a certain frequency of operation, the size of the beam waist radius is much smaller in region 1 than it is in 2.

Two conclusions are immediately obvious. For a smaller d_{in}, L reaches the two approximations more rapidly. On the other hand, however, for a fixed z_c, a smaller d_{in} enables a smaller distance L.

The equation $L = z_c + d_{in}^2/z_c$ can also be written as

$$z_c^2 - Lz_c + d_{in}^2 = 0 \tag{5.6}$$

and hence,

$$z_c = \frac{L \pm \sqrt{L^2 - 4d_{in}^2}}{2}, \tag{5.7}$$

(meaning that $L \gtrsim 2d_{in}$ as above). These solutions correspond to the above regions 1 and 2, respectively.

The input distance of $d_{in} = 1\,\mathrm{m}$ has been chosen for convenience while remaining a reasonable distance to implement the feed circuit. All the remaining analysis will be based on this value. The function will therefore assume the curve in Fig. 5.3:

5.2 Focal Length

We can also obtain the focal length of the reflectors from (5.2). Since f has a double solution when $L = z_c + d_{in}^2/z_c$, then,

$$f(z_c,\ d_{in},\ L) = \frac{Ld_{in} + d_{in}^2 + z_c^2}{L + 2d_{in}}. \tag{5.8}$$

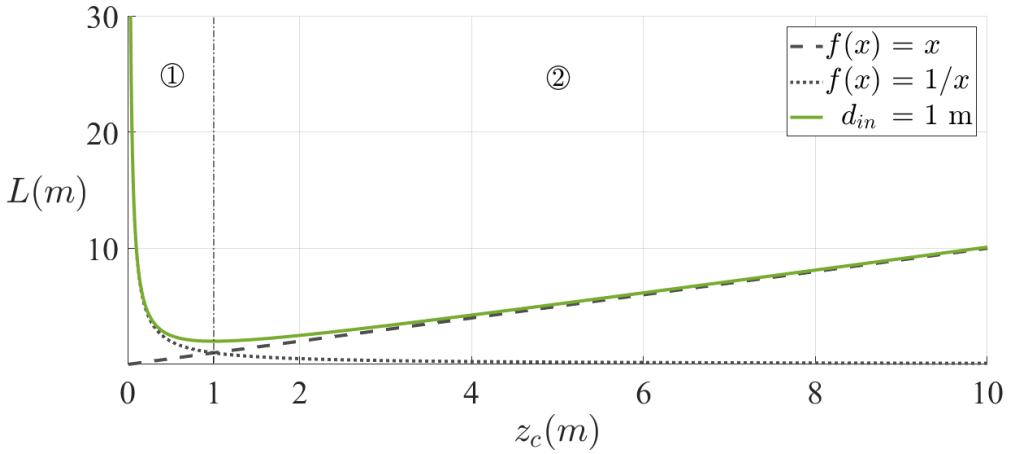

FIGURE 5.3: Distance between mirrors for $d_{in} = 1\,\text{m}$, where the approximations for each region are visible. In the regions well below and well above the minimum, for $z_c \lesssim 0.1\,\text{m}$ and $z_c \gtrsim 5\,\text{m}$, L can be approximated by d_{in}^2/z_c and z_c, respectively.

5.3 Beam in the Far-Field (Region 1, where $L \approx d_{in}^2/z_c$)

The assumption (5.5a) means that the beam propagates in the far-field region (region 1). The beam waist radius is, from (3.11),

$$\varpi_{0_S} = \sqrt{\frac{\lambda d_{in}^2}{\pi L}}, \tag{5.9}$$

where 's' stands for "small waist". In such a case,

$$\frac{\varpi_{0_S}}{\sqrt{\lambda}} = \frac{d_{in}}{\sqrt{\pi L}} = const, \tag{5.10}$$

which means that the ratio between the beam waist and the square root of the wavelength is a constant of the system. Therefore, if ν is the *frequency* and n is the *refraction index* of the propagation medium ($n \approx 1$ for air), then

$$\nu = \frac{c d_{in}^2}{\pi n L \varpi_{0_S}^2}. \tag{5.11}$$

This means that the choice of the components' size will be balanced with the frequency of operation.

In region 1, the focal length is

$$f_S = \frac{L^3 d_{in} + L^2 d_{in}^2 + d_{in}^4}{L^3 + 2L^2 d_{in}}. \tag{5.12}$$

5.4 Beam in the Near-Field (Region 2, where $L \approx z_c$)

It is apparent from Fig. 5.3 that the near-field is a good approximation for $z_c \gtrsim 5\,\mathrm{m}$.

In this case the beam waist radius from (3.11) is

$$\varpi_{0_B} = \sqrt{\frac{\lambda L}{\pi}}, \tag{5.13}$$

where the subscript 'B' means "big waist". This also means that,

$$\frac{\varpi_{0_B}}{\sqrt{\lambda}} = \sqrt{\frac{L}{\pi}} = const, \qquad \nu = \frac{Lc}{\pi n \varpi_{0_B}^2}.$$

Moreover, the focal length is,

$$f_B = \frac{L^2 + L d_{in} + d_{in}^2}{L + 2 d_{in}}. \tag{5.14}$$

5.5 Paraxial Limit

The paraxial approximation sets a limit for both of these regions. From (3.12),

$$\frac{z_c}{\varpi_0} > 0.9\pi, \tag{5.15}$$

and hence, considering the conditions in (5.5), the paraxial limits for the regions 1 and 2 are, respectively,

$$\frac{\varpi_{0_S} L}{d_{in}^2} < \frac{1}{0.9\pi}, \tag{5.16a}$$

and

$$\frac{\varpi_{0_B}}{L} < \frac{1}{0.9\pi}. \tag{5.16b}$$

These limits should be respected when designing the system in the paraxial approximation.

5.6 Beam Radius at the Reflector

The beam radius at the position of the reflector, ϖ_R, having travelled d_{in}, is

$$\varpi_R = \varpi_0 \sqrt{1 + \left(\frac{d_{in}}{z_c}\right)^2}. \tag{5.17}$$

This means that for the regions considered, we arrive at the same value,

$$\varpi_{R_S} = \varpi_{R_B} = \sqrt{\frac{\lambda}{\pi}\frac{(L^2 + d_{in}^2)}{L}}. \tag{5.18}$$

5.7 Relation Between Focal Lengths

The quotient between (5.12) and (5.14) gives

$$\frac{f_S}{f_B} = \frac{L^3 d_{in} + L^2 d_{in}^2 + d_{in}^4}{L^4 + L^3 d_{in} + L^2 d_{in}^2} \tag{5.19}$$

which is < 1 for $d_{in} < L$, which will always be the case. We then have

$$f_S < f_B. \tag{5.20}$$

5.8 Comparison Between Beams in the Near and Far-Field

In order to best understand the differences between both beam types Fig. 5.4 shows the two different possible scenarios.

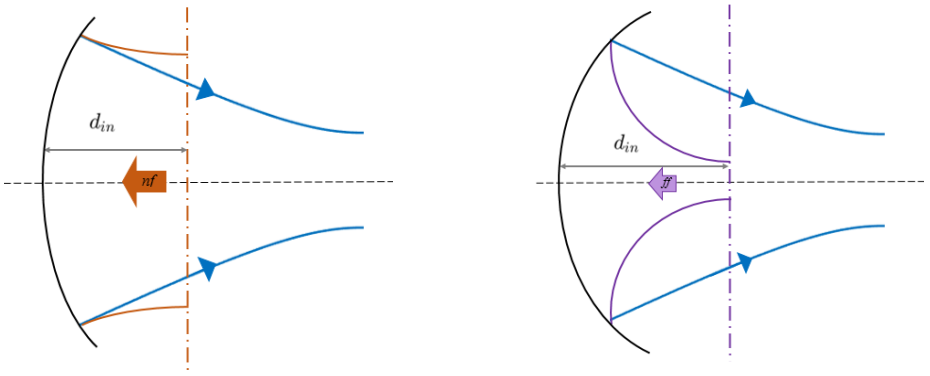

(a) (b)

FIGURE 5.4: Comparison between beams in the near and far-field: (a) beam in the far-field (*small*) (b) beam in the near-field (*Big*)

It is worth pointing out that the focal length representation is according to the result in the previous section.

5.9 Parabolic Reflector

The dimensions of a parabolic reflector are related as

$$4fD = R_R^2, \tag{5.21}$$

where R_R is the Reflector's Radius, D its Depth and f is the focal length.

The size of R_R must necessarily take ϖ_R into account, for obvious reasons. By defining the *reflector's coefficient* (c_R) as

$$R_R = c_R \varpi_R \quad \Rightarrow \quad \frac{R_R}{\sqrt{\lambda}} = c_R \sqrt{\frac{(L^2 + d_{in}^2)}{\pi L}} \tag{5.22}$$

and by substituting (5.18) one arrives at

$$D = \frac{c_R^2 \varpi_R^2}{4f} \quad \Rightarrow \quad \frac{D}{\lambda} = \frac{c_R^2}{4\pi f} \left(\frac{L^2 + d_{in}^2}{L} \right). \tag{5.23}$$

The coefficient c_R should be as large as possible, though a value of $\sqrt{2}$ is enough from a practical point of view (Fig. 3.1).

It is worth noting that due to (5.20), $D_S > D_B$. A beam in the far-field demands a larger reflector depth.

5.10 Elliptic Reflector

What if we want to use elliptic mirrors? While at first they may not seem very useful for our study that is not the case.

Ellipses are defined by two foci, F_1 and F_2, and if the beam originates at the first focus, the reflecting surface (centred at a point P) will direct the output beam waist to the second focus of the ellipse, as can be seen in Fig. 5.5, disabling the possibility of a reciprocal system.

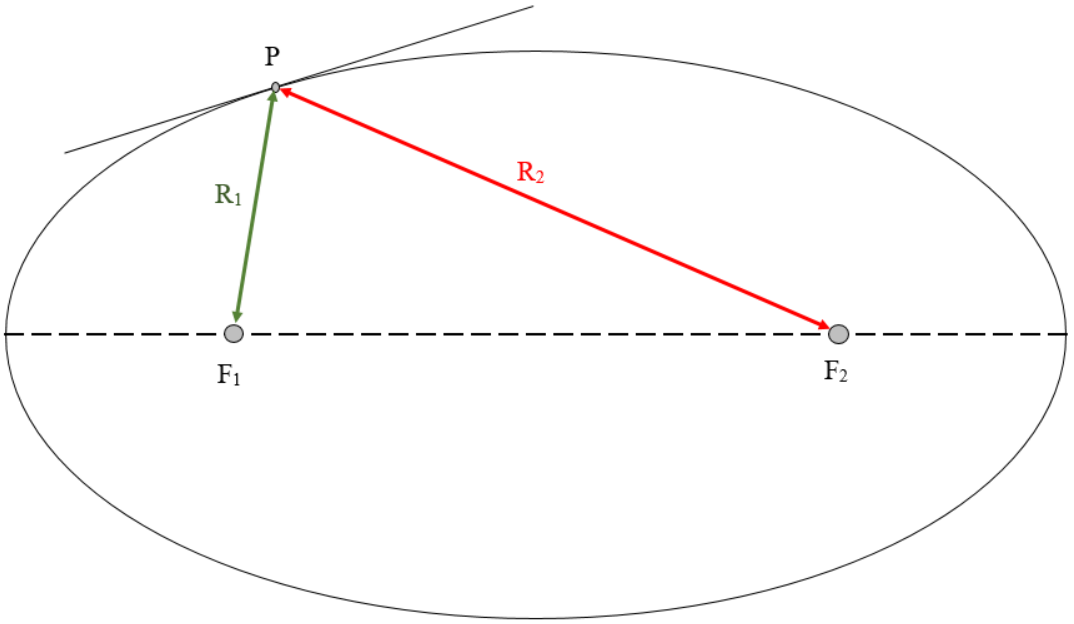

FIGURE 5.5: General ellipse representation with its main parameters. P is any point in the surface distanced away from the foci, F_1 and F_2, by $R_1 = \overline{F_1P}$ and $R_2 = \overline{F_2P}$.

The focal length of the elliptic reflecting surface centred in P is given by

$$f_e = \frac{R_1 R_2}{R_1 + R_2} \tag{5.24}$$

where $R_1 = \overline{F_1P}$ and $R_1 = \overline{F_2P}$.

To obtain the optimal performance of an elliptical focusing surface [2], we need to set the system in a way that the input beam has a value of radius of curvature such that $R_{in} = R_1$ and, similarly, the radius of curvature of the output beam $R_{out} = R_2$.

Although the use of elliptical reflectors made from surfaces of the same ellipse is not advantageous, we can use the surface from two equal ellipses which share one focal point (Fig. 5.6), thus arriving at a situation where the reciprocal principle is again obtainable.

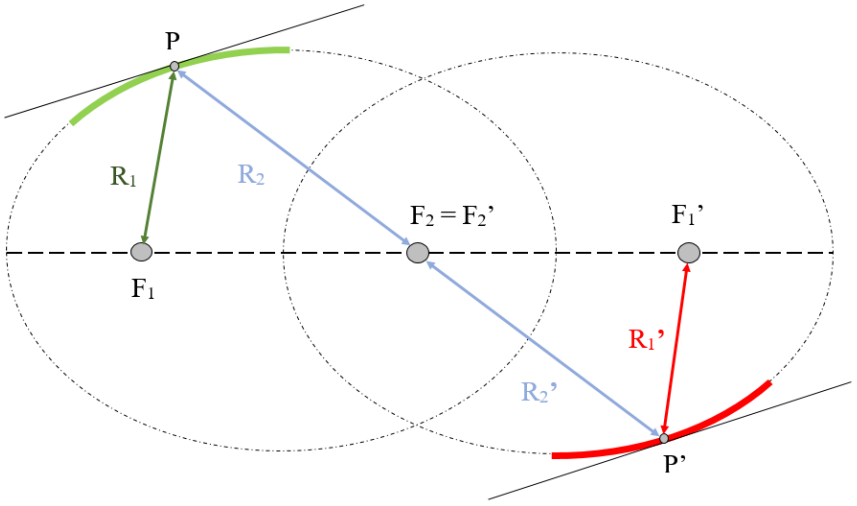

FIGURE 5.6: Double ellipse system. The second ellipse parameters are denoted by an inverted comma. The ellipses share one focus point, $F_2 = F_2'$, and, to respect reciprocity, $R_1 = R_1'$ and $R_2 = R_2'$.

Gaussian beams in that system are represented in Fig. 5.7. It is worth noting that, to satisfy the optimal condition for elliptical reflector, the requirement is not for the input beam waist to be located in the focus point, F_1, but for the input beam to have a value of radius of curvature at the reflector of $R_{in} = R_1$.

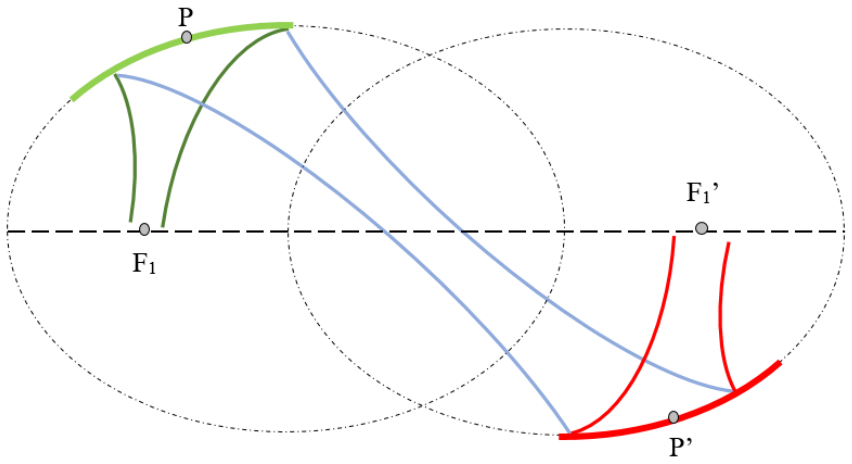

FIGURE 5.7: Schematic representation of a double ellipsoidal reflector quasi-optical system. The distance between mirrors is simply $L = \overline{PP'}$. To obtain the optimal condition the input and output beam waist must be located at a point which makes $R_{in} = R_1 = \overline{F_1 P}$ and $R_{out} = R_1' = \overline{F_1' P'}$.

5.11 Ellipsoidal Focal Length Validity

We will verify if the focal length of an ellipsoidal surface is equivalent to that of a general quasi-optical component.

As stated before, the focal length of an ellipsoidal reflector in the optimal quasi-optical condition is given by $f_e = (R_{in}R_{out})/(R_{in} + R_{out})$. From (3.7), we have that

$$R_{in} = d_{in} + \frac{(\pi\varpi_{0_{in}}^2/\lambda)^2}{d_{in}} \qquad \text{and} \qquad R_{out} = d_{out} + \frac{(\pi\varpi_{0_{out}}^2/\lambda)^2}{d_{out}}. \tag{5.25}$$

Now, since the ray transfer matrix of a reflector is generally given by $A = 1,\ B = 0,\ C = -1/f$ and $D = 1$, by replacing its values in (3.24) and (3.25), we get

$$\varpi_{0_{out}} = \frac{\frac{z_c^2 + d_{in}^2}{f} - d_{in}}{x} \tag{5.26}$$

and

$$\varpi_{0_{out}} = \frac{\varpi_{0_{in}}}{\sqrt{x}}, \tag{5.27}$$

where $x = (f^2 - 2fd_{in} + d_{in}^2 + z_c^2)/f^2$.

The elliptical focal length becomes

$$\frac{\left(d_{in} + \frac{z_c^2}{d_{din}}\right)\left(d_{out} + \frac{z_c^2}{d_{dout}}\right)}{d_{in} + \frac{z_c^2}{d_{din}} + d_{out} + \frac{z_c^2}{d_{dout}}} = \ldots = \frac{1}{\frac{d_{out}}{z_{c_{out}}^2 + d_{out}^2} + \frac{d_{in}}{z_{c_{in}}^2 + d_{in}^2}}. \tag{5.28}$$

At this point we can use (5.26) and (5.27) to arrive at the final form,

$$f_e = f. \tag{5.29}$$

We have proven that the focal length is indeed valid.

5.12 Theory Restraints

For the value of the distance between reflectors, L, we have two different equations[1]. One arises immediately from the quasi-optical formalism as $L_1 = 2d_{out}$, where d_{out} is given by (3.24). The other (L_2) is calculated from (5.8). The starting point is that these should be the same:

$$L_1 = 2f\frac{z_c^2 + d_{in}^2 - fd_{in}}{f^2 - 2fd_{in} + z_c^2 + d_{in}^2} = \frac{z_c^2 + d_{in}^2 - 2fd_{in}}{f - d_{in}} = L_2. \tag{5.30}$$

[1]The subscripts 1 and 2 will be used to differentiate them.

After working on the terms as a function of f, we arrive at

$$f^2(d_{in}^2 - z_c^2) - 2fd_{in}(z_c^2 + d_{in}^2) + (z_c^2 + d_{in}^2)^2 = 0, \tag{5.31}$$

which has the solution,

$$f = \frac{z_c^2 + d_{in}^2}{d_{in} \mp z_c}. \tag{5.32}$$

By replacing (5.32) in L_1 and L_2 we arrive at exactly the same solution, $L_1 = L_2 = \mp\left(z_c + \frac{d_{in}^2}{z_c}\right)$. Since $L > 0$, the solution of interest is,

$$f = \frac{z_c^2 + d_{in}^2}{z_c + d_{in}}. \tag{5.33}$$

5.13 d_{in} that Maximizes L_1

In the case that $f \neq (z_c^2 + d_{in}^2)(z_c + d_{in})$, we must use $L_1 = 2d_{out} = L$ as the distance between reflectors:

$$L = 2f\frac{z_c^2 + d_{in}^2 - fd_{in}}{f^2 - 2fd_{in} + z_c^2 + d_{in}^2}. \tag{5.34}$$

The distance d_{in} which maximizes L is obtained by optimising (5.34) as a function of d_{in},

$$\frac{\partial L}{\partial d_{in}} = \frac{-2f^2(f^2 - 2fd_{in} - z_c^2 + d_{in}^2)}{(f^2 - 2fd_{in} + z_c^2 + d_{in}^2)^2} = 0 \quad \Rightarrow \quad d_{in} = f \pm z_c.$$

Knowing that $\frac{\partial^2 L}{\partial {d_{in}}^2} = \mp\frac{f^2}{z_c^3}$, L is maximum when,

$$d_{in} = f + z_c. \tag{5.35}$$

5.14 Summary

Quasi-optical systems made up of two equal components, positioned in such a way that the reciprocity principle is respected, can be explained by two simple equations, (5.4) and (5.33), reproduced here:

$$f = \frac{z_c^2 + d_{in}^2}{z_c + d_{in}} \qquad \text{and} \qquad L = z_c + \frac{d_{in}^2}{z_c}.$$

The suggested system building procedure is as follows.

In most applications, L is normally the first variable to be defined. When that is the case, f and ϖ_0 must be adjusted to best fit the parameter requirements. As will be seen in the following chapters, ϖ_0 depends heavily on the feed antenna characteristics, normally

being the second parameter to be settled. Then, it is only a matter of calculating f and d_{in} (from (5.4), $d_{in} = \sqrt{z_c(L - z_c)}$) to obtain all of the parameter values.

For this study we used two parabolic reflectors and two antennas. The latter will be explained in the following chapter.

Chapter 6

Antennas

As is explained in [39], antennas are defined as "a means for radiating or receiving radio waves" by the *IEEE Standard Definitions of Terms for Antennas*. In the following section, a general introduction to antennas is presented based on [39].

6.1 Fundamental Parameters

There are many types of antennas assuming very different shapes so in order to compare their performance engineers have several common parameters that describe the antenna radiating characteristics.

6.1.1 Radiation Pattern

One of the most important parameters is the radiation pattern. It allows for an immediate visualization of the radiating characteristics of an antenna, as "a mathematical function or a graphical representation of the radiation properties of the antenna as a function of space coordinates" [39]. When analysed in the far field, it is a function of directional coordinates.

The radiation pattern can be studied in terms of electric or magnetic field (amplitude *field pattern*) or of the power density (amplitude *power pattern*), both of which can be normalised to their maximum value. In that case, we arrive at the *normalized field and power patterns*.

Quite usually, the radiation patterns are best represented in a logarithmic scale, in units of decibels (dB), because the finer details can be better observed that way.

The radiation pattern is separated into regions delimited by values of relatively weak radiation intensity. The region containing the direction of maximum radiation is called

the *major lobe*. The rest are all called *minor lobes*, which represent radiation in undesired directions. If a radiation lobe has the opposite direction of the major lobe ($\sim 180°$) it is called a *back lobe*, otherwise they are simply referred to as *side lobes*.

antennas are defined differently according to their radiation pattern directional characteristics:

Isotropic Ideal lossless antennas which equally radiate in all directions. They are impossible to achieve but used as a reference for real antennas;

Directional Antennas which are more effective in certain directions than in others. Generally used for antennas whose maximum directivity[1] is significantly greater than that of a half-wave dipole.

Omnidirectional Special type of directional antennas that are non directional (equally radiating) in a certain plane, but not in the remaining orthogonal planes.

6.1.2 Radiation Power Density

Electromagnetic radiation contains energy in the fields that compose it ($\mathcal{E}$ and $\mathcal{H}$. In order to arrive at the power in an electromagnetic wave, it is useful to introduce the power density (energy per unit time per unit area) vector, named *Poynting Vector* ($\mathrm{W/m^2}$):

$$\vec{\mathcal{S}} = \vec{\mathcal{E}} \times \vec{\mathcal{H}} \tag{6.1}$$

These are for time-dependant fields. The calculus will then allow us to know the instantaneous power density.

The total instantaneous power will then be

$$\vec{\mathcal{P}} = \oiint_S \vec{\mathcal{S}} \cdot \hat{\mathbf{n}}\, da \tag{6.2}$$

Once again it is possible to define the fields for a time variation of the form $\exp(i\omega t)$. In that case

$$\vec{\mathcal{E}}(x,y,z,t) = \mathrm{Re}[\vec{E}(x,y,z)e^{i\omega t}], \tag{6.3}$$

$$\vec{\mathcal{H}}(x,y,z,t) = \mathrm{Re}[\vec{H}(x,y,z)e^{i\omega t}]. \tag{6.4}$$

Knowing that the average value of these quantities is obtained by integrating them over one period and dividing by it, we arrive at

$$\vec{S}_{average}(x,y,z) = [\vec{\mathcal{S}}(x,y,z,t)]_{average} = \frac{1}{2}\,\mathrm{Re}[\vec{E} \times \vec{H}^*]. \tag{6.5}$$

[1] The directivity parameter is explained below.

It is common to name *radiation density* (S_{rad}) to the power density when analysed in the far-field. The 1/2 factor is to be omitted for RMS values.

The Average Power Radiated by an antenna is then

$$P_{rad} = \frac{1}{2} \oiint_S \mathrm{Re}[\vec{E} \times \vec{H}^*] \cdot \ d\vec{s} \tag{6.6}$$

6.1.3 Radiation Intensity

It is possible to analyse the power radiated from an antenna in a certain direction, per unit solid angle. Then we refer to the *Radiation Intensity* In the far

$$U = r^2 S_{rad} \tag{6.7}$$

We can then relate the radiation intensity with the far-field electric of the antenna as

$$U(\theta, \phi) = \frac{r^2}{2\eta} |\vec{E}(r, \theta, \phi)|^2 \simeq \frac{r^2}{2\eta} \left[|\mathring{E_\theta}(\theta, \phi)|^2 + |\mathring{E_\phi}(\theta, \phi)|^2 \right] \tag{6.8}$$

One can then arrive at the total power radiated by integrating over the entire solid angle (4π)

$$P_{rad} = \oiint_\Omega U \ d\Omega = \int_0^{2\pi} \int_0^{\pi} U \sin\theta \ d\theta \ d\phi \tag{6.9}$$

6.1.4 Beamwidth

The major lobe contains the radiation pattern maximum, oriented in a certain direction. The beamwidth is defined in terms of angular separation between two points of a plane containing that direction, with the same amplitude, on opposite sides of the pattern maximum. A multitude of beamwidths can be defined but generally it is assumed that beamwidth refers to the *Half-Power Beamwidth* (HPBW). Another useful beamwidth is the *First-Null Beamwidth* (FNBW).

There are two main advantages to the definition of the beamwidth. On one hand as a figure of merit since it is inversely related to the side lobes (as one increases, the other decreases). On the other hand as an antenna resolution "analyser" because an antenna is capable of distinguishing between sources if they are at least separated by angular distances of FNBW/2 $\approx$ HPBW.

6.1.5 Directivity

The directivity of an antenna is "the ratio of the radiation intensity in a given direction from the antenna to the radiation intensity averaged over all directions" (which is the total power radiated by the antenna divided by 4π). It is therefore dependent on the radiation pattern.

$$D = \frac{4\pi U}{P_{rad}} \tag{6.10}$$

If the direction is not specified, the direction of maximum intensity is used and we talk about the *maximum directivity* (D_{max}).

6.1.6 Antenna Efficiency

The total antenna efficiency (ϵ_0) relates the power introduced in the input terminals with the power of the output terminal (the radiated wave), accounting for the different losses:

- ϵ_r – reflections (due to mismatch) between the transmission line and the antenna;
- ϵ_c – conduction;
- ϵ_d – dielectric.

In general:

$$\epsilon_0 = \epsilon_r \epsilon_c \epsilon_d \tag{6.11}$$

where $\epsilon_r = (1 - |\Gamma|^2)$, $\Gamma = (Z_{in} - Z_0)/(Z_{in} + Z_0)$ is the voltage reflection coefficient at the input terminals of the antenna, Z_{in} is the antenna input impedance and Z_0 the characteristic impedance of the transmission line. A common engineering concept based on Γ is the voltage standing wave ratio, $VSWR = (1 + |\Gamma|)/(1 - |\Gamma|)$.

It is usually difficult to compute ϵ_c and ϵ_d although they are measurable. However, even by measurements, they are not separable, hence the definition of the antenna radiation efficiency ($\epsilon_{cd} = \epsilon_c \epsilon_d$), where the overall antenna efficiency can be written as:

$$\epsilon_0 = \epsilon_{cd}(1 - |\Gamma|^2) \tag{6.12}$$

6.1.7 Gain

The gain of an antenna is somewhat similar to the directivity while also taking into account the antenna efficiency. "It is a ratio of the intensity in a certain direction, to the radiation intensity that would be obtained if the power accepted" were radiated isotropically.

$$G = \frac{4\pi U}{P_{in}} \tag{6.13}$$

Again, the direction of maximum radiation is taken by default.

We can relate the gain with the directivity as

$$G = \epsilon_{cd} D \tag{6.14}$$

6.2 Gaussian Coupling Efficiency

The *Gaussian Coupling Efficiency* or *gaussicity* (η_G) translates the amount of power from an antenna which is coupled to the fundamental gaussian beam (with a certain ϖ_0 and z_0) [40]. When designing an antenna as a function of ϖ_0, it is important to maximize η_G.

In [2] some antenna types have their η_G discriminated as well as the correspondent ϖ_0 and z_0. However, for different types of antenna one can still arrive at the Gaussian Coupling Efficiency by an algorithm explained in [40], by using the antenna's far field data. This is especially relevant when considering the sub-efficiencies which amount to η_G.

The gaussian coupling efficiency can also be calculated from the near field [2, 40],

$$\eta_G = \frac{\iint |E_A \cdot E_G^*|^2 \, dx \, dy}{\left[\iint |E_A|^2 dx \, dy\right] \left[\iint |E_G|^2 dx \, dy\right]} \tag{6.15}$$

6.3 Smooth Surface Conical Horn Antenna

After studying [2], the smooth surfaced conical horn antenna strikes as balancing a relative ease of manufacturing with a high gaussicity and that is the reason why they were the chosen antenna type. A schematic of the antenna is shown in Fig. 6.1.

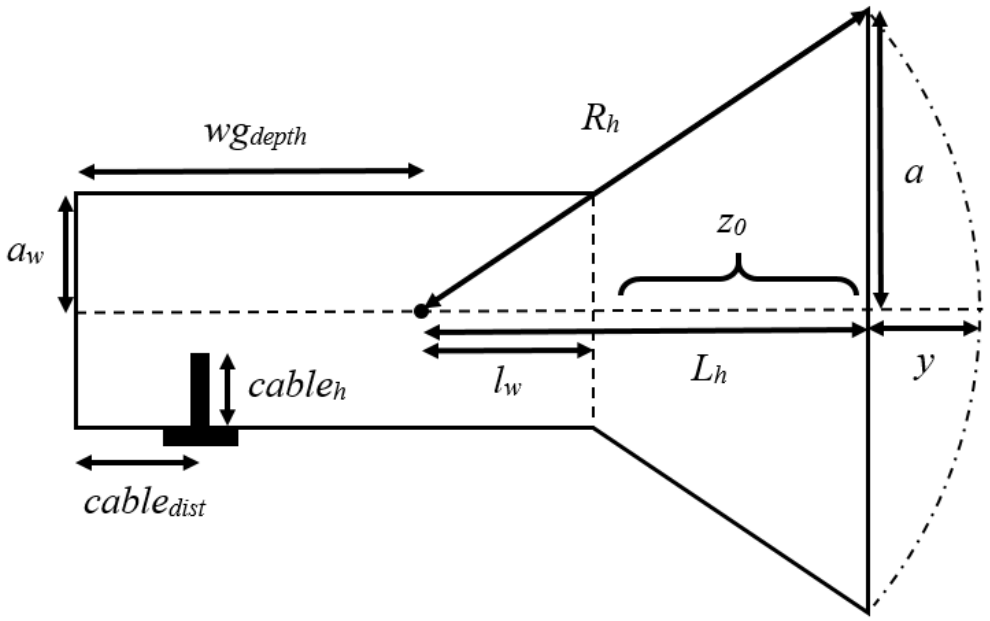

FIGURE 6.1: Conical horn antenna schematic where a is the aperture radius, a_w is the waveguide radius, L_h is the length between the aperture and the centre of curvature and R_h is the horn slant length.

In Tab. 6.1 the main horn antenna parameters are explained.

TABLE 6.1: Conical horn antennas parameters.

Symbol	Terminology
a	Aperture Radius
a_w	Waveguide Radius
R_h	Slant Length
L_h	Horn Length[2]
l_w	Horn Length in Waveguide
$cable_{dist}$	Distance to the Connector[3]
z_0	Beam Waist Location
y	Beam Offset

6.3.1 Conical Horn Gaussicity

The optimum gaussian coupling efficiency for the smooth surfaced conical horn type is $\eta_G = 0.91$, where the beam radius at the aperture has the form

$$\varpi = c_g a. \tag{6.16}$$

c_g was called the *gaussian coefficient*, useful for connecting the gaussian beam radius with the aperture radius. For smooth surfaced conical horn antennas $c_g = 0.76$. The beam waist and its location are respectively given, for any conical horn, by

$$\varpi_0 = \frac{\varpi}{\sqrt{1 + \left(\frac{\pi\varpi^2}{\lambda R}\right)^2}}, \tag{6.17}$$

$$z_0' = \frac{R}{1 + \left(\frac{\lambda R}{\pi\varpi^2}\right)^2}. \tag{6.18}$$

An important note regarding the beam waist location must now be made. From (6.18) we obtain the distance to the beam waist *from the wave front*, not from the antenna aperture. For that we need to subtract y:

$$z_0 = z_0' - y. \tag{6.19}$$

y is the difference between the slant length and the horn length $y = R_h - L_h$. By replacing it in the equation above we arrive at

$$z_0 = \frac{L_h + \left(\frac{\lambda R_h}{\pi\varpi^2}\right)^2 (L_h - R_h)}{1 + \left(\frac{\lambda R_h}{\pi\varpi^2}\right)^2} \tag{6.20}$$

6.3.2 Design Procedure

All the antenna parameters influence the radiation output. A very clear design procedure can be found in [41].

The directivity of conical horn antennas can be related with its directivity,

$$D(\text{dB}) = 10\log\left[\varepsilon_{ap}\frac{4\pi}{\lambda^2}(\pi a^2)\right] = 10\log\left(\frac{C}{\lambda}\right)^2 - L_{fig}(s) \tag{6.21}$$

where ε_{ap} is the *aperture efficiency*, the ratio of maximum *effective area*[4], $A_e = P_T/W_i$, to the physical area. C is the aperture circumference $C = 2a\pi$ and L_{fig} is the *loss figure*,

$$L_{fig}(s) = -10\log\varepsilon_{ap} \;\simeq\; (0.8 - 1.87s + 26.25s^2 - 17.79s^3)(\text{dB}). \tag{6.22}$$

s is the maximum phase deviation (in number of wavelengths), $s = \frac{a}{2\lambda R_h}$. Knowing that the aperture diameter ($2a$) for optimal gain is $2a \cong \sqrt{3R_h\lambda}$, then $s = \frac{3}{8}$ leading to $L_{fig}(\frac{3}{8}) \cong 2.9\,\text{dB}$.

[4]Ratio of the available power at the terminals of a receiving antenna to the power flux density of a plane wave incident on the antenna from that direction" [39]

The recommended steps are as follows:

1. Calculate $C = \lambda\sqrt{10^{\frac{D_C + L_{fig}(s)}{10}}}$ (from (6.21));
2. This allows us to obtain the aperture radius, $a = \frac{C}{2\pi}$,
3. and from it determine the slant length, $R_h = \frac{4a^2}{3\lambda}$;
4. Finally, through the Pythagoras Theorem, we get the horn length, $L_h = \sqrt{R_h^2 - a^2}$.

There is a condition arising from point 4, the Pythagoras Theorem: since L must have a positive value, $R_h^2 > a^2 \Leftrightarrow \frac{a}{\lambda} > \frac{3}{4}$.

We can then obtain $l_w = \frac{a_w L_h}{2a}$ from triangle similarity.

6.3.2.1 Gaussian Beam Parameters as a Function of Directivity

From (6.17) and (6.18)[5] and the equations presented in the previous section we can relate the directivity of an antenna with the gaussian beam it produces, by substituting ϖ for (6.16), $R_h = \frac{4a^2}{3\lambda}$ and $a = \frac{C}{2\pi}$:

$$\varpi_0 = \frac{c_g \lambda}{2\pi}\sqrt{\frac{10^{\frac{D_C + L_{fig}(s)}{10}}}{1 + \frac{9}{16}\pi^2 c_g^4}}, \tag{6.23}$$

$$z_0' = \lambda\frac{10^{\frac{D_C + L_{fig}(s)}{10}}}{3\pi^2 + \frac{1}{\frac{3}{16}c_g^4}}. \tag{6.24}$$

6.3.2.2 Gaussian Beam Parameters as a Function of Antenna Parameters

Alternatively we can have ϖ_0 and z_0' as a function of the remaining antenna parameters:

$$\varpi_0 = \frac{c_g a}{\sqrt{1 + \frac{\pi^2 c_g^4 a^4}{\lambda^2}}}, \tag{6.25}$$

$$z_0' = \frac{R_h}{1 + \frac{1}{\frac{9}{16}\pi^2 c_g^4}}. \tag{6.26}$$

[5] All the beam waist location presented in the following sections will be z_0', related with z_0 by (6.19).

6.3.2.3 Circular Antenna Parameters as a Function of the Gaussian Beam

Sometimes it can be useful to know how to produce a certain gaussian beam from a conical horn. The analysis is then reversed and from ϖ_0 we obtain the remaining parameters.

For a certain beam, the directivity is

$$D_C = 10\log\left[\left(\frac{2\varpi_0\pi}{c_g\lambda}\right)^2\left(1+\frac{9}{16}\pi^2c_g^4\right)\right] - 2.91, \tag{6.27}$$

and the antenna must have

$$a = \frac{4\varpi_0}{c_g}\sqrt{1+\frac{9}{16}\pi^2c_g^4}, \tag{6.28}$$

$$R_h = \frac{4\varpi_0^2}{3\lambda c_g^2}\left(1+\frac{9}{16}\pi^2c_g^4\right), \tag{6.29}$$

and finally

$$L_h = \frac{\varpi_0}{c_g}\sqrt{\frac{19\,\varpi_0^2}{9\lambda^2c_g^2}\left(1+\frac{9}{16}\pi^2c_g^4\right)^2 - \left(1+\frac{9}{16}\pi^2c_g^4\right)}. \tag{6.30}$$

6.4 Proposed Antenna

In order to best achieve a gaussian beam with a horn antenna while respecting the paraxial limit (3.12) at the operating frequency of 5.8 GHz, an Excel workbook was created. It allowed for the settling of a conical horn antenna with the parameters declared in Tab. 6.2.

TABLE 6.2: Designed conical horn antenna parameters.

Symbol	Value (cm)
a	10.893
R_h	30.587
L_h	28.582
l_w	5.224

The remaining parameters will be explained further down.

The antenna's directivity is $D = 19.52\,\text{dB}$ and its output radiation is expected to approximate a gaussian beam with $\varpi_0 = 4.902\,\text{cm}$ and $z_0 = 8.719\,\text{cm}$.

6.4.1 Waveguide

In order to feed the antenna a waveguide which allows the propagation of the TE_{11} is necessary for the best gaussian coupling efficiency. The waveguide is also circular. In that case the *cut-off frequency* is,

$$\nu_c = \frac{1.841\, c}{2\,\pi\, a_w\, \sqrt{\epsilon_r}}, \tag{6.31}$$

The chosen waveguide has a radius of $a_w = 2\,\text{cm}$, designed for a cut-off frequency of 4.395 GHz.

6.4.2 SMA Connector

To excite the waveguide and consequently the antenna, a SMA connector was used to plug in a cable to the signal generator. The most appropriate was Farnell's 1052522-1 SMA connector (Fig. 6.2). The gold finish was chosen for it allows a better soldering grip.

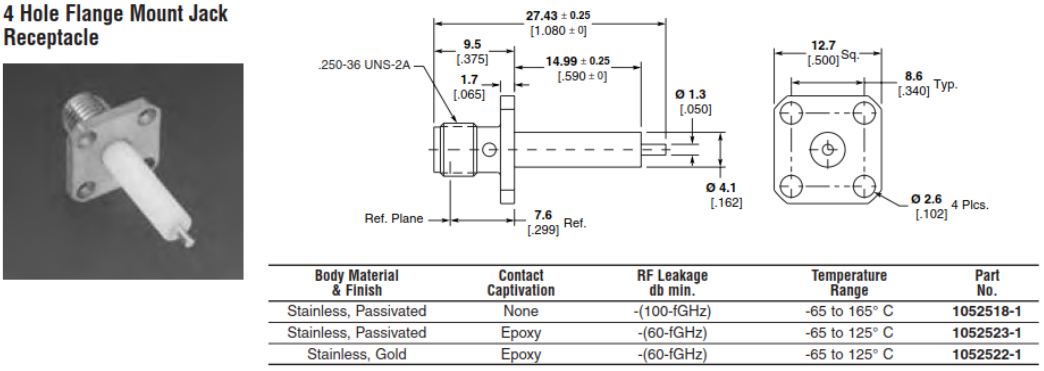

Body Material & Finish	Contact Captivation	RF Leakage db min.	Temperature Range	Part No.
Stainless, Passivated	None	-(100-fGHz)	-65 to 165° C	**1052518-1**
Stainless, Passivated	Epoxy	-(60-fGHz)	-65 to 125° C	**1052523-1**
Stainless, Gold	Epoxy	-(60-fGHz)	-65 to 125° C	**1052522-1**

FIGURE 6.2: SMA Connector used.

6.5 CST Simulation

This antenna was designed in *CST Studio Suite* for simulation of the antennas characteristics (for a frequency interval of [5.0 - 6.6] GHz). Since the ultimate goal was to 3D print the antenna, several layers were included in the simulation to obtain the most realistic results. Two different antenna layers were drawn, the PLA (Polylactic acid, a common 3D printing filament) and the conducting layer (copper), as can be observed in Fig. 6.3. The PLA has a thickness of 1 mm.

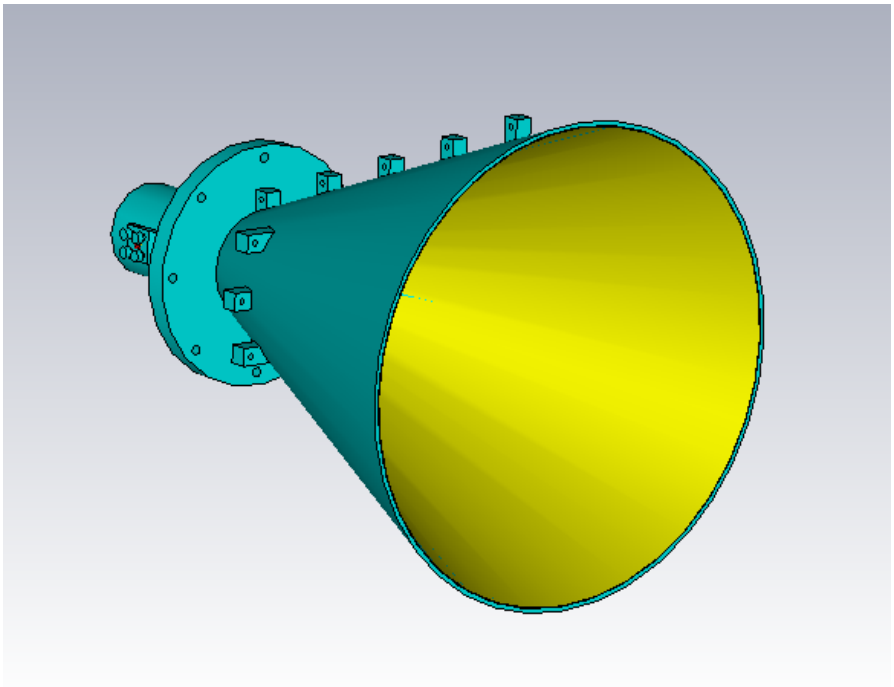

FIGURE 6.3: Horn antenna designed in CST. The blue and yellow layers are respectively PLA and copper.

The SMA connector were included as well as the screws and nuts used to hold the connector to the antenna (Fig. 6.4).

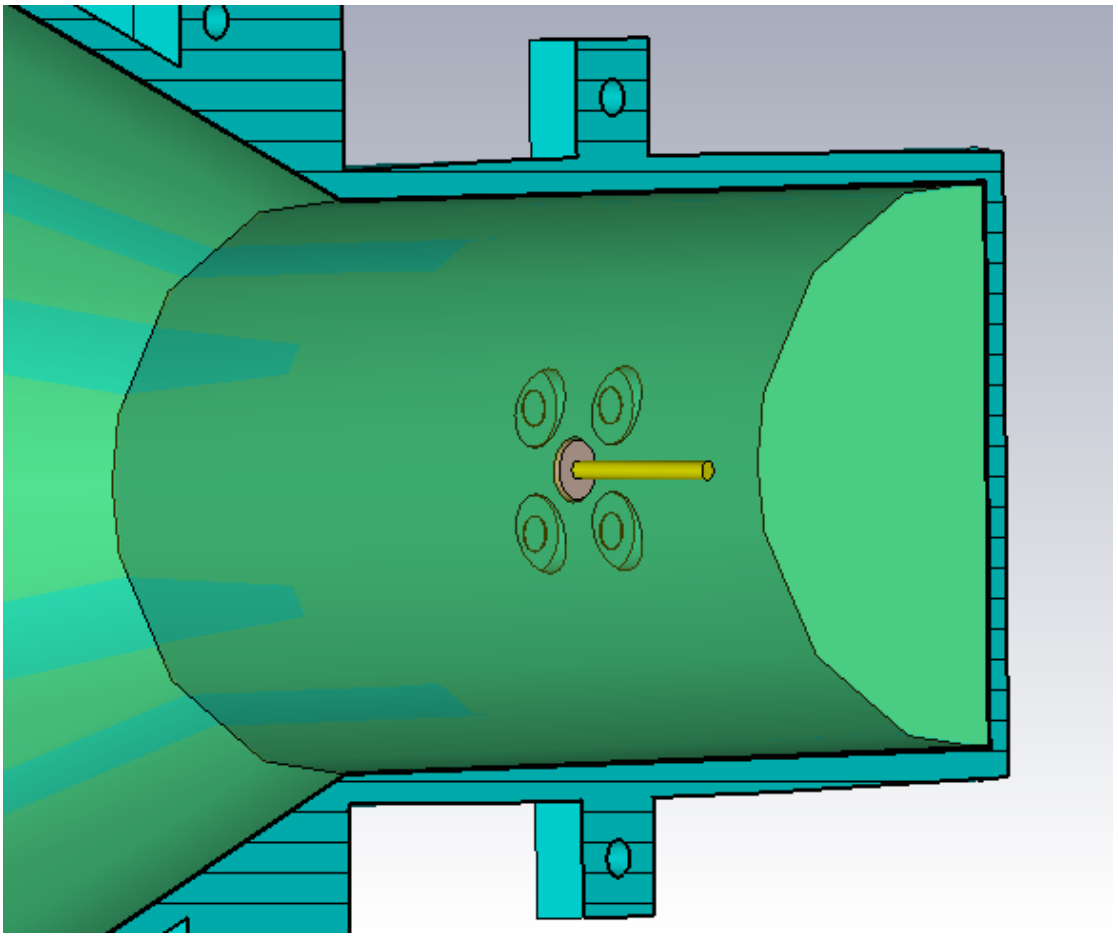

FIGURE 6.4: Detail of the SMA connector on the horn antenna.

The port of excitation was the SMA connector.

6.5.1 Simulation Results

Before saving the results, an optimization was performed for the different parameters. The results presented are the final ones obtained. The parameters changed were the waveguide radius, a_w, the waveguide depth, wg_{depth}, the connector distance from the waveguide basis, $cable_{dist}$, and the connector height, $cable_h$.

TABLE 6.3: Designed SMA connector parameters.

Symbol	Value (cm)
a_w	1.991
wg_{depth}	2.200
$cable_{dist}$	2.278
$cable_h$	1.123

6.5.1.1 Port Modes

The first obtainable result are the port modes. At the SMA connector we have,

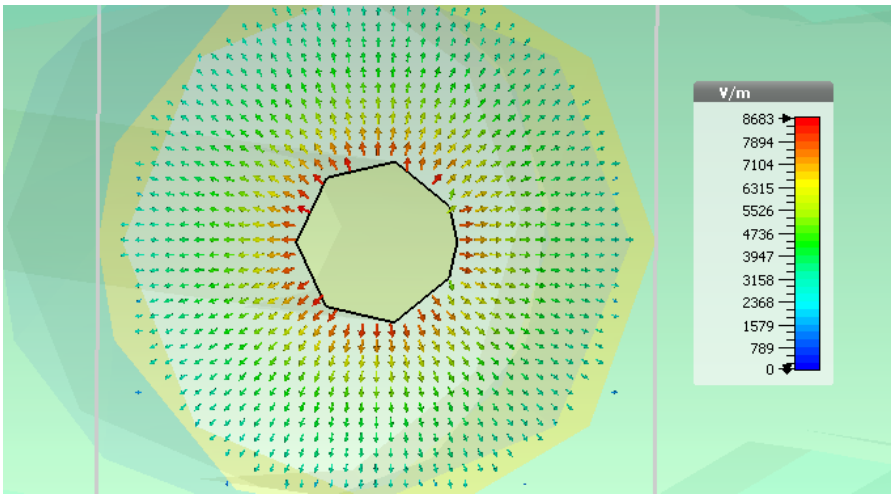

FIGURE 6.5: Port modes at the SMA connector.

6.5.1.2 S_{11} Parameter

The S_{11} parameter is a measure of how much energy is returning to the port of excitation, hence the smaller the better.

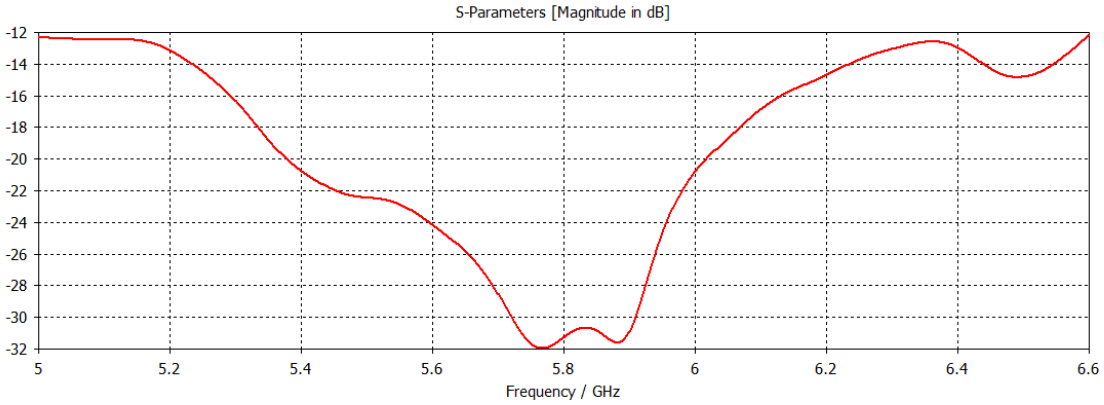

FIGURE 6.6: S_{11} Parameter of the simulated antenna in dB.

6.5.1.3 VSWR

The Voltage Standing Wave Ratio is a measure of how well is the antenna matched to the transmission line (in this case the SMA connector), by measuring the reflection coefficient.

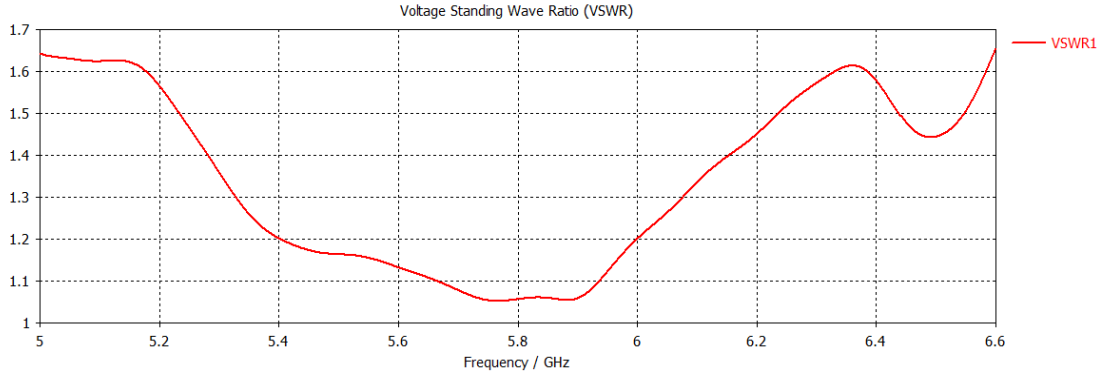

FIGURE 6.7: VSWR of the simulated antenna.

6.5.1.4 Smith Chart

Another way to analyse the S_{11} result is in the Smith Chart. The usefulness of this representation is improved due to the fact that it includes the input impedance.

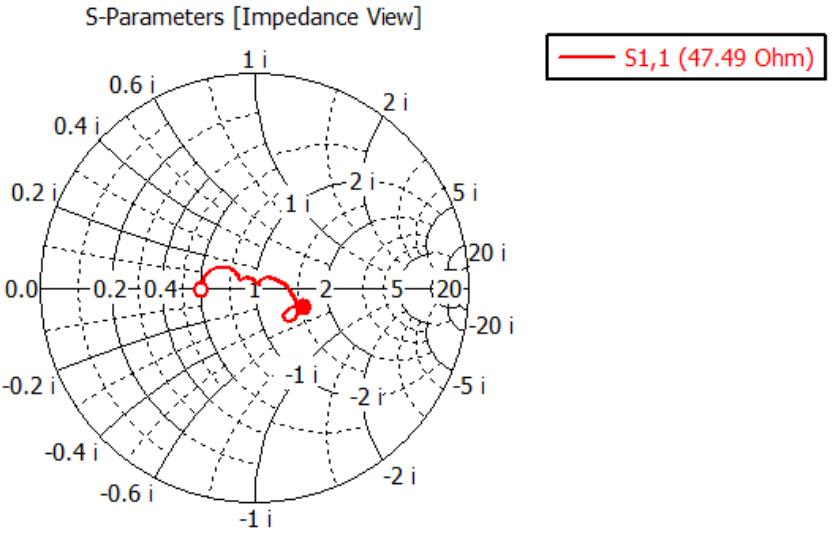

FIGURE 6.8: Smith chart of the simulated antenna, where it is possible to observe the input impedance.

6.5.1.5 Far Field

One of the most useful results is the far field radiation pattern. As can be seen in Fig. 6.9, the gain is $G = 19.7\,\text{dB}$, higher that what the antenna was designed to be.

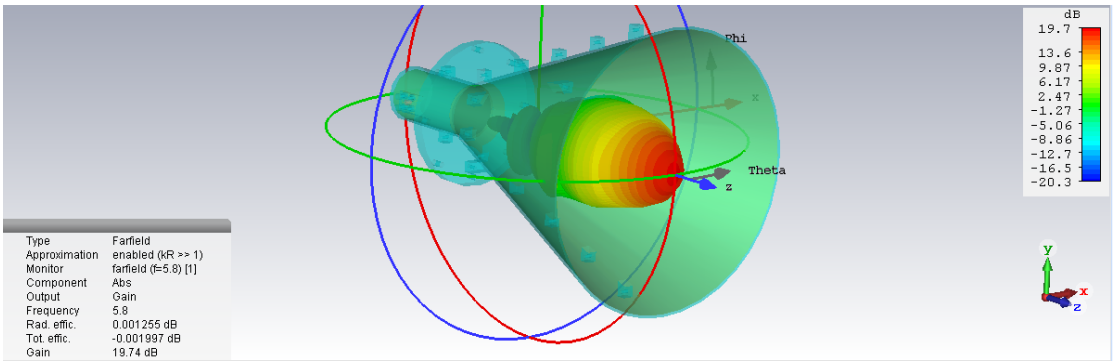

FIGURE 6.9: Far field of the simulated antenna.

This ends the analysis of the simulated antenna. The positive results were a good incentive to 3D print the antennas.

6.6 3D Printing

Firstly only one antenna was printed. These were divided into 4 pieces because of the 3D printer size (Fig. 6.10), whereas ideally only two pieces would be printed. They were printed in PLA (Polylactic Acid) filament for support. The conducting material is copper, applied using copper tape (one surface has glue). It is fairly easy to cut and place the copper into place. That is one of the reasons why this method was used.

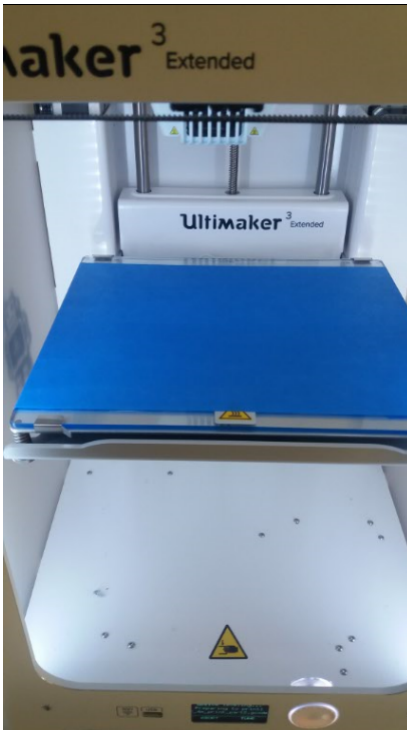

FIGURE 6.10: The 3D printer used, *Ultimaker 3 Extended*.

Since the PLA parts had to be placed and fixed into place, several supports have been added to the design where screws would be later placed.

Immediately after printing the pieces, several work had to be done to work on natural imperfections. The first obvious were the deformations made by the quick cooling of the PLA filament (Fig. 6.11). These would be compensated when screwing the pieces together.

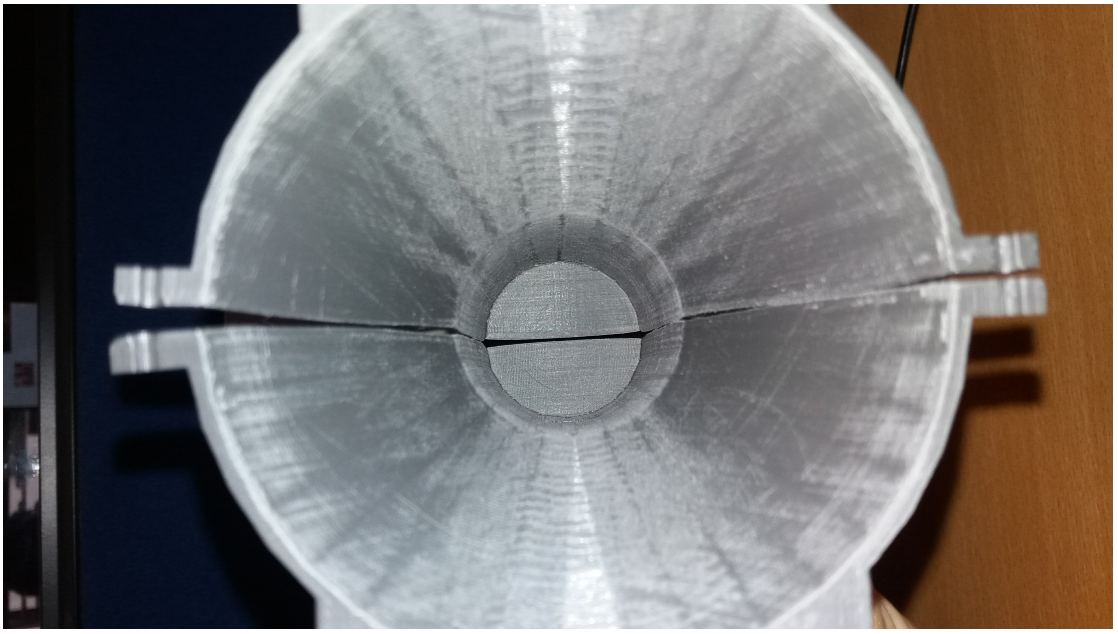

FIGURE 6.11: PLA deformation by cooling.

Later on, filing and widening the screw holes would be necessary. Only after that could the copper tape be applied.

FIGURE 6.12: Several PLA pieces on different stages.

Finally the end result can be seen in Fig. 6.13.

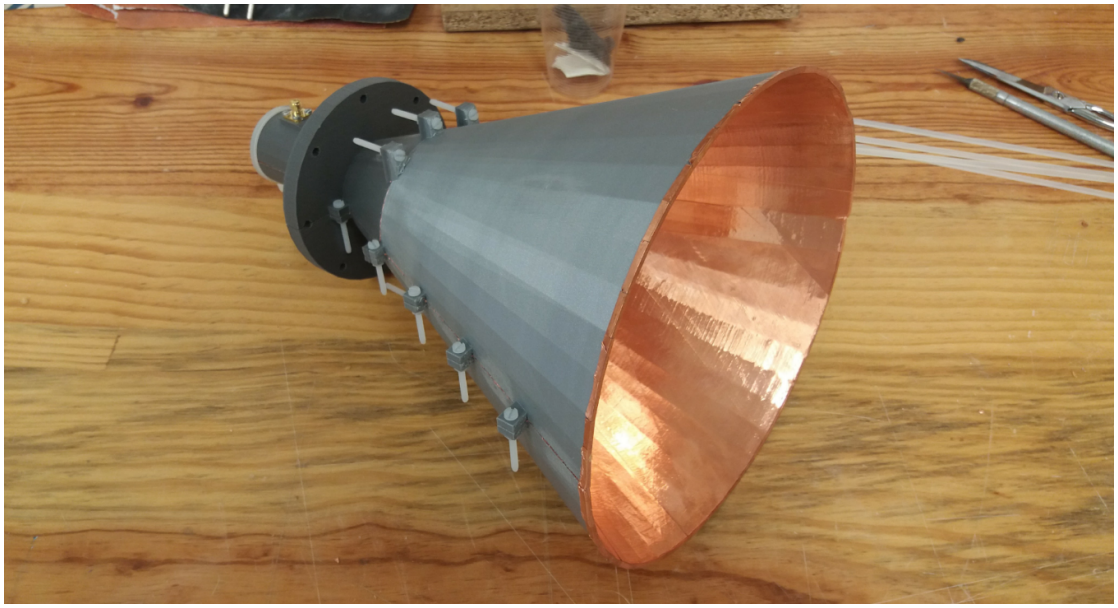

FIGURE 6.13: Finished antenna. One can see the connector on top.

6.7 Printed Antennas Results

Both antennas present similar results in all the parameters. The measurements were made in an anechoic room and the results are presented here with the simulated results of the previous section repeated for a better comparison.

6.7.1 S_{11} Parameter

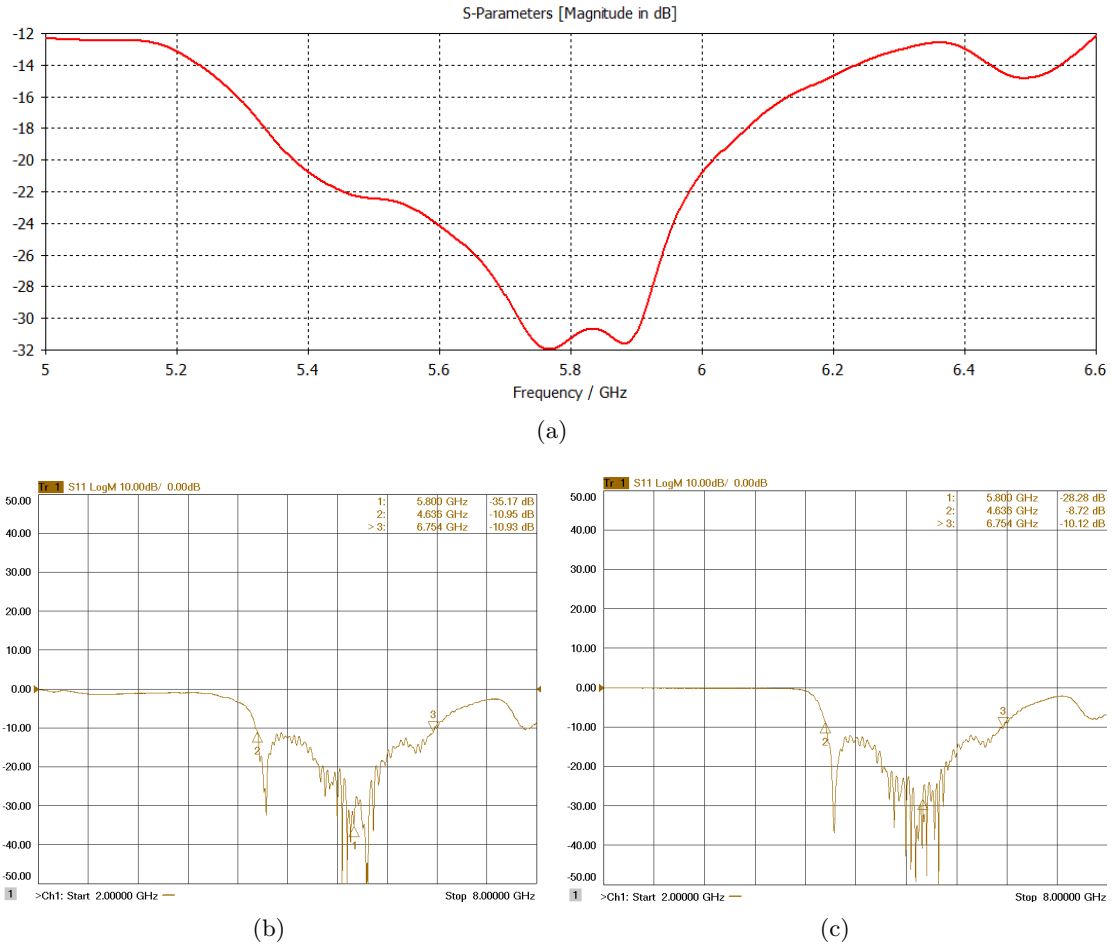

(a)

(b)

(c)

FIGURE 6.14: S_{11} parameters of the printed antennas in dB. (a) CST Simulation (b) Antenna 1 (c) Antenna 2

Both antennas present a good result for the S_{11} parameter.

6.7.2 Smith Chart

Antenna 1 and 2 have an input impedance value of 49.04 Ω and 46.42 Ω, respectively.

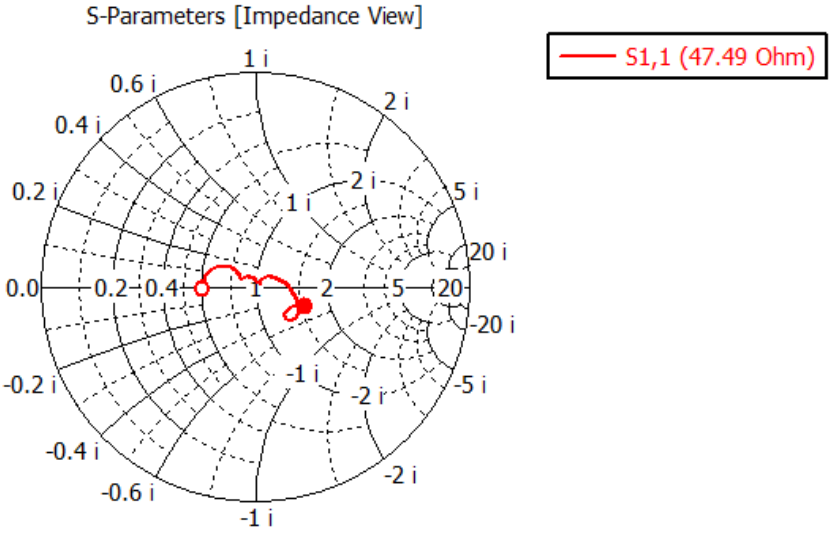

(a)

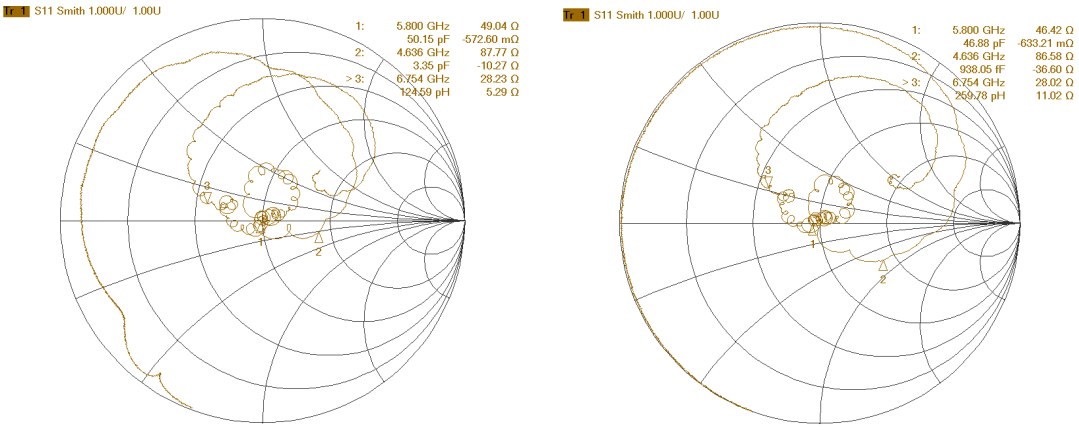

(b) (c)

FIGURE 6.15: Smith chart of the printed antennas. (a) CST Simulation (b) Antenna 1 (c) Antenna 2

6.7.3 Far Field

The radiation pattern of both antennas are compared in Fig. 6.16.

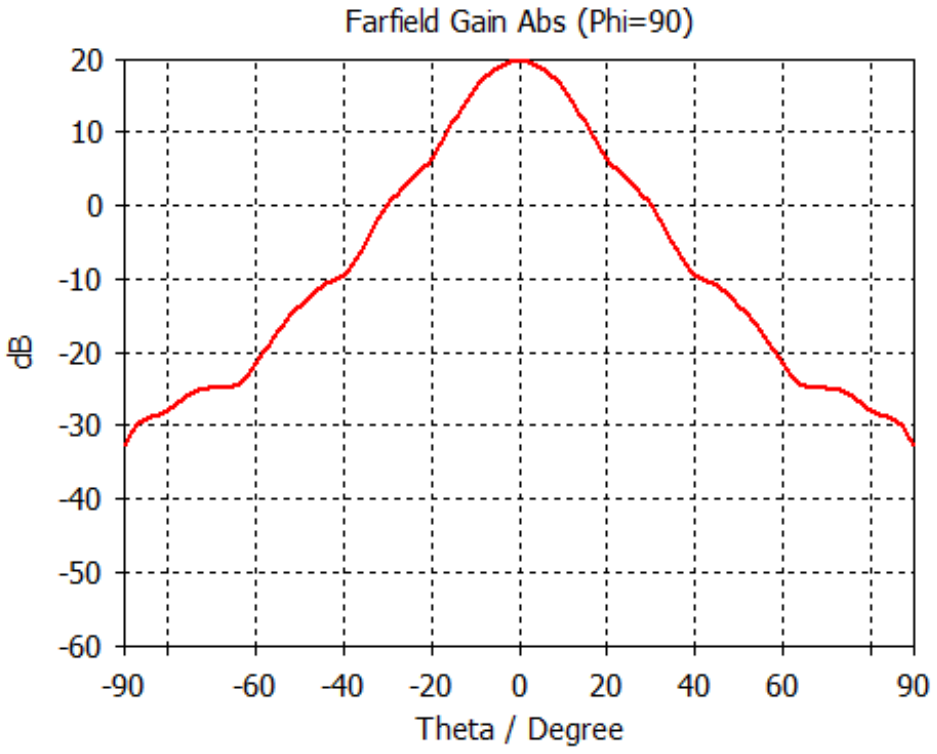

(a)

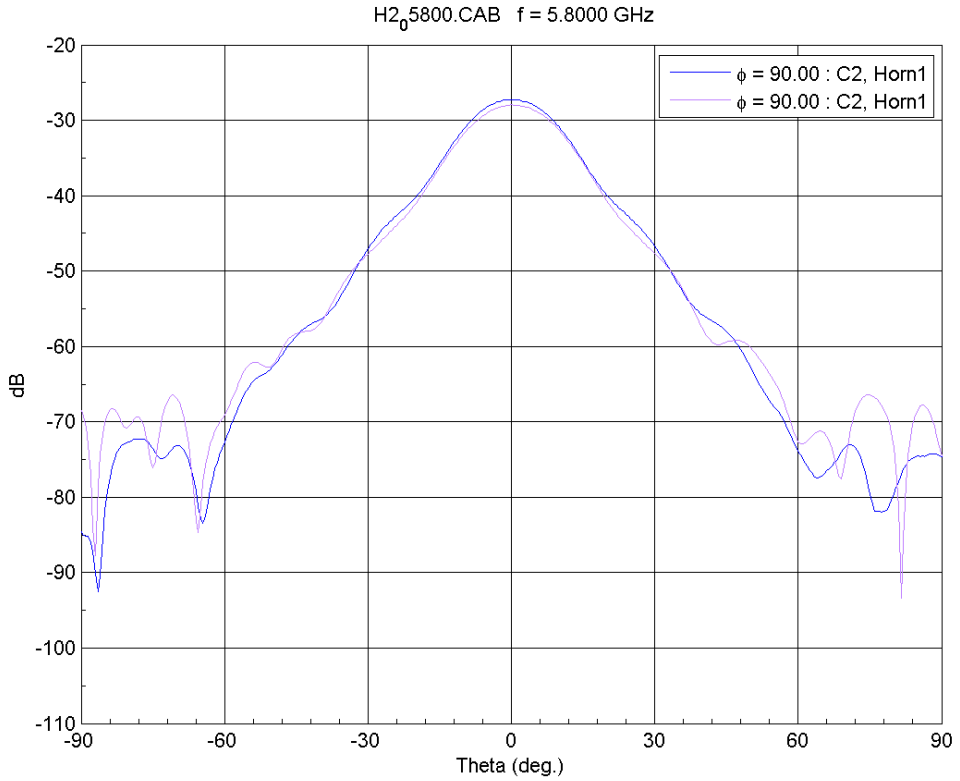

(b)

FIGURE 6.16: Far field of the printed antennas. (a) CST Simulation (b) Antenna 1 is labelled on top of antenna 2.

One finds them to be very similar. A S_{21} measurement was performed in order to know the gain of the antennas, by comparing it to that of a reference antenna (Fig. 6.17) whose gain is known, G_{ref}.

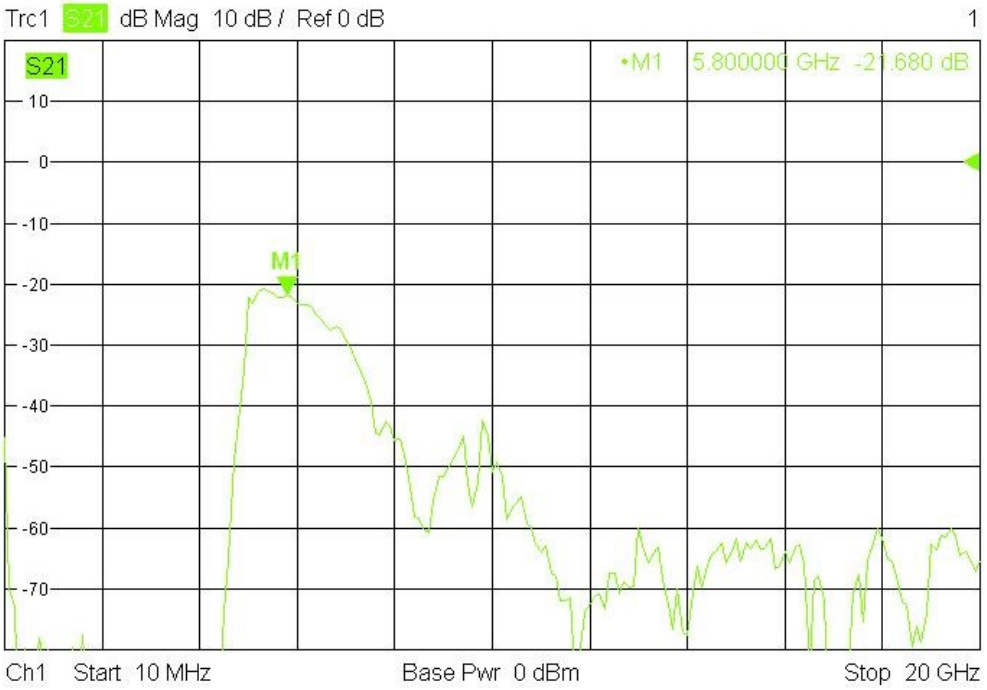

(a)

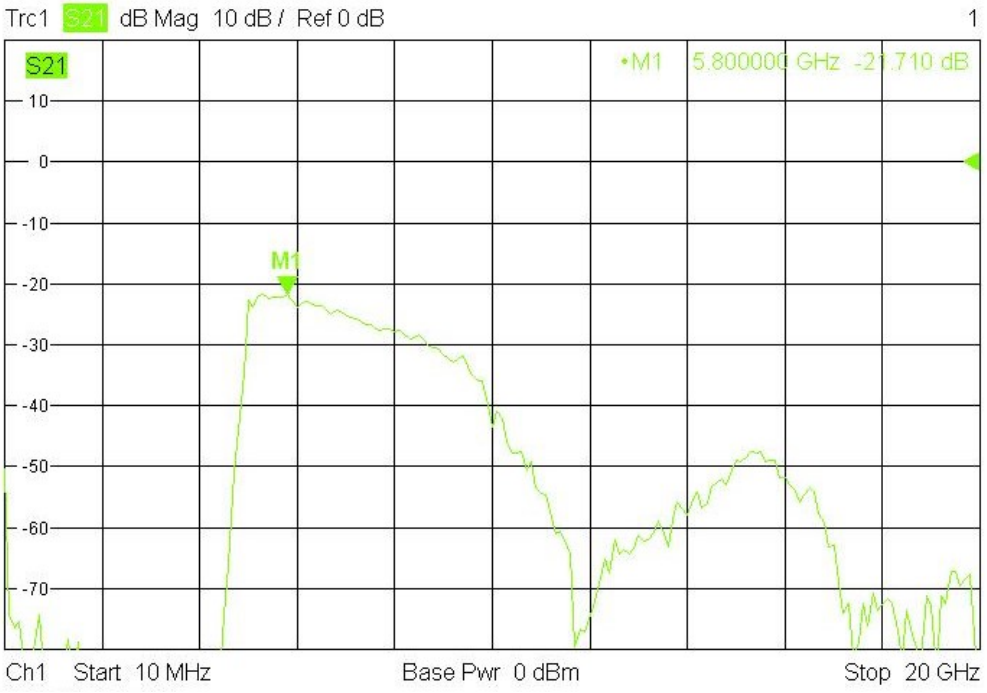

(b)

FIGURE 6.17: S21 parameters of the printed and reference antenna. (a) Antenna 1 (b) Reference Antenna

The following equation was used:

$$G_{Ant} = G_{ref} - (\mathrm{S}_{21_{ref}} - \mathrm{S}_{21_{Ant}}).$$

The reference antenna has a gain of $G_{ref} = 19.034\,\mathrm{dB}$, and by observing that $\mathrm{S}_{21_{ref}} = -21.710\,\mathrm{dB}$ and $\mathrm{S}_{21_{Ant}} = -21.680\,\mathrm{dB}$, the printed antenna (Antenna 1) can be determined to have $G_{Ant_1} = 19.064\,\mathrm{dB}$. The difference between this value and the one it was designed to be ($G = 19.5\,\mathrm{dB}$) on the gaussian beam it produces is unknown, since we still the means to measure gaussian beam output.

In all of the parameters, there is clearly one antenna which outperforms the other (Antenna 1). There may be two main factors that explain the difference. The nuts and screws used to fix the connector in Antenna 1 were made of metal, whereas those of Antenna 2 were plastic. This came as unexpected since it was thought that metal would interfere destructively with the whole structure, reducing the radiation efficiency.

The contrary result may be due to the fact that the metal makes a better connection between the copper surface of the antenna and the SMA connector.

Chapter 7

Parabolic Reflectors

The final element necessary for this study are the parabolic reflectors. Two of these were obtained from the Portuguese company Famaval, along with the necessary supports, whose schematic can be seen in Fig. 7.1.

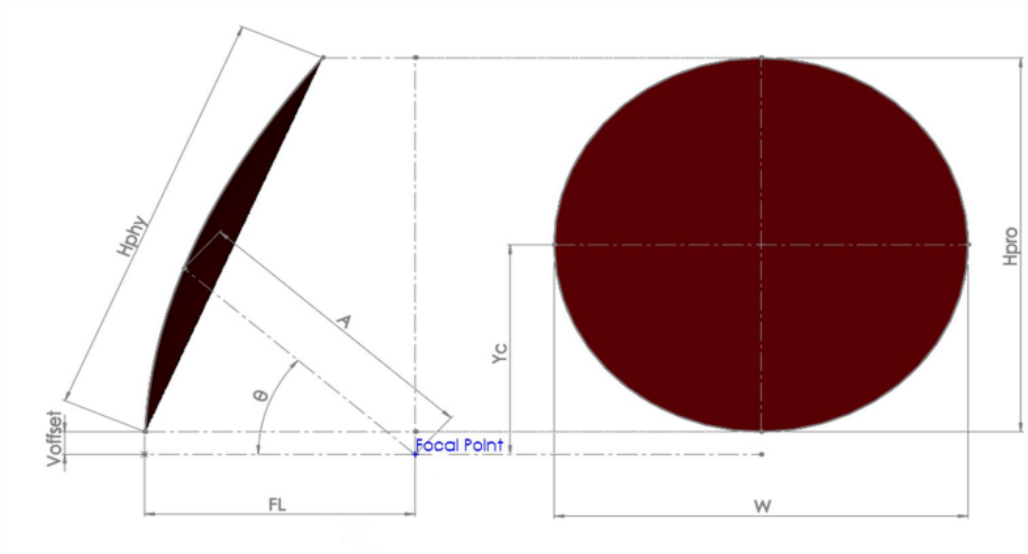

FIGURE 7.1: Parabolic reflector schematic.

The reflectors have their parameters explained in Tab. 7.1

TABLE 7.1: Reflector parameters

Symbol	Terminology	Value (cm)
W	Width	105.879
f	Focal Length	72.675
H_{phy}	Physical Height	114.531
H_{pro}	Projected Height	105.879
V_{offset}	Offset Distance[1]	7.000
Y_C	Vertical Centre	59.939
Θ	Offset Angle	40.59 °

This value of focal length, along with the antenna built in the previous chapter, can be used to set-up a system where $L \approx 5\,\text{m}$ as can be seen in Fig. 7.2.

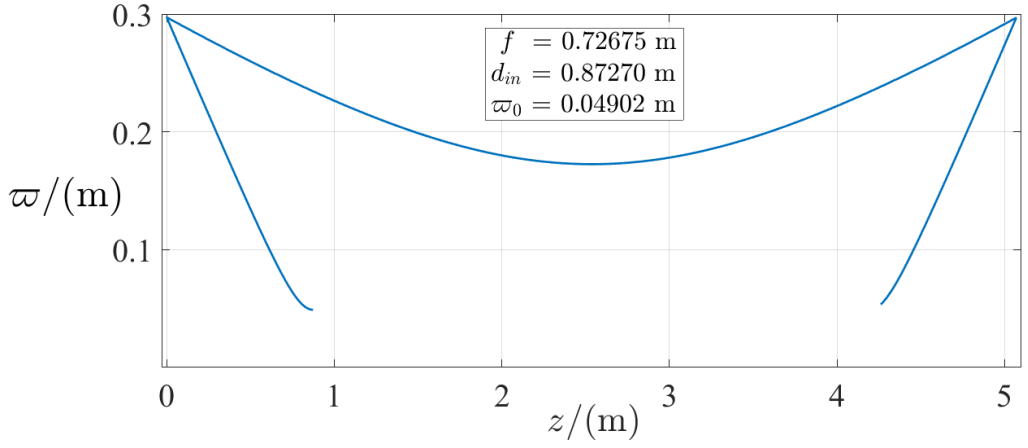

FIGURE 7.2: Script representation for the proposed system.

7.1 Feed Blockage

After being reflected from the parabolic dish, the beam may encounter the feed antenna, suffering blockage from it. To avoid it, we start by comprehending how much of the antenna is above the axis of symmetry of the parent parabola of the parabolic reflector (Fig. 7.3).

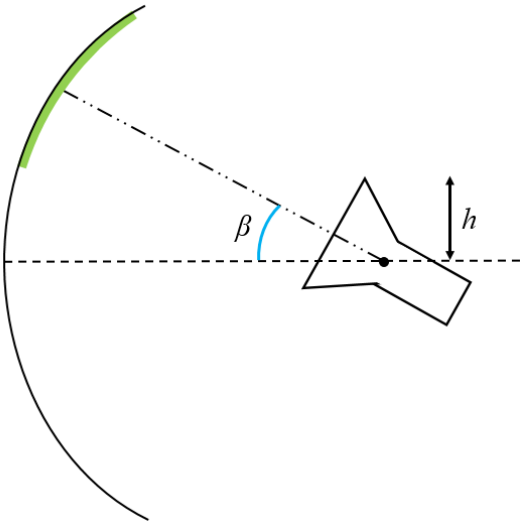

FIGURE 7.3: Feed and dish antenna schematic. An off-set parabolic reflector is represented in green whose parent parabola is in black. β is the angle that the optical axis makes with the parent parabola axis of symmetry and h is the *feed antenna's height* above the latter.

Depending on the angle β, h will vary. The extremes can be seen in Fig. 7.4:

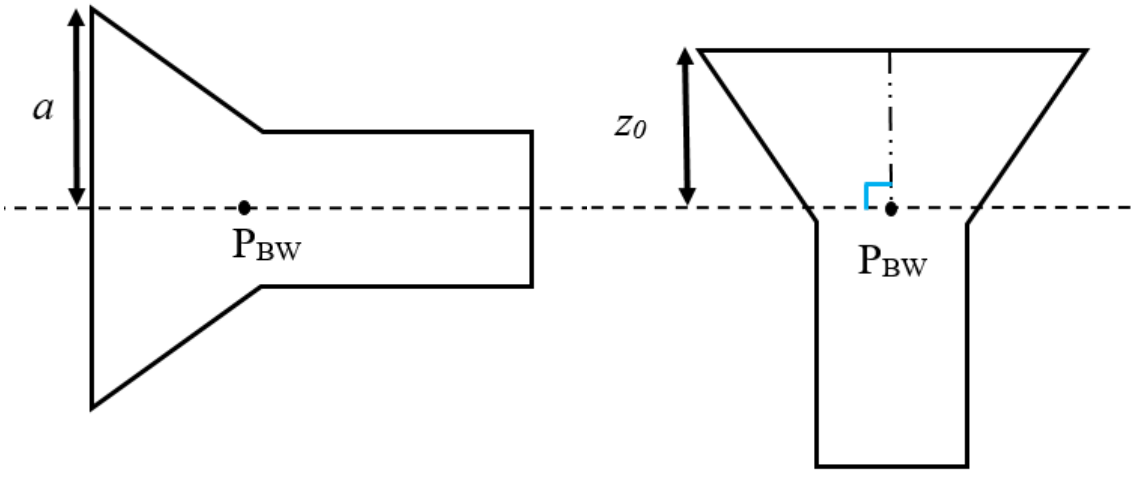

(a) (b)

FIGURE 7.4: Feed antenna height above the parabola's symmetry axis. P_{BW} is the antenna rotation point because it is the beam waist location. In (a) $\beta = 0^{\circ}$, $h = a$ and (b) $\beta = 90^{\circ}$, $h = z_0$

One can obtain an equation for h by acknowledging that the only interesting part in this analysis is the triangle shown in green in Fig. 7.5:

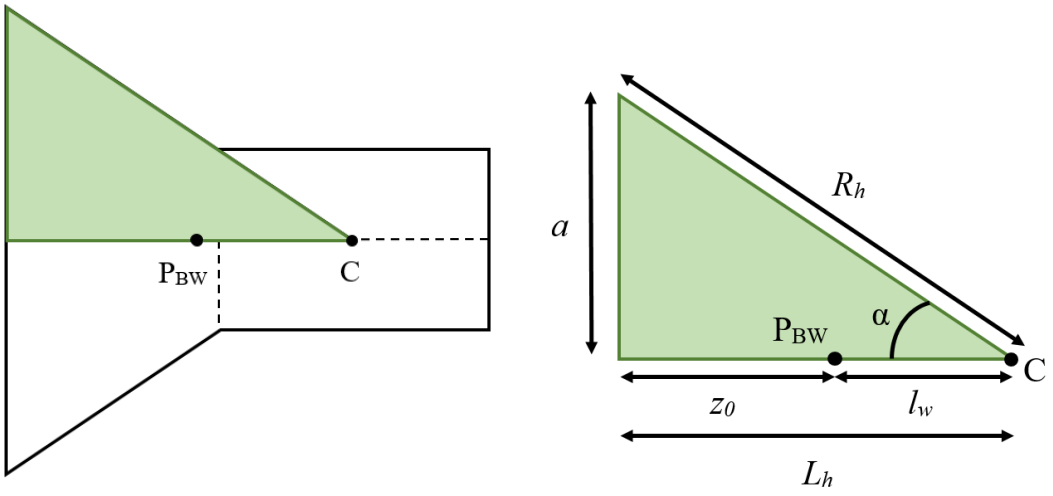

(a) (b)

FIGURE 7.5: Blockage Triangle: (a) on the horn antenna, (b) on its own.

α is the horn slant angle, characteristic of the horn. For a general angle β, the triangle becomes (Fig. 7.6),

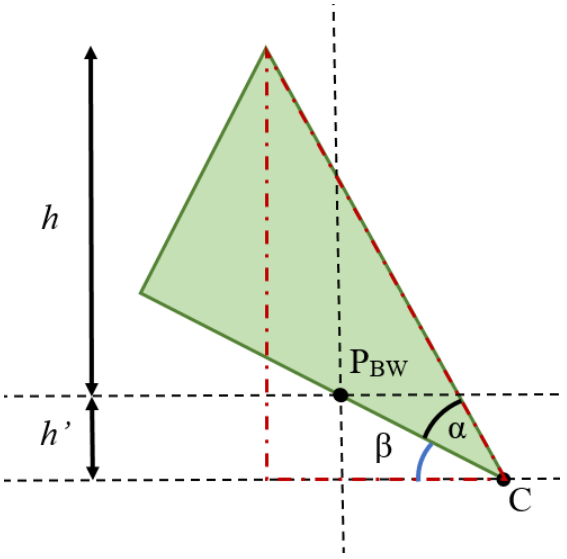

FIGURE 7.6: Blockage triangle at an arbitrary angle β. h is the triangle height above the parabola symmetry axis and h' is the perpendicular distance between this axis and the center of curvature of the horn antenna.

By trigonometry we conclude that $\sin\beta = \frac{h'}{L_h - z_0}$, $\alpha = \text{atan}\left(\frac{a}{L_h}\right)$ and $\sin(\beta+\alpha) = \frac{h+h'}{R_h}$. By using the trigonometric relation, $\sin(A+B) = \sin A\cos B + \cos A \sin B$,

$$h = R_h\left[\sin\beta + \text{atan}\left(\frac{a}{L_h}\right)\right] - (L_h - z_0)\sin\beta \tag{7.1}$$

By rearranging the terms,

$$h = \sin\beta\,[R_h\cos\alpha - (L_h - z_0)] + R_h\cos\beta\sin\alpha. \tag{7.2}$$

Furthermore, knowing that $R_h = \sqrt{L_h^2 + a^2} \Leftrightarrow R_h\sin\alpha = a \Leftrightarrow R_h\cos\alpha = L$, we can simplify the result to the form,

$$h = z_0\sin\beta + L_h\cos\beta. \tag{7.3}$$

Chapter 8

Preliminary Experiment

The final set-up was arranged to complete a first round of experiments (Fig. 8.1).

FIGURE 8.1: Emitter antenna and first parabolic reflector.

A detailed view of the emitter antenna and the first parabolic reflector is presented in Fig. 8.2

FIGURE 8.2: Emitter antenna and first parabolic reflector.

Here it is possible to observe that the parabolic dish is supported by a metal pole whose base is held to the ground by the use of iron weights. The pole base is screwed to one of these weights while having another on top of it. After positioning the dishes at exactly 5 m from each other, bubble levels were used to try and align both structures (Fig. 8.3).

(a) (b)

FIGURE 8.3: Parabolic antennas leveling: (a) horizontally (b) vertically

Although the use of a single VNA was pondered (as a signal source and detector), the necessary cables would have to be so long that the losses would be immense. Instead, two separate devices were used: it is possible to observe the signal generator in Fig. 8.4, a Rohde & Schwarz SMR 50,

FIGURE 8.4: The signal generator used to feed the emitter antenna.

and the spectrum analyser in Fig. 8.5, a Rohde & Schwarz FSH4,

FIGURE 8.5: The spectrum analyser used to detect the incoming wave.

From a first trial, only the detection of the signal was possible with attenuations of the order of -40 dB. However, several adjustments were made for a second trial.

Firstly, the cables' attenuation was measured, by connecting the signal generator directly to the spectrum analyser. As a measure of safety, a 6 dB signal attenuator was used. The cables were CBL-3FT-SMSM+, and had attenuations of 2.44 and 2.33 dB. An example can be seen in Fig. 8.6.

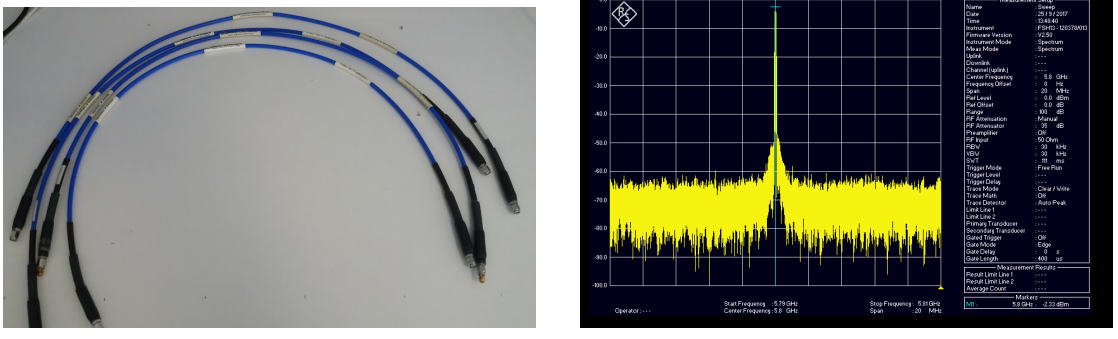

(a) (b)

FIGURE 8.6: The cables used. (a) Picture of the cables (b) example of an attenuation measurement.

After this measurement, the devices were taken outside where the experiment was conducted having changed the antennas distance from the parabolic, but using the metal tubes as reference. Only after not being able to achieve satisfactory results, were the tubes removed and the antennas positioned by hand, with the help of two colleagues (Fig. 8.7).

FIGURE 8.7: The final set-up which consisted on hand positioning the antennas.

The final result is shown below,

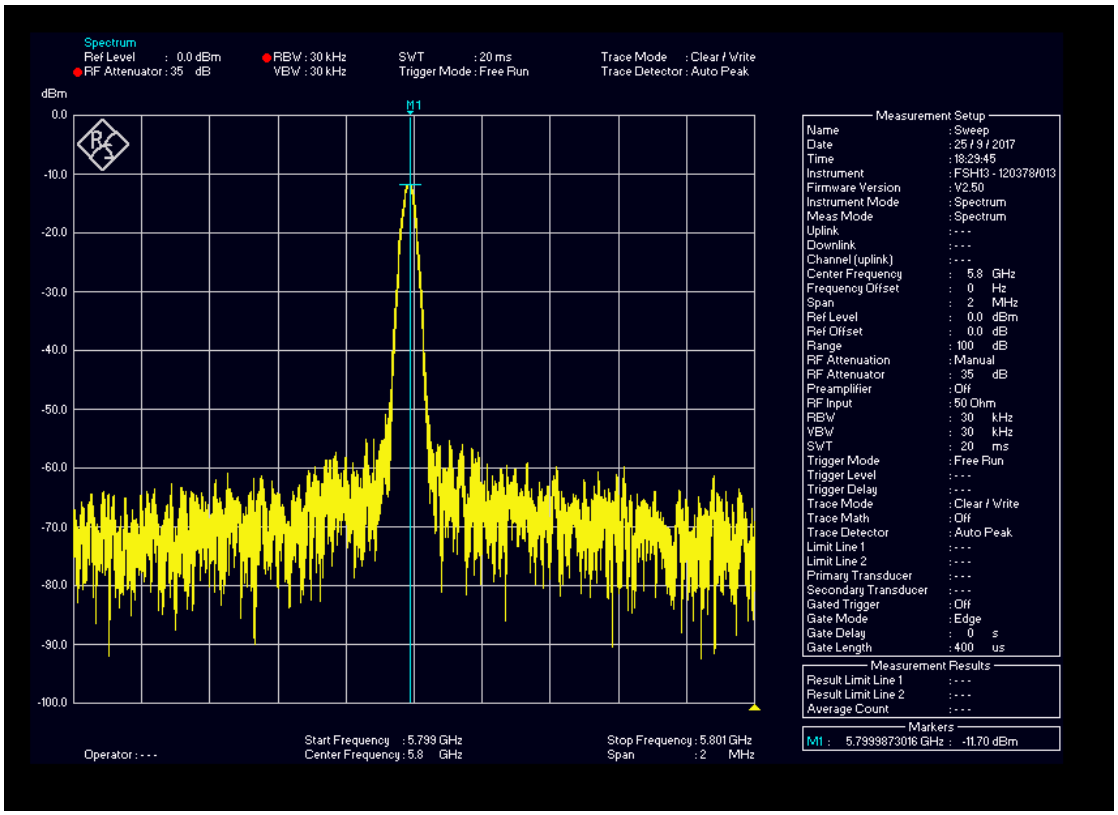

FIGURE 8.8: The maximum efficiency tranfered.

8.1 Efficiency

In order to arrive at the total efficiency, on must take into account all the components used.

The reflectors' efficiency were accounted as being $\sim 74\%$[1] which equals a power attenuation of $\sim -1.308\,\text{dB}$. Since we have two reflectors, we sum the attenuation. The cables were measured and we found that their insertion loss was $-2.33\,\text{dB}$ and $-2.44\,\text{dB}$. On the other hand, the signal attenuator used was a Minicircuit VAT-6W2+, which has an attenuation of 6.40 dB at 5.8 GHz. We accounted for 6 dB, hence 0.40 dB must be subtracted from the measured attenuation of the cables. On the other hand, the SMA connectors have an insertion loss of ~ -0.145 dB. Finally, a DC blocker was in the spectrum analyser, which is $\sim 1\,\text{dB}$, further reducing the cables attenuation.

The cables attenuation are therefore $-1.04\,\text{dB}$ and $-0.93\,\text{dB}$. By summing it all up we have,

$$-1.308 \times 2 - 0.40 - 1.04 - 0.93 - 0.145 \times 2 = -5.82\,\text{dB}.$$

This equals an overall attenuation of $-11.7 - (-5.82) = -5.88\,\text{dB}$, which in percentage is the same as to say that a total efficiency of 25.8% was achieved.

The power emitted was of $0\,\text{dBm}$, $1\,\text{mW}$, enabling the conclusion that at the receiving end arrived $0.258\,\text{mW}$.

8.2 Result Discussion

Although the efficiency is not great, several important conclusions can be made.

First of all, the existence of a focus point is very clear. In order to achieve the -11.7 dB attenuation, there were a lot of patience required for putting the antennas into position. A variation of single millimetres would reduce the value by various dB. Obviously there were too many free variables which must be fixed in order to obtain better results.

On the other hand, this also means that a better efficiency value can be achieved by building a proper supporting structure. Only after being able to control variations on the order of millimetres and degrees, will we be able to know for sure the position of maximum intensity and how the beam parameters influence the system. Furthermore, we can not forget that this value was achieved having changed only the antennas. By adjusting the parabolic dishes, it is likely that the overall efficiency will increase.

There is another important point to make. All the gaussian beam parameters were simply supposed to be as the theory indicates, but that is most likely not the case,

[1] Information given by Famaval.

having been possible to have variations on the beam waist and its location, throughout the system. Better control must be made to include analysis of the gaussian beam. Only then can we know for sure how the beam is propagating, and what to expect at the system's end.

Finally, one can end this discussion with the statement that it is necessary to repeat the experiment with a more thorough and extensive analysis, so as to make sure everything is aligned and in the proper position, and all the parameters are exhausted. However, having found that the expected system behaves as planned is motivating and helps to ensure that the theory may be useful after being perfected,

The final note is that, although positive, the results are not satisfactory, being necessary further work.

Chapter 9

Conclusion

One can summarise the original contents of this dissertation in three different major areas. Firstly, a theoretical analysis of the quasi-optical system. Then the scripts developed which allow for the visualisation of the beam along a general system and finally the practical aspect. In the latter, an experimental set-up was conceived as well as the necessary components. The ultimate goal was to validate an original quasi-optical system in the sense that the basis for achieving a higher efficiency was to reduce spillover losses, by controlling the beam radius.

All of this provided the author with exciting challenges and the opportunity to work with different tools, software and people while learning a lot both on the academic and personal level.

Although the experimental part could not be completed, several important steps have been achieved that enable a basis for further analysis in this subject. The first most evident future topic to be done is to develop a method to analyse the gaussian beam emitted from any source, base on [40]. A complete efficiency analysis is also vital to any power analysis, including this one. Further down the line, different antenna types shall be included in the study, all with the goal of achieving the pretended beam, which may no longer be gaussian since other beam types must also be pondered.

9.1 Publication

The work done on this dissertation enabled the writing of a paper submitted to the Wireless Power Transfer Journal:

- Pereira, R. A. M.; Carvalho, N. B.; Pinto da Cunha, J.: Quasi-Optical Analysis of a Double Reflector Microwave Antenna System

Bibliography

[1] Brown, W. C.: Adapting Microwave Techniques to Help Solve Future Energy Problems, 1973 IEEE G-MTT International Microwave Symposium, 1973, pp. 189-191.

[2] Goldsmith, P. F.: Quasioptical Systems: Gaussian Beam Quasioptical Propagation and Applications, IEEE Press, Piscataway, NJ, 1998.

[3] Sherman, J. W.: Properties of Focused Apertures in the Fresnel Region, IRE Transactions on Antennas and Propagation, vol. 10, no. 4, July 1962, pp. 399-408.

[4] Balanis, C. A.: Advanced Engineering Electromagnetics, John Wiley & Sons Comp., Hoboken, 2012.

[5] Goodman, J. W.: Introduction to Fourier Optics, Roberts & Company Publishers, Greenwood Village, 2005.

[6] Brown, W. C.: The History of Power Transmission by Radio Waves, IEEE Transactions on Microwave Theory and Techniques, vol. 32, no. 9, Sept. 1984, pp. 1230-1242.

[7] Marincic, A. S.: Nikola Tesla and the Wireless Transmission of Energy, IEEE Transactions on Power Apparatus and Systems, vol. PAS-101, no. 10, Oct. 1982, pp. 4064-4068.

[8] Lumpkins, W.: Nikola Tesla's Dream Realized: Wireless power energy harvesting, IEEE Consumer Electronics Magazine, vol. 3, no. 1, Jan. 2014, pp. 39-42.

[9] Carvalho, N. B. et al.: Wireless Power Transmission: R&D Activities Within Europe, IEEE Transactions on Microwave Theory and Techniques, vol. 62, no. 4, April 2014, pp. 1031-1045.

[10] Song, M.; Belov, P.; Kapitanova, P.: Wireless Power Transfer Inspired by the Modern Trends in Electromagnetics, Applied Physics Review 4, 021102, 2017.

[11] Choudhary, V.; Singh, S. P.; Kumar, V; Prashar, D.: Wireless Power Transmission: An Innovative Idea, Intern. Journal of Educ. Planning & Admin., vol. 1, no. 3, 2011, pp. 203-210.

[12] Report SM.2392-0: Applications of Wireless Power Transmission via Radio Frequency Beam, Radiocommunication Sector of International Telecommunication Union (ITU-R), Aug. 2016.

[13] Gómez-Tornero, J. L.; Poveda-García, M.; Guzmán-Quirós, R.; Sánchez-Arnause, J. C.: Design of Ku-band Wireless Power Transfer System to Empower Light Drones, 2016 IEEE Wireless Power Transfer Conference, 2016, pp. 1-4.

[14] Brown, W. C.: Progress in the Design of Rectennas, Journal of Microwave Power, vol. 4, no. 3, 1969, pp. 168-175

[15] Furukawa, M. et al.: 5.8-GHz Planar Hybrid Rectenna for Wireless Powered Applications, 2006 Asia-Pacific Microwave Conference, 2006, pp. 1611-1614.

[16] McSpadden, J. O.; Mankins, J. C.: Space Solar Power Programs and Microwave Wireless Power Transmission Technology, IEEE Microwave Magazine, vol. 3, no. 4, Dec 2002, pp. 46-57.

[17] Koert, P.; Cha, J. T.: Millimeter Wave Technology for Space Power Beaming, IEEE Transactions on Microwave Theory and Techniques, vol. 40, no. 6, Jun 1992, pp. 1251-1258.

[18] Nagababu, M.; Airani, K. C.; Karthik, K. S.; Shambulinga, M.: 4x4 Microstrip Antenna Array for Wireless Power Transmission, 2015 International Conference on Applied and Theoretical Computing and Communication Technology, 2015, pp. 719-722.

[19] Oliveri, G.; Poli, L.; Massa, A.: Maximum Efficiency Beam Synthesis of Radiating Planar Arrays for Wireless Power Transmission, IEEE Transactions on Antennas and Propagation, vol. 61, no. 5, May 2013, pp. 2490-2499.

[20] Alvarez, J. et al.: Near field Multifocusing on Antenna Arrays via Non-convex Optimisation, IET Microwaves, Antennas & Propagation, vol. 8, no. 10, July 2014, pp. 754-764.

[21] Clarricoats, P. J. B.; Poulton, G. T.: High-efficiency Microwave Reflector Antennas - A review, Proceedings of the IEEE, vol. 65, no. 10, Oct. 1977, pp. 1470-1504.

[22] Hasselmann, F.; Felsen, L.: Asymptotic Analysis of Parabolic Reflector Antennas, IEEE Transactions on Antennas and Propagation, vol. 30, no. 4, Jul 1982, pp. 677-685.

[23] Rudge, A. W.; Adatia, N. A.: Offset-parabolic-reflector Antennas: A review, in Proceedings of the IEEE, vol. 66, no. 12, Dec. 1978, pp. 1592-1618.

[24] Murphy, J. A.: Distortion of a Simple Gaussian Beam on Reflection from Off-axis Ellipsoidal Mirrors, International Journal of Infrared and Millimeter Waves, vol. 8, Sept. 1987, pp. 1165-1187.

[25] Sauleau, R.; Fernandes, C. A.; Costa, J. R.: Review of Lens Antenna Design and Technologies for mm-wave Shaped-beam Applications, 11th International Symposium on Antenna Technology and Applied Electromagnetics, 2005, pp. 1-5.

[26] Fernandes, C. A.; Costa, J. R.; Lima, E. B.; Silveirinha, M. G.: Review of 20 Years of Research on Microwave and Millimeter-wave Lenses at "Instituto de Telecomunicações", IEEE Antennas and Propagation Magazine, vol. 57, no. 1, Feb. 2015, pp. 249-268.

[27] Shavit, R.: Dielectric Spherical Lens antenna for Wireless Millimeter-wave Communications, Microw. and Opt. Tech. Lett., vol. 39, no. 1, Oct. 2003, pp. 28–33.

[28] Piksa, P.; Zvanovec, S.; Cerny, P.: Elliptic and Hyperbolic Dielectric Lens Antennas in mm-Waves, Radio Eng., vol. 20, no. 1, April 2011, p. 271.

[29] Hristov, H. D.; Herben, M. H. A. J.: Millimeter-wave Fresnel-zone Plate Lens and Antenna, IEEE Transactions on Microwave Theory and Techniques, vol. 43, no. 12, Dec. 1995, pp. 2779-2785.

[30] Karimkashi, S.; Kishk, A. A.: Focusing Properties of Fresnel Zone Plate Lens Antennas in the Near-Field Region, IEEE Transactions on Antennas and Propagation, vol. 59, no. 5, May 2011, pp. 1481-1487.

[31] Xue, L.; Fusco, V.: Electronically Reconfigurable Microwave Lens Antennas, Queen's University Belfast, Dec. 2005

[32] Jones, E.: Paraboloid reflector and hyperboloid lens antennas, Transactions of the IRE Professional Group on Antennas and Propagation, vol. 2, no. 3, Jul 1954, pp. 119-127.

[33] Fernandes, C. A.; Costa, J. R.; van der Vorst, M.: Design of a Shaped Double-shell Lens Feed for a Quasi-optical Reflector System, 2007 IEEE Antennas and Propagation Society International Symposium, 2007, pp. 5331-5334.

[34] Smith, D. R. et al.: An Analysis of Beamed Wireless Power Transfer in the Fresnel Zone Using a Dynamic, Metasurface Aperture, J. Appl. Phys., vol. 121, no. 1, Jan. 2017, pp. 014901.

[35] Friberg, A. T.; Jaakkola, T.; Tuovinen, J.: Electromagnetic Gaussian Beam Beyond the Paraxial Regime, in IEEE Transactions on Antennas and Propagation, vol. 40, no. 8, Aug 1992, pp. 984-989.

[36] Sheppard, C. J. R.; Saghafi, S.: Electromagnetic Gaussian beams Beyond the Paraxial Approximation, J. Opt. Soc. Am. A 16, 1999, 1381-1386.

[37] Tuan, S. C.; Chou, H. T.; Lu, K. Y. and Chou, H. H.: Analytic Transient Analysis of Radiation From Ellipsoidal Reflector Antennas for Impulse-Radiating Antennas

Applications, in IEEE Transactions on Antennas and Propagation, vol. 60, no. 1, Jan. 2012, pp. 328-339.

[38] Chou, H. T.; Tuan, S. C.; Lu, K. Y. and Chou, H. H.: An Analytic Solution of Transient Scattering From Perfectly Conducting Ellipsoidal Surfaces Illuminated by an Electromagnetic Plane Wave, in IEEE Transactions on Antennas and Propagation, vol. 60, no. 1, Jan. 2012, pp. 340-350.

[39] Balanis, C. A.: Antenna Theory: Analysis and Design, John Wiley & Sons, Inc., Hoboken, NJ, 2005.

[40] Karandikar, Y.: Factorization of Gaussian Coupling Efficiency and Algorithm to Compute It, 6th European Conference on Antennas and Propagation (EUCAP), Prague, 2012.

[41] Lo, Y. T. and Lee, S. W.: Antenna Handbook: Volume II Antenna Theory, Van Nostrand Reinhold, New York, NY, 1993.

[42] Kalialakis, C.; Carvalho, N. B.; Shinohara, N. and Georgiadis, A.: Selected Developments in Wireless Power Transfer Standards and Regulations, IEEE Standards University E-Magazine, vol.6, no. 2, 2016.

[43] Pozar, D. M.: Microwave Engineering, John Wiley & Sons, Inc., Hoboken, NJ, 2012.

Appendices

A - WPT Paper

Quasi-Optical Analysis of a Double Reflector Microwave Antenna System

Journal:	*Wireless Power Transfer*
Manuscript ID	WPT-WPTF-17-006.R2
Manuscript Type:	Wirelessly Powering: The Future
Date Submitted by the Author:	13-Sep-2017
Complete List of Authors:	Pereira, Ricardo; Universidade de Coimbra Faculdade de Ciencias e Tecnologia, Departamento de Física Carvalho, Nuno; Instituto de Telecomunicações Universidade de Aveiro, Dep Electrónica, Telecomunicações e Informática Pinto da Cunha, José; Universidade de Coimbra Faculdade de Ciencias e Tecnologia, Departamento de Física
Keywords:	quasi-optics, microwave, wireless power transfer, gaussian beam, double reflector

Quasi-Optical Analysis of a Double Reflector Microwave Antenna System

Ricardo A. M. Pereira[1], Nuno Borges Carvalho[2], José Pinto da Cunha[1]

[1]Physics Department, University of Coimbra, Rua Larga, P-3004 516, Coimbra, Portugal

[2]Institute of Telecommunications, University of Aveiro, 3810-193, Aveiro, Portugal

By using Quasi-Optical tools it is possible to approximate Microwave radiation to Gaussian Beams, which enables the study of its propagation and coupling to different components. Hence their usefulness for Wireless Power Transfer and rapid system design. In this paper a system composed by two reflectors is analysed both theoretically and by discussing two cases where quasi-optical tools were applied. The Near and Far Field regimes were considered and corresponding frequencies of operation, beam radius and radius of curvature were computed.

Corresponding author: R. A. M. Pereira; Email: ricardo6pereira@gmail.com; Phone: +351 91 906 18 24

I INTRODUCTION

Microwave's high directionality along with a high transmission efficiency in the atmosphere made this type of radiation interesting for long distance transmissions.

These features made the millimeter and sub-mm waves also convenient for power transmission in the air [1]. However, the divergence effects are significant and have to be considered. The common theory of optics has then been adapted to contexts with high diffraction (such as microwave propagation), being referred to as "quasi-optics"[2, 3]. There is vast literature on this subject with compreensive treatment, both on electromagnetics [4] and optics [5], which dedicate sections to the diffraction effect.

Wireless Power Transfer (WPT) using Radio Frequencies (RF) can be traced back to the XIX century, with the work of Heinrich Hertz [6]. His experiments demonstrated the propagation of electromagnetic waves and their reflection on parabolic mirrors at the receiver and transmitter ends. Later on, Nikola Tesla pioneered a different concept of WPT by using low frequency standing waves along the surface of the Earth which would power strategically located antennas. There was no focusing and the radiation would propagate in every direction[7, 8].

Since then, many efforts and important contributions have been done. For a summary of the state-of-the-art on WPT refer to [9, 10]. WPT has immense potential for numerous applications, ranging from distances of a few centimeters (with inductive and capacitive fields) all the way to kilometers using microwaves [11]. Long distance WPT remains a field of interest since there is still much to be done in order to improve the overall efficiency.

A review of the general applications for RF and, specifically, microwave power transfer can be found in [12]. Microwaves have been used to power drones [6, 13] by using rectennas (rectifying antennas) as receivers [14, 15]. The use of microwaves and rectennas form the basis of a Space Solar System for power harvesting where the Sun energy would be converted to electricity in space

via solar panels, and transferred to Earth by microwaves [16, 17].

In general, emitting antennas can have any form but the use of planar arrays is very interesting in various situations due to their relatively small size and low manufacturing costs. Their use in WPT has been contemplated [18] and interesting studies developed, namely on the maximization of the power transfer efficiency [19] or the possibility of focusing multiple targets [20].

That brings us to another important aspect in electromagnetic waves which is the focusing of the radiation. It is common to use reflectors or lenses to create systems that focus the beam, thus reducing the spillover losses. On one hand parabolic reflectors are advantageous to avoid spherical aberration and are common in the industry [21, 22]. Off-set parabolic reflectors are crucial to avoid blockage from the feed [23] at the price of some undesired beam aberrations [24]. On the other hand, depending on the application, lenses can eventually be more advantageous [25, 26] with dielectric lenses receiving a lot of attention [27, 28], due to their simplicity. Fresnel Zone Plate Lens [29, 30] and electronically reconfigurable Luneburg lenses [31] are also worth interesting. Several studies make use of both reflectors and lenses [32, 33].

An interesting application of the quasi-optical theory applied to WPT that considers a meta-surface aperture to dynamically focus a radiation beam to specific points is discussed in [34].

The present study applies the quasi-optical theory in the study of a double-reflector WPT system, using the reciprocity principle to simplify the analysis.

Gaussian Beams

The wave front of a light beam can be approximated to plane waves in most applications if the wavelength is much smaller than the size of the components involved (e.g. reflectors, lenses, etc.) That is not the case for microwaves since generally the wavelength (λ) is about the same size as the antennas' components (at 5.8 GHz, $\lambda = 51.7\,\text{mm}$ in air). In such a case, a better approximation is to consider that the waves are gaussian beams.

Let's assume that these beams propagate in the $\hat{z}$ direction, with z_0 being the point at which the power is most concentrated and the diffraction less evident - the beam wave front can correctly be approximated by a plane wave at the surroundings of this point; we will assume $z_0 = 0$ throughout the discussion. As z increases (i.e. as the beam propagates), the beam spreads and the wave front, i.e. the surface of equal phase of the electric field, assumes a curved shape.

The electric field of a gaussian beam that propagates freely in the fundamental mode is axially symmetric; its value depends only on the *distance from the axis of propagation (radius)*, r, and the *position along the axis*, z, and can be written as

$$E(r,z) = \sqrt{\frac{2}{\pi\varpi^2}} \exp\left(-\frac{r^2}{\varpi^2} - ikz - \frac{i\pi r^2}{\lambda R} + i\phi_0\right) \tag{1}$$

where ϖ is the beam radius, R is the radius of curvature of the wave front, $\phi_\mathbf{0}$ is the phase shift and λ is the wavelength. This field is normalized such that $\int |E|^2 \cdot 2\pi r \; dr = 1$ for convenience and is represented in Fig. 1.

Although most of the radiation propagates in the fundamental mode there is also some power in higher order modes. The percentage of each depends mostly on the type of antenna used. In some cases the fundamental mode alone is not a good enough approximation. A more general definition allows us to define the electric field for Higher Order Modes [2].

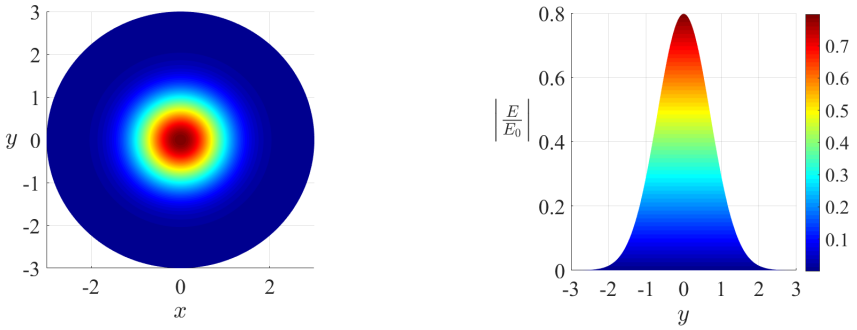

Figure 1: Normalized electric field distribution of a gaussian beam in the fundamental mode ($\varpi_0 = 1\,\mathrm{m}$): (a) front view and (b) transverse view

Gaussian beams are therefore described by three important parameters, ϖ, R and ϕ_0:

- The *Beam Radius*, $\varpi(z)$, is the distance to the axis at which the field drops to $1/e$ of its on-axis value and is generally a function of the position along the propagation direction. Its minimum value, which is characteristic of the beam, is called the *Beam Waist Radius* (ϖ_0) and it is located at the *Beam Waist* point, z_0, which is defined according to a reference point (e.g. the aperture of a horn antenna). In (2) it is assumed that $z_0 = 0$. It can be shown that [2],

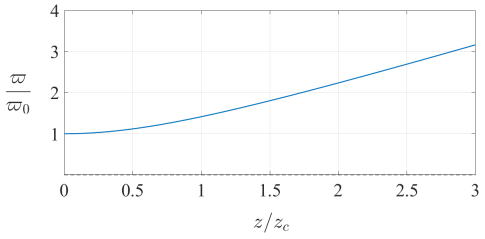

$$\varpi = \varpi_0 \sqrt{1 + \left(\frac{z}{z_c}\right)^2}, \qquad (2)$$

Figure 2: The normalized beam radius is plotted as a function of the propagation axis, z.

where $z_c = (\pi\varpi_0^2)/\lambda$ is the confocal distance, an important quantity which will be defined below.

- The *Radius of Curvature*, $R(z)$, is the radius of curvature of a wave front at z, if the wave was plane at $z = 0$,

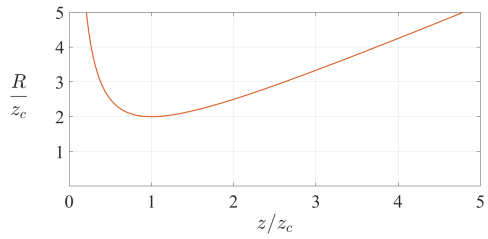

$$R = z + \frac{z_c^2}{z}. \tag{3}$$

Figure 3: The radius of curvature of the wave front along z.

Naturally, at the beam waist $z = z_0 = 0$ and $R \to \infty$, typical of a plane surface.

- The *Beam Phase Shift*, ϕ_0, (sometimes called the *Guoy Phase Shift*) is the difference between the on-axis wave front phase and that of a corresponding plane wave. It generally changes along z, being

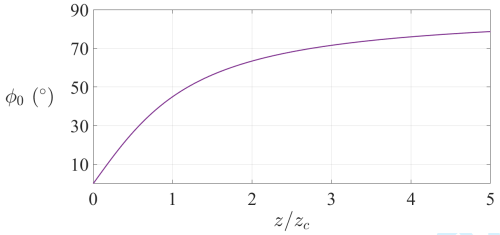

$$\phi_0 = \arctan\left(\frac{z}{z_c}\right). \tag{4}$$

Figure 4: Phase shift along z.

- When studying beam transformations it is particularly convenient to define the so called *Gaussian Beam Parameter*, q,

$$\frac{1}{q} = \frac{1}{R} - i\frac{\lambda}{\pi\varpi^2} \tag{5}$$

or (as a function of ϖ_0)

$$q = z + iz_c. \tag{6}$$

- The crucial quantity after which all the other parameters are written is the *Confocal Distance* (or *Rayleigh Range*),

$$z_c = \frac{\pi\varpi_0^2}{\lambda}. \tag{7}$$

This parameter sets the scale at which a gaussian beam remains collimated (i.e. the beam's rays remain parallel, with minimum divergence). Therefore, z_c parameterizes the transition between the near-field region, $z \ll z_c$, and the far-field, $z \gg z_c$.

It is important to differentiate between the definition of the field regions of gaussian beams from that of antennas'. The antenna's near-field is the region where non-radiative fields dominate, while the far-field is associated with the emission of radiation. On the other hand, since gaussian beams are a representation of electromagnetic waves the field regions are always related to the beam of radiation and the way it behaves and propagates. The diffraction is the major differentiator between the near and far-field of gaussian beams, with z_c being the transition region.

Paraxial Approximation

The paraxial approximation refers to near axis wave fronts. These have wave vectors (rays) that are almost parallel to the optical axis at any point (i.e. the divergence angle is $\theta \lesssim 10\ ^\circ$). In such an approximation,

$$\sin\theta \approx \theta, \quad \tan\theta \approx \theta \quad \text{and} \quad \cos\theta \approx 1.$$

and the analysis is linear. Generally the paraxial approximation is considered valid as long as

$$\frac{\varpi_0}{\lambda} \gtrsim 0.9. \tag{8}$$

However, studies of gaussian beams beyond the paraxial limits can be found in [36, 37].

Beam Transformation

Rays propagating freely in a homogeneous medium can be ascribed at each point to their distance (r) and slope (θ) to the optical axis. If a ray encounters a quasi-optical component it is formally transformed and an output ray will emerge. In the paraxial approximation these transformations are linear, hence the output ray is linearly related to the input one:

$$\begin{bmatrix} r_{out} \\ \theta_{out} \end{bmatrix} = \begin{bmatrix} A & B \\ C & D \end{bmatrix} \cdot \begin{bmatrix} r_{in} \\ \theta_{in} \end{bmatrix}.$$

The $ABCD$ elements form the so called *Ray Transfer Matrix* ($\mathbf{M}$), which is characteristic of the system with its components. It can be calculated by multiplying the matrices of each component that interacts with a ray in reverse order (e.g. if a ray enters a system and encounters the component A and then B, the overall matrix is $M = M_B \times M_A$).

The radius of curvature of the wave front of a beam is $R = r/\theta$ and, therefore, the gaussian beam parameter, q, can be related to the ray parameters. Defining q_{in} as the input gaussian beam parameter at the input beam waist we can arrive at the output gaussian beam parameter (at the output beam waist), q_{out},

$$q_{out} = \frac{A \cdot q_{in} + B}{C \cdot q_{in} + D}. \tag{9}$$

By using (5) we can obtain the beam radius (ϖ) and the radius of curvature (R) of the output beam as a function of z.

A general system matrix, M_{sys}, can be written by taking the matrices representing the propagation of the incoming and outgoing rays together with the ray transfer matrix, M. It enables us to write the input and output parameters for any system configuration in simple terms:

$$\begin{aligned} M_{sys} &= \begin{bmatrix} 1 & d_{out} \\ 0 & 1 \end{bmatrix} \cdot \begin{bmatrix} A & B \\ C & D \end{bmatrix} \cdot \begin{bmatrix} 1 & d_{in} \\ 0 & 1 \end{bmatrix} \\ &= \begin{bmatrix} A + Cd_{out} & Ad_{in} + B + d_{out}(Cd_{in} + D) \\ C & Cd_{in} + D \end{bmatrix} \\ &= \begin{bmatrix} A' & B' \\ C' & D' \end{bmatrix} \end{aligned} \tag{10}$$

where d_{in}, the *input distance*, is the distance from the input beam waist to the first element of the system and d_{out} is the *output distance* from the last element of the system to the output beam waist (see Fig. 5).

Since the beam parameter (6) at the beam waist (where $z = 0$) is $q_{in} = iz_c$ then, by inserting $A'B'C'D'$ elements of the overall matrix, M_{sys}, in (9), the output beam parameter q_{out} becomes,

$$q_{out} = \frac{(A + Cd_{out})iz_c + [(A + Cd_{out})d_{in} + (B + Dd_{out})]}{Ciz_c + Cd_{in} + D}, \tag{11}$$

and, given that at the output beam waist, $z_{out} = 0$, q_{out} is imaginary, and

$$d_{out} = -\frac{(Ad_{in} + B)(Cd_{in} + D) + ACz_c^2}{(Cd_{in} + D)^2 + C^2 z_c^2} \tag{12}$$

and finally the output beam waist radius $\varpi_{0_{out}}$ (knowing that $\det M = 1$),

$$\varpi_{0_{out}} = \frac{\varpi_{0_{in}}}{\sqrt{(Cd_{in} + D)^2 + C^2 z_c^2}}. \tag{13}$$

Gaussian Coupling Efficiency, the Beam Waist Radius (ϖ_0) and Its Location (z_0)

The *Gaussian Coupling Efficiency* (η_G) translates the amount of power from an antenna which is coupled to the fundamental gaussian beam (with a certain ϖ_0 and z_0) [35]. When designing an antenna as a function of ϖ_0, it is important to maximize η_G.

In [2] some antenna types have their η_G discriminated as well as the correspondent ϖ_0 and z_0. However, for different types of antenna one can still arrive at the Gaussian Coupling Efficiency by an algorithm explained in [35]. This is especially relevant when considering the sub-efficiencies which amount to η_G.

The quantities explained in this section are fundamental when designing a concrete system because only with them can the antennas be approximated to gaussian beams.

II QUASI-OPTICAL SYSTEM

The proposed quasi-optical system for this study is a double reflector configuration (represented in Fig. 5), somewhat inspired by the acoustic mirror. The idea is that:

1. A feed antenna radiates on the first reflector;
2. The mirror transforms the radiation in order for it to better propagate through space, directing the beam at the second mirror;
3. This last one will in turn transform the beam so that it can be better received in the final antenna.

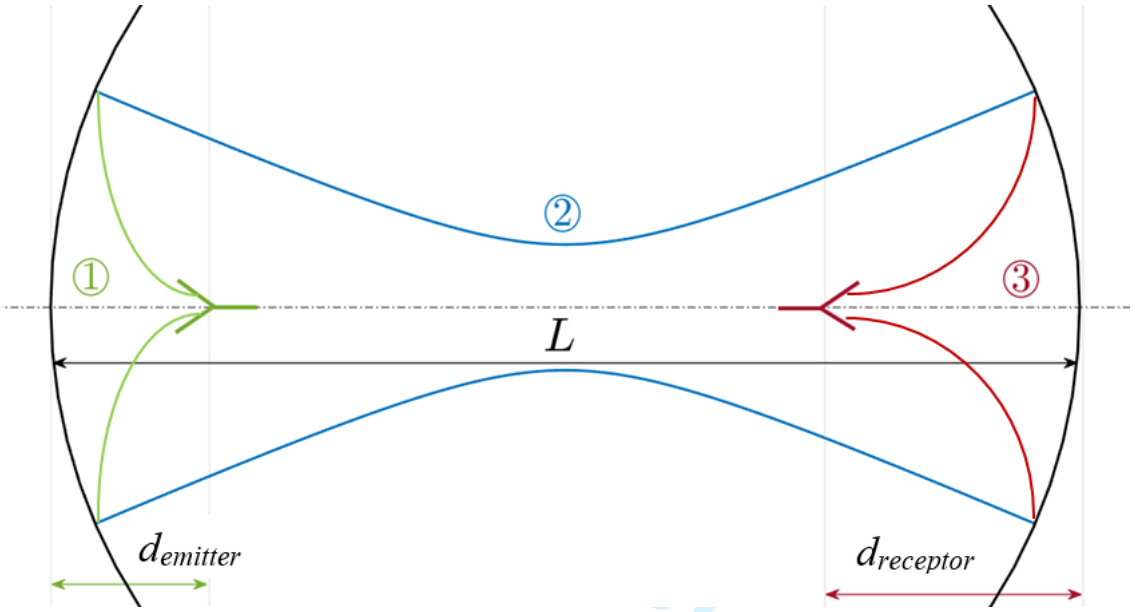

Figure 5: Double-Reflector configuration. $d_{emitter}$ is the distance from the input beam waist radiated by the emitter antenna to the first reflector, after which one can find a beam waist clearly located at $z = L/2$. $d_{receptor}$ is the distance from the final reflector to the output beam waist, at the reception antenna.

Although represented on-axis, an offset reflector should be mandatory since most energy flows in the center of the axis. This set-up was chosen for being the most simple (reflectors are the only type of components used besides the mandatory feed antennas) which serves the purpose of theory validation and preparation for more advanced systems (e.g. adding lenses will enable increasingly complex and improved solutions). Parabolic reflectors were chosen in order to avoid spherical aberration.

The *separation between reflectors* (L) is the quantity that specially characterizes the system. Our final goal is to understand how to achieve the maximum power transmission efficiency, for the maximum L possible.

It is extremely necessary to make a note here. Every quasi-optical system analysis is made by considering an incident beam, with a certain beam waist radius $\varpi_{0_{in}}$ located at a distance d_{in} from

the first component of the system, that suffers transformations by the system. The result is an output beam with a certain $\varpi_{0_{out}}$ that will be located at a distance d_{out} from the last component of the system. A representation of a general quasi-optical system is represented in Fig. 6.

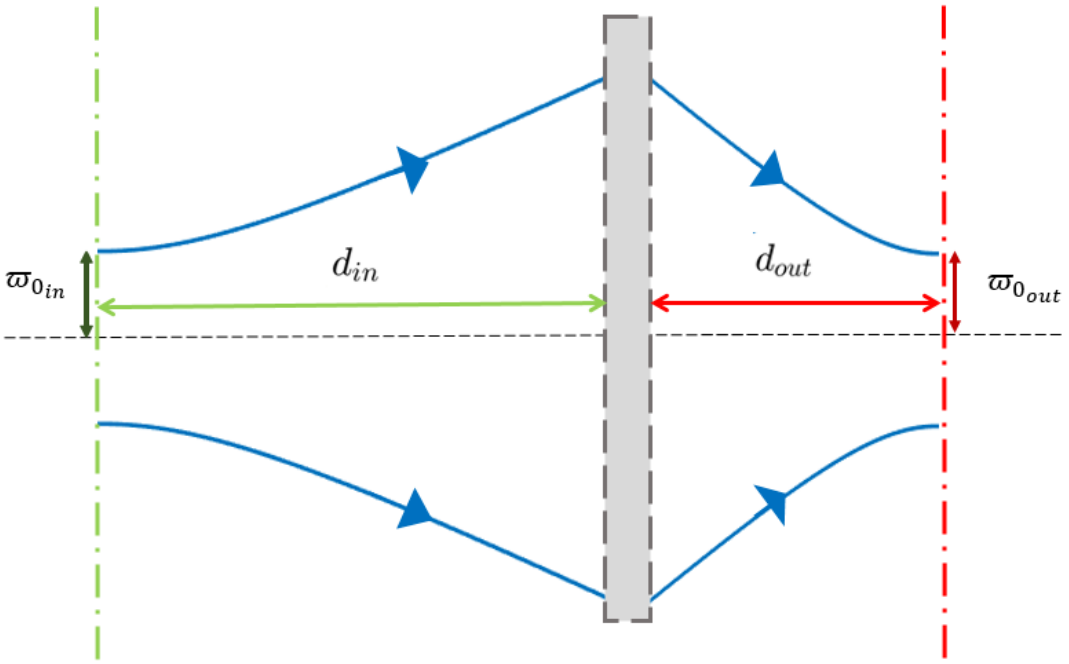

Figure 6: General quasi-optical system. d_{in} is the distance from the input beam waist to the first system's component whereas d_{out} is the distance from the final component to the output beam waist. The grey box illustrates the general system which can be composed of various components.

For our double-reflector system, the quasi-optical system is composed by three components: the first reflector, the distance between reflectors and the final reflector, where $d'_{in} = d_{emitter}$, $d'_{out} = d_{receptor}$ (the inverted comas are used for quantities referring to the total double-reflector system).

However, we can begin our analysis by simplifying the double mirror set-up by making both mirrors and antennas equal: in optics and quasi-optics, rays respect the reciprocity principle, therefore the same laws apply to incoming or outgoing beams - the transformations are simply reversed. One can then analyse the mirrors' effect by studying only one of them.

By doing so, the quasi-optical system represents only one reflector and although $d_{in} = d_{emitter}$ remains exactly the same, the output beam waist will now be the beam after the first reflector. By observing Fig. 5, it is clear that $d_{out} = L/2$.

In that case, the ray transfer matrix is exactly that of a single mirror with a certain *focal length* (f),

$$\begin{bmatrix} 1 & 0 \\ -\frac{1}{f} & 1 \end{bmatrix}. \tag{14}$$

To clarify, the feed antenna originates a beam whose beam waist is at certain distance d_{in} from

the reflector. This beam will diverge until it is transformed by the reflector. The output beam will converge until it reaches $L/2$ where the output beam waist is located by definition (i.e. $d_{out} = L/2$). That finalises the quasi-optical system analysis, but not the beam propagation, which proceeds until the receptor. Because of reciprocity, the beam is expected to diverge until it reaches L, the position where the second mirror is, with the same characteristics (parameters' values) it had in the first mirror. Then the beam will be transformed by the mirror and focused at the receiving antenna, which, reciprocally, is at a distance of d_{in} from the last reflector. In this case $d_{emitter} = d_{receptor} = d_{in}$.

In the end, the incoming beam at the receiving antenna should have the same characteristics of the outgoing beam at the transmitting antenna,

$$\varpi_{0_{final}} = \varpi_{0_{initial}}.$$

At this point the wave front is approximately a plane wave, which might be advantageous for conversion efficiency (at the receptor).

By substituting the parameters of (14): $A = 1,\ B = 0,\ C = -1/f$ and $D = 1$ into (11) and (12), and solving as a function of the mirror's focal length (f) we arrive at

$$af^2 - bf + c = 0, \tag{15}$$

with $a = \frac{L}{2} + d_{in},\ b = -\left(Ld_{in} + d_{in}^2 + z_c^2\right)$ and $c = \frac{L}{2}\left(d_{in}^2 + z_c^2\right)$. This is a quadratic polynomial equation, which has two solutions. In order for the focal length to be a real quantity

$$b^2 - 4ac \geq 0 \tag{16}$$

Therefore,

$$\left[-\left(Ld_{in} + d_{in}^2 + z_c^2\right)\right]^2 - 4\left[\frac{L}{2} + d_{in}\right]\left[\frac{L}{2}\left(d_{in}^2 + z_c^2\right)\right] \geq 0,$$

which can be solved for L, yielding the condition,

$$L \leq z_c + \frac{d_{in}^2}{z_c}. \tag{17}$$

III RESULTS

A) Maximum Distance Between Mirrors

We have arrived at an interval of possible values for L, ranging from zero up to $L_{max}(d_{in}, z_c) = z_c + d_{in}^2/z_c$.

For the sake of simplicity, L will always refer to its maximum value.

In order to maximize the distance between mirrors it is necessary to optimize on z_c and d_{in}. Hence,

$$\begin{cases} \dfrac{\partial L}{\partial z_c} = 1 - \dfrac{d_{in}^2}{z_c^2} = 0 \quad \Rightarrow \quad z_c^2 = d_{in}^2 \quad \Rightarrow \quad z_c = \pm d_{in} \\ \dfrac{\partial L}{\partial d_{in}} = \dfrac{2d_{in}}{z_c^2} = 0 \quad \Rightarrow \quad d_{in} = 0 \end{cases}$$

The only critical point is therefore $z_c = d_{in} = 0$ which is obviously of no interest since we look forward to quantities that have positive non-zero values. Hence, it should be assumed that d_{in} is a controllable parameter and optimize for z_c.

In so doing we find that L is minimum at $z_c = d_{in}$, given that $\frac{d^2L}{dz_c{}^2} = \frac{2d_{in}^2}{z_c^3} = \frac{2}{z_{c_{crit}}} > 0$. The function $L(z_c)$ is represented in Fig. 7 for different values of d_{in}.

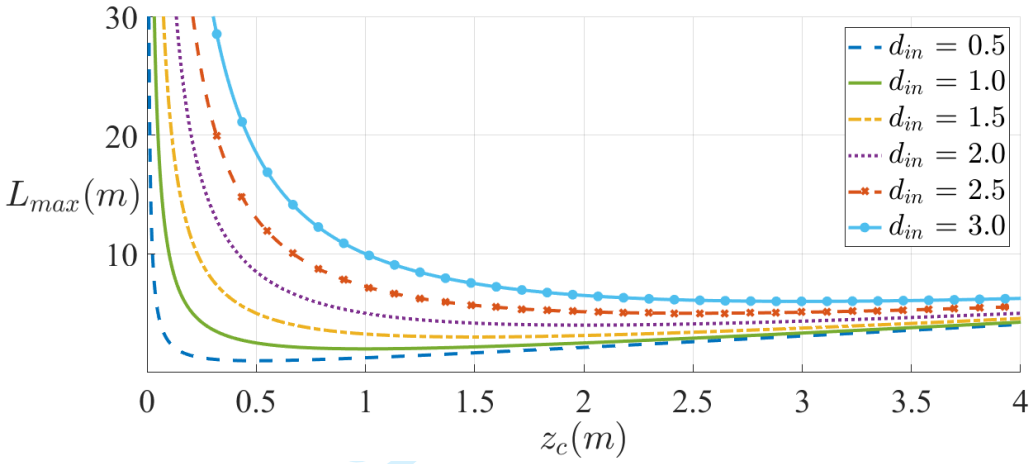

Figure 7: Distance between mirrors, L, for different values of d_{in}.

It is convenient to consider separately the regions below and above the minimum of L, $L_{min} = 2d_{in}$. For each of the regions an assumption can be made, which allows for a simplification of L. These regions correspond respectively to,

$$z_c \ll d_{in} \Rightarrow L \approx d_{in}^2/z_c \tag{18a}$$

and

$$z_c \gg d_{in} \Rightarrow L \approx z_c, \tag{18b}$$

which means that in the two regions the beam is propagating in the far and near-field, respectively. To avoid any possible ambiguity with near and far-field antennas, we shall call the above regions simply *region 1* and *2* or instead *small* and *big beam regions* because, as will be seen in section IV, for a certain frequency of operation, the size of the beam waist radius is much smaller in region 1 than it is in 2.

Two conclusions are immediately obvious. For a smaller d_{in}, L reaches the two approximations more rapidly. On the other hand, however, for a fixed z_c, a smaller d_{in} enables a smaller distance L.

The equation $L = z_c + d_{in}^2/z_c$ can also be written as

$$z_c^2 - Lz_c + d_{in}^2 = 0 \tag{19}$$

and hence,

$$z_c = \frac{L \pm \sqrt{L^2 - 4d_{in}^2}}{2}, \tag{20}$$

(meaning that $L \gtrsim 2d_{in}$ as above). These solutions correspond to the above regions 1 and 2, respectively.

The input distance of $d_{in} = 1\,\text{m}$ has been chosen for convenience while remaining a reasonable distance to implement the feed circuit. All the remaining analysis will be based on this value. The function will therefore assume the curve in Fig. 8:

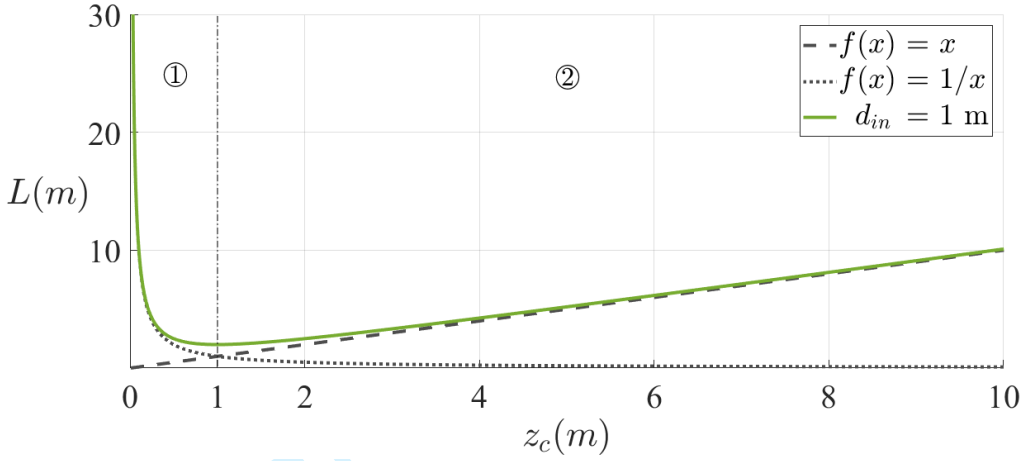

Figure 8: Distance between mirrors for $d_{in} = 1\,\text{m}$, where the approximations for each region are visible. In the regions well below and well above the minimum, for $z_c \lesssim 0.1\,\text{m}$ and $z_c \gtrsim 5\,\text{m}$, L can be approximated by d_{in}^2/z_c and z_c, respectively.

B) Focal Length

We can also obtain the focal length of the reflectors from (15). Since f has a double solution when $L = z_c + d_{in}^2/z_c$, then,

$$f(z_c,\ d_{in},\ L) = \frac{Ld_{in} + d_{in}^2 + z_c^2}{L + 2d_{in}}. \tag{21}$$

C) Beam in the Far-Field (Region 1, where $L \approx d_{in}^2/z_c$)

The assumption (18a) means that the beam propagates in the far-field region (region 1). The beam waist radius is, from (7),

$$\varpi_{0_S} = \sqrt{\frac{\lambda d_{in}^2}{\pi L}}, \tag{22}$$

where 's' stands for "small waist". In such a case,

$$\frac{\varpi_{0_S}}{\sqrt{\lambda}} = \frac{d_{in}}{\sqrt{\pi L}} = const, \tag{23}$$

which means that the ratio between the beam waist and the square root of the wavelength is a constant of the system. Therefore, if ν is the *frequency* and n is the *refraction index* of the propagation medium ($n \approx 1$ for air), then

$$\nu = \frac{cd_{in}^2}{\pi n L \varpi_{0_S}^2}. \tag{24}$$

This means that the choice of the components' size will be balanced with the frequency of operation.

In region 1, the focal length is

$$f_S = \frac{L^3 d_{in} + L^2 d_{in}^2 + d_{in}^4}{L^3 + 2L^2 d_{in}}. \tag{25}$$

D) Beam in the Near-Field (Region 2, where $L \approx z_c$)

It is apparent from Fig. 8 that the near-field is a good approximation for $z_c \gtrsim 5\,\mathrm{m}$.

In this case the beam waist radius from (7) is

$$\varpi_{0_B} = \sqrt{\frac{\lambda L}{\pi}}, \tag{26}$$

where the subscript 'B' means "big waist". This also means that,

$$\frac{\varpi_{0_B}}{\sqrt{\lambda}} = \sqrt{\frac{L}{\pi}} = const, \qquad \nu = \frac{Lc}{\pi n \varpi_{0_B}^2}.$$

Moreover, the focal length is,

$$f_B = \frac{L^2 + L d_{in} + d_{in}^2}{L + 2 d_{in}}. \tag{27}$$

E) Paraxial Limit

The paraxial approximation sets a limit for both of these regions. From (8),

$$\frac{z_c}{\varpi_0} > 0.9\pi, \tag{28}$$

and hence, considering the conditions in (18), the paraxial limits for the regions 1 and 2 are, respectively,

$$\frac{\varpi_{0_S} L}{d_{in}^2} < \frac{1}{0.9\pi}, \tag{29a}$$

and

$$\frac{\varpi_{0_B}}{L} < \frac{1}{0.9\pi}. \tag{29b}$$

These limits should be respected when designing the system in the paraxial approximation.

F) Beam Radius at the Reflector

The beam radius at the position of the reflector, ϖ_R, having travelled d_{in}, is

$$\varpi_R = \varpi_0 \sqrt{1 + \left(\frac{d_{in}}{z_c}\right)^2}. \tag{30}$$

This means that for the regions considered, we arrive at the same value,

$$\varpi_{R_S} = \varpi_{R_B} = \sqrt{\frac{\lambda}{\pi} \frac{(L^2 + d_{in}^2)}{L}}. \tag{31}$$

G) Relation Between Focal Lengths

The quotient between (25) and (27) gives

$$\frac{f_S}{f_B} = \frac{L^3 d_{in} + L^2 d_{in}^2 + d_{in}^4}{L^4 + L^3 d_{in} + L^2 d_{in}^2} \tag{32}$$

which is < 1 for $d_{in} < L$, which will always be the case. We then have

$$f_S < f_B. \tag{33}$$

H) Comparison Between Beams in the Near and Far-Field

In order to best understand the differences between both beam types Fig. 9 shows the two different possible scenarios.

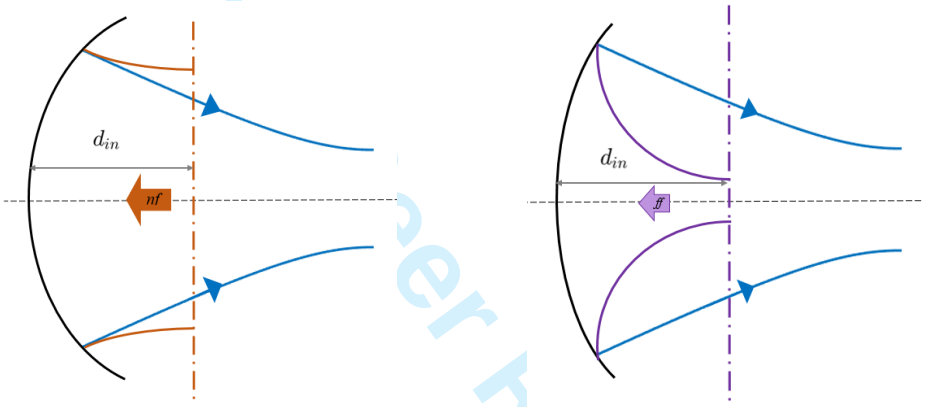

(a) (b)

Figure 9: Comparison between beams in the near and far-field: (a) beam in the far-field (*small*) (b) beam in the near-field (*Big*)

It is worth pointing out that the focal length representation is according to the result in the previous section.

I) Parabolic Reflector

The dimensions of a parabolic reflector are related as

$$4fD = R_R^2, \tag{34}$$

where R_R is the Reflector's Radius, D its Depth and f is the focal length.

The size of R_R must necessarily take ϖ_R into account, for obvious reasons. By defining the *reflector's coefficient* (c_R) as

$$R_R = c_R \varpi_R \quad \Rightarrow \quad \frac{R_R}{\sqrt{\lambda}} = c_R \sqrt{\frac{(L^2 + d_{in}^2)}{\pi L}} \tag{35}$$

and by substituting (31) one arrives at

$$D = \frac{c_R^2 \varpi_R^2}{4f} \quad \Rightarrow \quad \frac{D}{\lambda} = \frac{c_R^2}{4\pi f}\left(\frac{L^2 + d_{in}^2}{L}\right). \tag{36}$$

The coefficient c_R should be as large as possible, though a value of $\sqrt{2}$ is enough from a practical point of view (Fig. 1).

It is worth noting that due to (33), $D_S > D_B$. A beam in the far-field demands a larger reflector depth.

IV CASE DISCUSSION

A script has been developed in order to verify the expected beam radius value as the beam propagates, undergoes a transformation by the reflectors and reaches the final antenna. It enables the graphical representation of the beam propagating through the system, by implementing the equations described in the paper.

A gaussian beam is started at z_0 with a user defined beam waist radius (ϖ_0) and direction of propagation. The position of the different components as well as their $ABCD$ parameters must also be defined, prior to the beam propagation throughout the system, so that if the beam position coincides with that of a certain component, it will suffer a transformation, as described in section I.

Taking an input distance of $d_{in} = 1\,\mathrm{m}$ and a distance between reflectors of $L = 100\,\mathrm{m}$, the paraxial limit dictates that

Region 1	*Region 2*
$\varpi_0 < 3.537 \times 10^{-3}\,\mathrm{m}$	$\varpi_0 < 35.368\,\mathrm{m}.$

which respectively translates into the wavelength limits,

$\lambda < 3.929 \times 10^{-3}\,\mathrm{m}$	$\lambda < 39.297\,\mathrm{m},$

or

$\nu > 76.341\,\mathrm{GHz}$	$\nu > 7.634\,\mathrm{MHz}.$

In order to arrive at an optimum system it is necessary to consider the size of the components and the frequency of operation. Defining one quantity may lead to undesired values for the other.

The focal length of the reflectors' is given by (25) and (27) for the regions concerned, yielding

$$f_S = 0.990\,\mathrm{m} \qquad \text{and} \qquad f_B = 99.029\,\mathrm{m}.$$

Beam in the Far-Field (Region 1)

The minimum frequency of operation for working with a small beam, for an input distance of 1 m and a distance between mirrors of 100 m, is 76.341 GHz. For easing the calculations we choose $\nu = 80\,\mathrm{GHz}$, and hence,

$$\lambda = 3.750 \times 10^{-3}\,\mathrm{m}, \qquad \varpi_{0_S} = \sqrt{\frac{\lambda d_{in}^2}{\pi L}} = 3.455\,\mathrm{mm}.$$

We obtain a relatively small beam waist radius, which will be advantageous in terms of the size of the components, while needing a high frequency of operation.

Beam in the Near-Field (Region 2)

On the other hand, a big beam can have a much smaller frequency, starting at $\nu = 8\,\text{MHz}$, giving,

$$\lambda = 37.500\,\text{m}, \qquad \varpi_{0_B} = \sqrt{\frac{\lambda L}{\pi}} = 34.549\,\text{m}.$$

A huge beam waist radius is obtained. However, by choosing $\nu = 80\,\text{GHz}$, then

$$\lambda = 3.750 \times 10^{-3}\,\text{m}, \qquad \varpi_0 = 0.346\,\text{m}.$$

It is worth noting that by properly choosing the frequency, the size of the beam waist radius will define if the beam is propagating in the near or in the far-field.

Graphical Representation

Several beams have been represented as a function of the frequency of operation (whose values were spread in order to account for different beam waist radii) from both region 1 (Fig. 10) and region 2 (Fig. 11). A logarithmic scale was used in the latter, due to the significant difference in the beam waist radius value between the beam in MHz and the remaining in GHz.

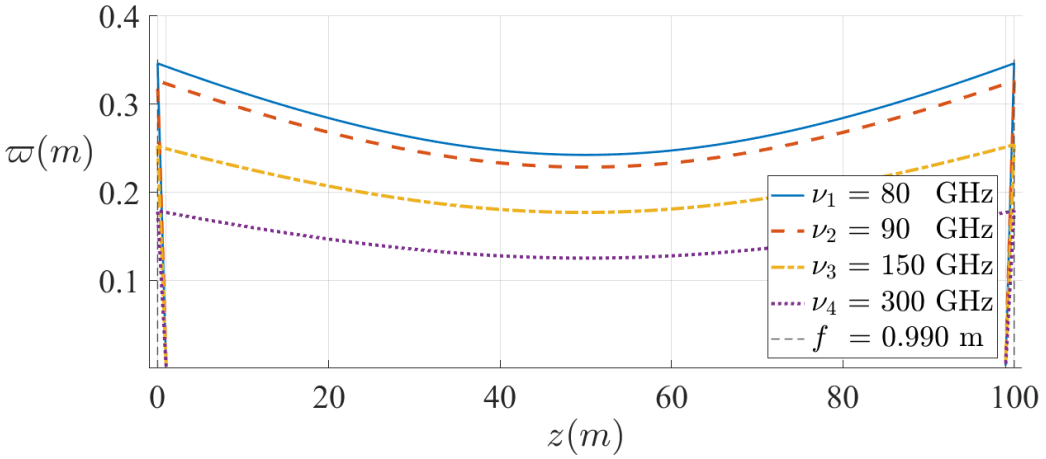

Figure 10: Beams propagating in the far-field (region 1). ϖ is the beam radius, z is the position along the propagation direction, ν is the characteristic frequency of operation and f is the focal distance.

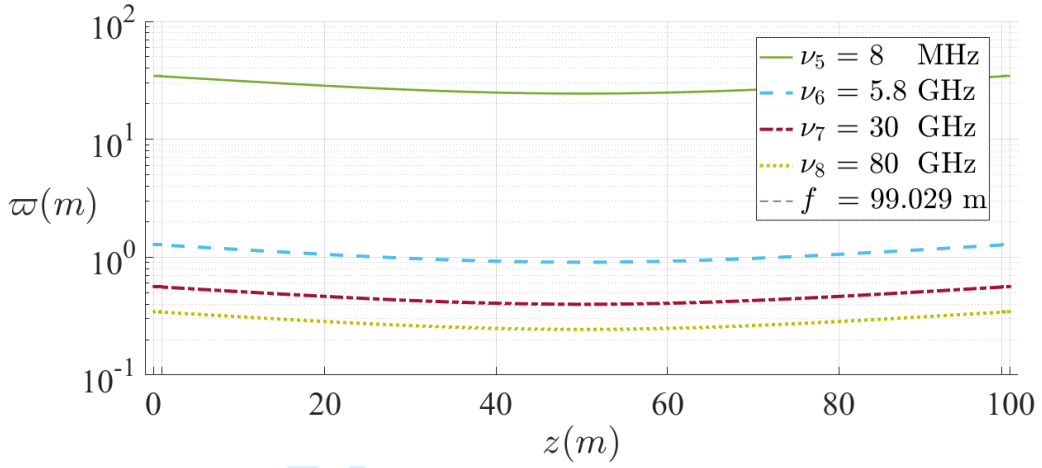

Figure 11: Beams propagating in the near-field (region 2). ϖ is the beam radius, z is the position along the propagation direction, ν is the characteristic frequency of operation and f is the focal distance.

In order to analyse the difference between the beams propagating in each of the regimes, another plot in the near-field was made (Fig. 12), operating at the same frequencies as that in Fig. 10.

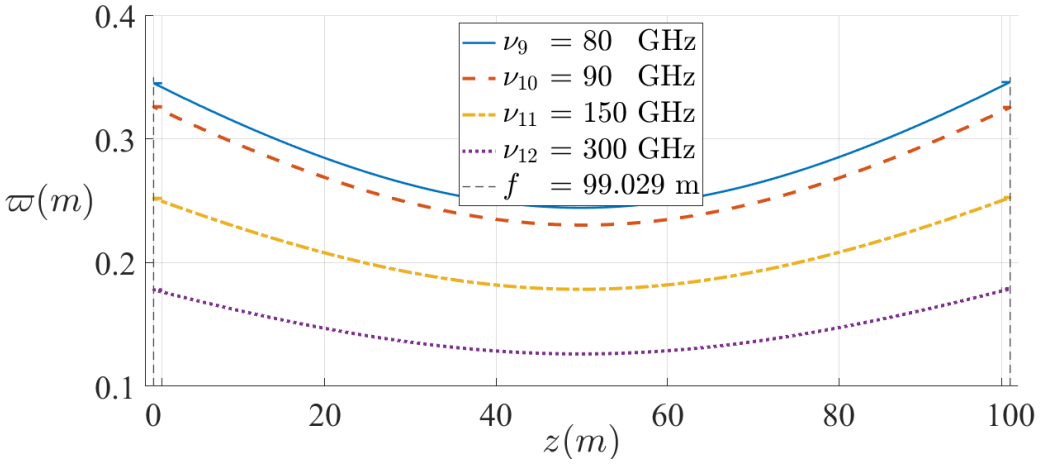

Figure 12: Beams propagating in the near-field with the same frequency as those in Fig. 10. ϖ is the beam radius, z is the position along the propagation direction, ν is the characteristic frequency of operation and f is the focal distance.

A few observations are in order:

- As the frequency increases, the average size of the beam radius decreases. Since the size of the antenna (reflector) are related to that of the beam waist radius (beam radius at the reflector), beams in the far-field regime appear more advantageous in this sense;
- The beam radius of the beam between the reflectors is independent of the beam type (whether it is a near or far-field beam) which originate from the antenna. Beams in the near-field have beam radius larger than the beam radius of the beam between reflectors, while beams in the far-field have a smaller beam radius, as can be seen in Fig. 9. When implementing this study, the size of various components may be constrained, forcing us to choose a feed beam in the near or far-field.

Regarding beams propagating with the same frequency, for either of the regimes, the beam radius at the reflector as well as the output beam waist radius (at $L = 50\,\mathrm{m}$) have nearly identical values. One can conclude that although the initial conditions have been different (emitting a beam in the near or far-field), at the reflector and after the transformation, the beam propagating the L distance has nearly the same characteristics.

V CONCLUSION

The theoretical study of a double reflector quasi-optical system was presented in the paraxial approximation, discussing the beam radii of two different beam types, propagating in the near and far-field, respectively. Different parameters have been considered for each of the beam types.

The preliminary results are consistent to what was expected considering the validity of the reciprocity between the source and the receptor. This study shows that we can have a framework simple enough in order to access the parameters concerned and to gain insight about their relevance.

We now have a tool to quickly prototype simple systems (the script enables the implementation of reflectors and lenses) which serves as basis for more complex analyses.

Further studies are necessary to analyse the power transfer efficiency and improve the model, alongside to simulations to all the process that exhaust the parameter space and allow proper optimization. A case study of a system with a double ellipsoidal mirror is also being considered [38, 39].

Upon completion of this work we plan on making a double reflector prototype aimed at measuring the effect of the various parameters on the power transfer between the emitting and receptor antennas and access the validity of the paraxial calculations. Several components have already been chosen and the main system parameters shall have the following values:

ν	λ	w_0	z_c	f
5.8 GHz	5.172 cm	4.902 cm	14.595 cm	72.675 cm

The goal is to be able to transfer power over the distance of $L = 5\,\mathrm{m}$ using two conical smooth surfaced antennas, which will reflect on two parabolic reflectors with the diameter of 1 m.

We can conclude that the goal of this study was achieved since preliminary results were obtained for building a system with reduced spillover losses, important for guaranteeing that the maximum beam arrives at the receiver antenna.

REFERENCES

[1] Brown, W. C.: Adapting Microwave Techniques to Help Solve Future Energy Problems, 1973 IEEE G-MTT International Microwave Symposium, 1973, pp. 189-191.

[2] Goldsmith, P. F.: Quasioptical Systems: Gaussian Beam Quasioptical Propagation and Applications, IEEE Press, Piscataway, NJ, 1998.

[3] Sherman, J. W.: Properties of Focused Apertures in the Fresnel Region, IRE Transactions on Antennas and Propagation, vol. 10, no. 4, July 1962, pp. 399-408.

[4] Balanis, C. A.: Advanced Engineering Electromagnetics, John Wiley & Sons Comp., Hoboken, 2012.

[5] Goodman, J. W.: Introduction to Fourier Optics, Roberts & Company Publishers, Greenwood Village, 2005.

[6] Brown, W. C.: The History of Power Transmission by Radio Waves, IEEE Transactions on Microwave Theory and Techniques, vol. 32, no. 9, Sept. 1984, pp. 1230-1242.

[7] Marincic, A. S.: Nikola Tesla and the Wireless Transmission of Energy, IEEE Transactions on Power Apparatus and Systems, vol. PAS-101, no. 10, Oct. 1982, pp. 4064-4068.

[8] Lumpkins, W.: Nikola Tesla's Dream Realized: Wireless power energy harvesting, IEEE Consumer Electronics Magazine, vol. 3, no. 1, Jan. 2014, pp. 39-42.

[9] Carvalho, N. B. et al.: Wireless Power Transmission: R&D Activities Within Europe, IEEE Transactions on Microwave Theory and Techniques, vol. 62, no. 4, April 2014, pp. 1031-1045.

[10] Song, M.; Belov, P.; Kapitanova, P.: Wireless Power Transfer Inspired by the Modern Trends in Electromagnetics, Applied Physics Review 4, 021102, 2017.

[11] Choudhary, V.; Singh, S. P.; Kumar, V; Prashar, D.: Wireless Power Transmission: An Innovative Idea, Intern. Journal of Educ. Planning & Admin., vol. 1, no. 3, 2011, pp. 203-210.

[12] Report SM.2392-0: Applications of Wireless Power Transmission via Radio Frequency Beam, Radiocommunication Sector of International Telecommunication Union (ITU-R), Aug. 2016.

[13] Gómez-Tornero, J. L.; Poveda-García, M.; Guzmán-Quirós, R.; Sánchez-Arnause, J. C.: Design of Ku-band Wireless Power Transfer System to Empower Light Drones, 2016 IEEE Wireless Power Transfer Conference, 2016, pp. 1-4.

[14] Brown, W. C.: Progress in the Design of Rectennas, Journal of Microwave Power, vol. 4, no. 3, 1969, pp. 168-175

[15] Furukawa, M. et al.: 5.8-GHz Planar Hybrid Rectenna for Wireless Powered Applications, 2006 Asia-Pacific Microwave Conference, 2006, pp. 1611-1614.

[16] McSpadden, J. O.; Mankins, J. C.: Space Solar Power Programs and Microwave Wireless Power Transmission Technology, IEEE Microwave Magazine, vol. 3, no. 4, Dec 2002, pp. 46-57.

[17] Koert, P.; Cha, J. T.: Millimeter Wave Technology for Space Power Beaming, IEEE Transactions on Microwave Theory and Techniques, vol. 40, no. 6, Jun 1992, pp. 1251-1258.

[18] Nagababu, M.; Airani, K. C.; Karthik, K. S.; Shambulinga, M.: 4x4 Microstrip Antenna Array for Wireless Power Transmission, 2015 International Conference on Applied and Theoretical Computing and Communication Technology, 2015, pp. 719-722.

[19] Oliveri, G.; Poli, L.; Massa, A.: Maximum Efficiency Beam Synthesis of Radiating Planar Arrays for Wireless Power Transmission, IEEE Transactions on Antennas and Propagation, vol. 61, no. 5, May 2013, pp. 2490-2499.

[20] Alvarez, J. et al.: Near field Multifocusing on Antenna Arrays via Non-convex Optimisation, IET Microwaves, Antennas & Propagation, vol. 8, no. 10, July 2014, pp. 754-764.

[21] Clarricoats, P. J. B.; Poulton, G. T.: High-efficiency Microwave Reflector Antennas - A review, Proceedings of the IEEE, vol. 65, no. 10, Oct. 1977, pp. 1470-1504.

[22] Hasselmann, F.; Felsen, L.: Asymptotic Analysis of Parabolic Reflector Antennas, IEEE Transactions on Antennas and Propagation, vol. 30, no. 4, Jul 1982, pp. 677-685.

[23] Rudge, A. W.; Adatia, N. A.: Offset-parabolic-reflector Antennas: A review, in Proceedings of the IEEE, vol. 66, no. 12, Dec. 1978, pp. 1592-1618.

[24] Murphy, J. A.: Distortion of a Simple Gaussian Beam on Reflection from Off-axis Ellipsoidal Mirrors, International Journal of Infrared and Millimeter Waves, vol. 8, Sept. 1987, pp. 1165-1187.

[25] Sauleau, R.; Fernandes, C. A.; Costa, J. R.: Review of Lens Antenna Design and Technologies for mm-wave Shaped-beam Applications, 11th International Symposium on Antenna Technology and Applied Electromagnetics, 2005, pp. 1-5.

[26] Fernandes, C. A.; Costa, J. R.; Lima, E. B.; Silveirinha, M. G.: Review of 20 Years of Research on Microwave and Millimeter-wave Lenses at "Instituto de Telecomunicações", IEEE Antennas and Propagation Magazine, vol. 57, no. 1, Feb. 2015, pp. 249-268.

[27] Shavit, R.: Dielectric Spherical Lens antenna for Wireless Millimeter-wave Communications, Microw. and Opt. Tech. Lett., vol. 39, no. 1, Oct. 2003, pp. 28–33.

[28] Piksa, P.; Zvanovec, S.; Cerny, P.: Elliptic and Hyperbolic Dielectric Lens Antennas in mm-Waves, Radio Eng., vol. 20, no. 1, April 2011, p. 271.

[29] Hristov, H. D.; Herben, M. H. A. J.: Millimeter-wave Fresnel-zone Plate Lens and Antenna, IEEE Transactions on Microwave Theory and Techniques, vol. 43, no. 12, Dec. 1995, pp. 2779-2785.

[30] Karimkashi, S.; Kishk, A. A.: Focusing Properties of Fresnel Zone Plate Lens Antennas in the Near-Field Region, IEEE Transactions on Antennas and Propagation, vol. 59, no. 5, May 2011, pp. 1481-1487.

[31] Xue, L.; Fusco, V.: Electronically Reconfigurable Microwave Lens Antennas, Queen's University Belfast, Dec. 2005

[32] Jones, E.: Paraboloid reflector and hyperboloid lens antennas, Transactions of the IRE Professional Group on Antennas and Propagation, vol. 2, no. 3, Jul 1954, pp. 119-127.

[33] Fernandes, C. A.; Costa, J. R.; van der Vorst, M.: Design of a Shaped Double-shell Lens Feed for a Quasi-optical Reflector System, 2007 IEEE Antennas and Propagation Society International Symposium, 2007, pp. 5331-5334.

[34] Smith, D. R. et al.: An Analysis of Beamed Wireless Power Transfer in the Fresnel Zone Using a Dynamic, Metasurface Aperture, J. Appl. Phys., vol. 121, no. 1, Jan. 2017, pp. 014901.

[35] Karandikar, Y.: Factorization of Gaussian Coupling Efficiency and Algorithm to Compute It, 6th European Conference on Antennas and Propagation (EUCAP), Prague, 2012.

[36] Friberg, A. T.; Jaakkola, T.; Tuovinen, J.: Electromagnetic Gaussian Beam Beyond the Paraxial Regime, in IEEE Transactions on Antennas and Propagation, vol. 40, no. 8, Aug 1992, pp. 984-989.

[37] Sheppard, C. J. R.; Saghafi, S.: Electromagnetic Gaussian beams Beyond the Paraxial Approximation, J. Opt. Soc. Am. A 16, 1999, 1381-1386.

[38] Tuan, S. C.; Chou, H. T.; Lu, K. Y. and Chou, H. H.: Analytic Transient Analysis of Radiation From Ellipsoidal Reflector Antennas for Impulse-Radiating Antennas Applications, in IEEE Transactions on Antennas and Propagation, vol. 60, no. 1, Jan. 2012, pp. 328-339.

[39] Chou, H. T.; Tuan, S. C.; Lu, K. Y. and Chou, H. H.: An Analytic Solution of Transient Scattering From Perfectly Conducting Ellipsoidal Surfaces Illuminated by an Electromagnetic Plane Wave, in IEEE Transactions on Antennas and Propagation, vol. 60, no. 1, Jan. 2012, pp. 340-350.

List of Figures

B - Famaval Report

Relatório

Localização do Ponto de Maior Intensidade e Centro de Fase das Antenas F23 e F30

Trabalho realizado por:

- Ricardo Pereira – ricardo6pereira@gmail.com

Introdução

A radiação eletromagnética na gama dos micro-ondas pode ser estudada na maioria dos casos utilizando a quasiótica [1]. Tal como o nome indica, esta teoria aproxima a radiação a um feixe de radiação, como na ótica, mas implementa-se o efeito da difração, caraterística dos micro-ondas, usando-se feixes gaussianos. As antenas corneta corrugadas são as que melhor emitem radiação nessa forma (direcionada).

Utilizando as ferramentas da quasiótica é possível descobrir a distância ao ponto onde a radiação tem maior intensidade, relativamente a um ponto de referência (***z***) (muito usualmente usa-se a boca ("aperture") da corneta como referência).

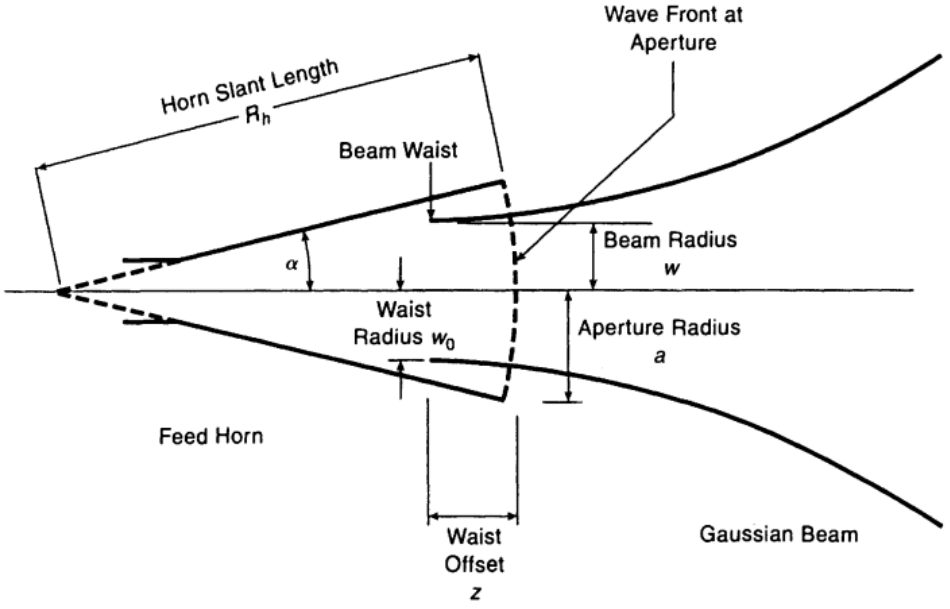

Fig. 1 - Esquema da Antena Corrugada e do Feixe Gaussiano [1].

Na Fig. 1 está esquematizada uma antena corneta e o feixe gaussiano criado pela mesma. O ponto de maior intensidade de radiação é a Cintura de Feixe ("Beam Waist"), onde o feixe tem o menor raio (***w₀***). Este ponto distancia-se da Frente de Onda da Boca da Corneta ("Wave Front at Aperture") por uma quantidade denominada de Distância à Cintura ("Waist Offset") (***z***).

Podemos encontrar o valor das diferentes grandezas na literatura [1]:

$$z = \frac{R_h}{1 + [\lambda R_h / \pi (0.644a)^2]^2}.$$

em que:

a – Raio do Orifício da corneta;

$\boldsymbol{R_h}$ – Comprimento de inclinação da boca.

Neste momento é necessário alertar que a este valor tem de ser subtraído a distância desde a frente de onda da boca da corneta até à boca da mesma (***y***):

$$y = R_h - L\left(\frac{a}{a - a_0}\right)$$

Podemos finalmente definir $\boldsymbol{z_0}$ como sendo a distância do ponto de maior intensidade de campo elétrico desde a boca da corneta:

$$z_0 = z - \left[R_h - L\left(\frac{a}{a - a_0}\right)\right]$$

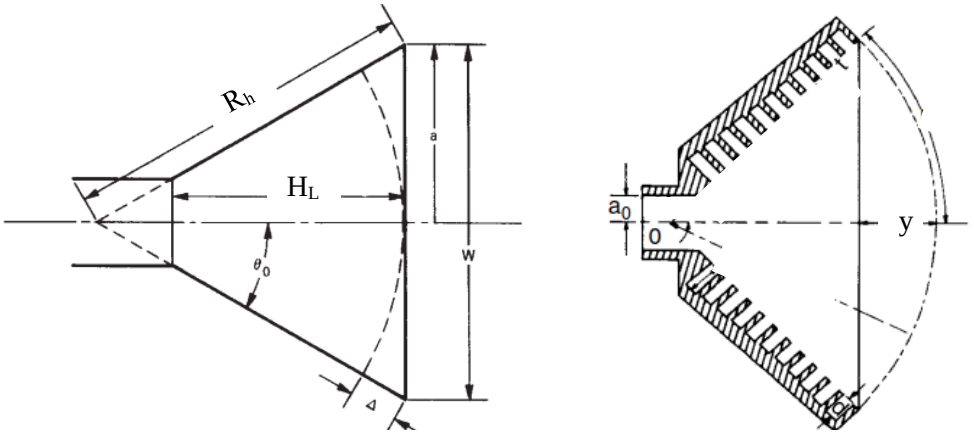

Fig. 3 – (esquerda) Esquema geral de antenas corneta com os principais parâmetros. (direita) Esquema de uma antena corneta corrugada escalar em que a distância da frente de onda na boca da corneta à boca propriamente dita é evidenciada (***y***).

No contexto da engenharia é útil falar também do Centro de Fase, o ponto a partir do qual a radiação eletromagnética propaga-se para o exterior esfericamente, com a fase do sinal sendo igual em qualquer ponto da esfera. Quando a radiação é emitida unicamente para certos ângulos, utiliza-se o Aparente Centro de Fase, como nas antenas corneta (Fig. 2).

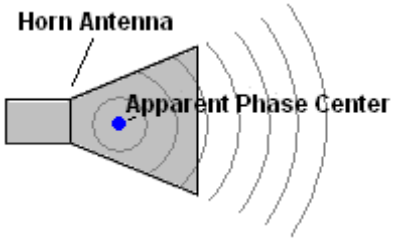

Fig. 2 - Esquema de uma antena corneta e do aparente centro de fase [2].

A diferença entre o centro de fase e a cintura de feixe é dada por:

$$\Delta_{pc} = z_{pc} - R = -\frac{(\pi w_0^2/\lambda)^2}{z_{pc}}.$$

O ponto de centro de fase varia com a distância à cintura de feixe a que a observação é efetuada (***z**pc*). Quando a observação é efetuada a uma distância muito maior que a distância de coerência (***z**c* = ***πw**0*^{2}/λ), $z_{pc} >> z_c$. a diferença é desprezável e pode-se afirmar que o ponto de maior intensidade e o ponto de centro de fase são exatamente o mesmo. De notar que aqui utiliza-se o raio de curvatura (***R***) à distância $\mathbf{z_{pc}}$, dado por $\boldsymbol{R = z_{pc} + z_c^2/z_{pc}}$.

Através da literatura [3], é possível obter o ponto de centro de fase para antenas corrugadas através da seguinte tabela:

Tab. 1 – Distância ao ponto de centro de fase de uma antena corneta circular corrugada desde a boca da corneta em direção ao seu interior (***Lp***) como rácio do comprimento de inclinação da boca.

S	L_p / R_h	S	L_p / R_h
0.00	0.0	0.36	0.386
0.04	0.005	0.40	0.464
0.08	0.020	0.44	0.542
0.12	0.045	0.48	0.614
0.16	0.080	0.52	0.673
0.20	0.124	0.56	0.718
0.24	0.178	0.60	0.753
0.28	0.240	0.64	0.783
0.32	0.310	0.68	0.811

em que $S = a^2/(2\lambda R_h)$.

Neste estudo, as antenas em questão são a F23 e F30:

F23

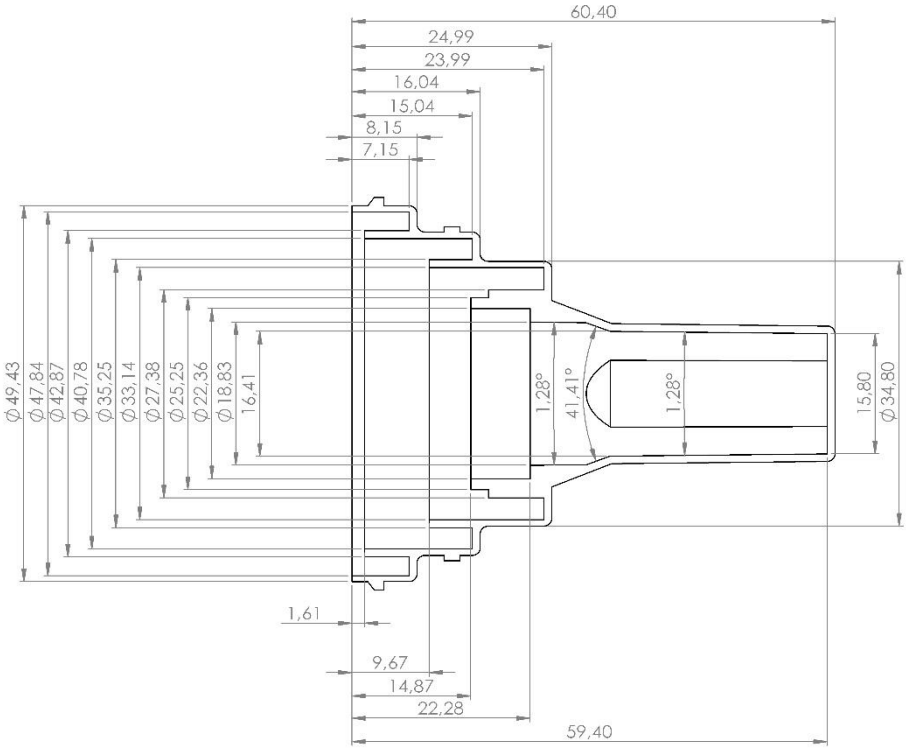

F30

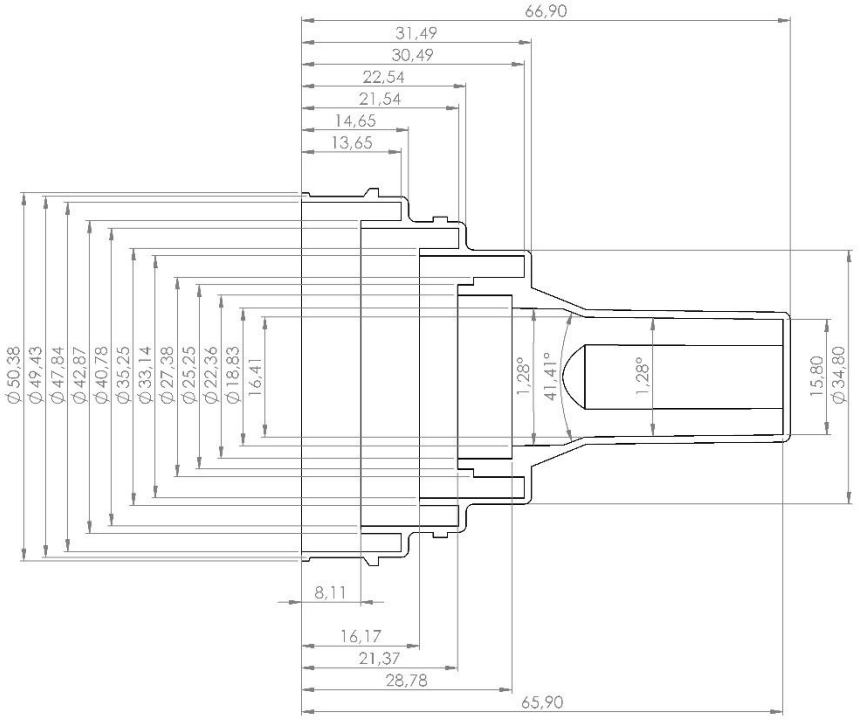

Desenvolvimento

Utilizando as fórmulas apresentadas na secção anterior é possível desenvolver e chegar a valores para as antenas em questão (F23 e F30).

Primeiro que tudo utilizou-se o Software CST para simular as antenas e obter os parâmetros mais comuns:

Modos dos Portos de Excitação (Frequência de operação = 11.5 GHz)

F23

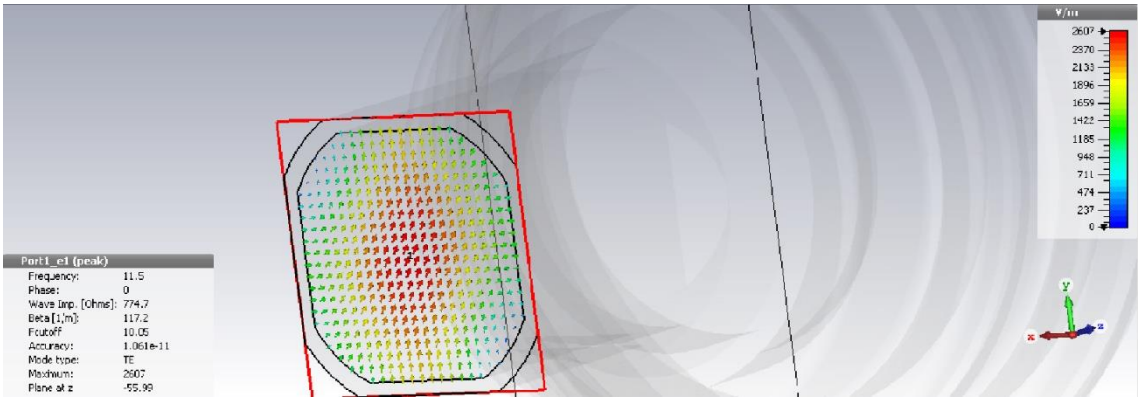

F30

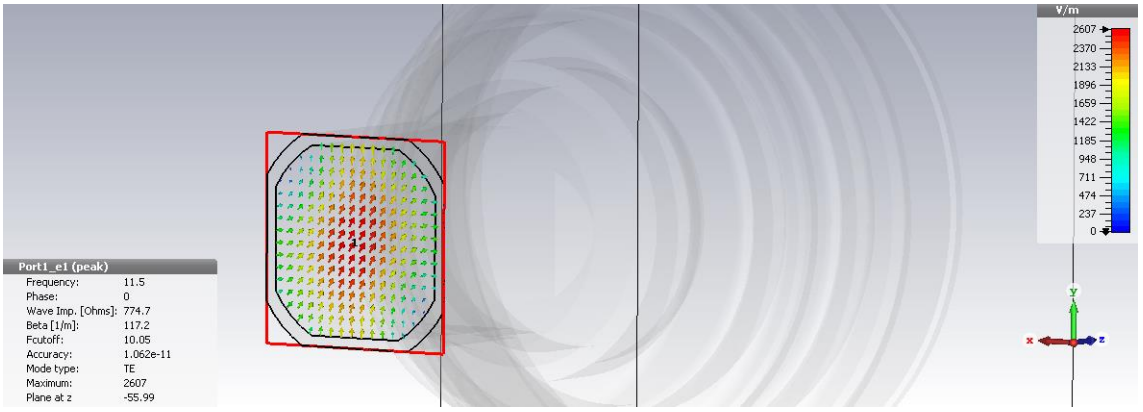

Parâmetros S11

F23

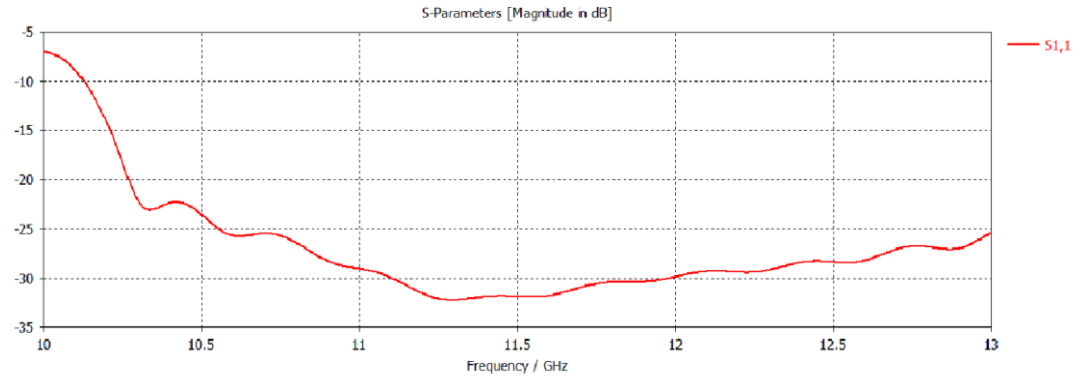

F30

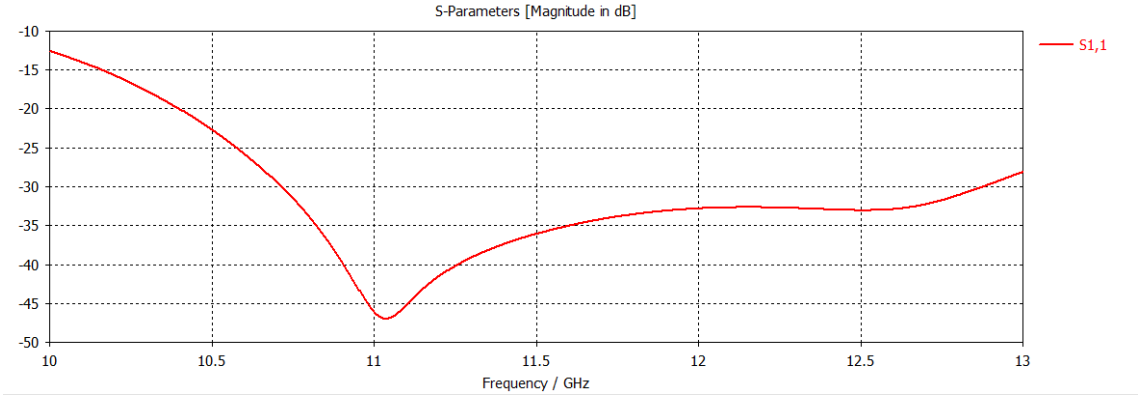

VSWR

F23

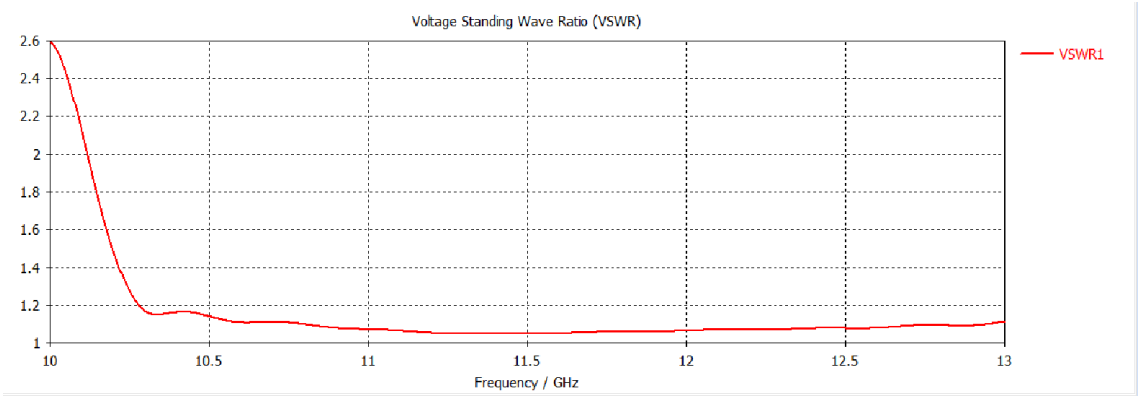

F30

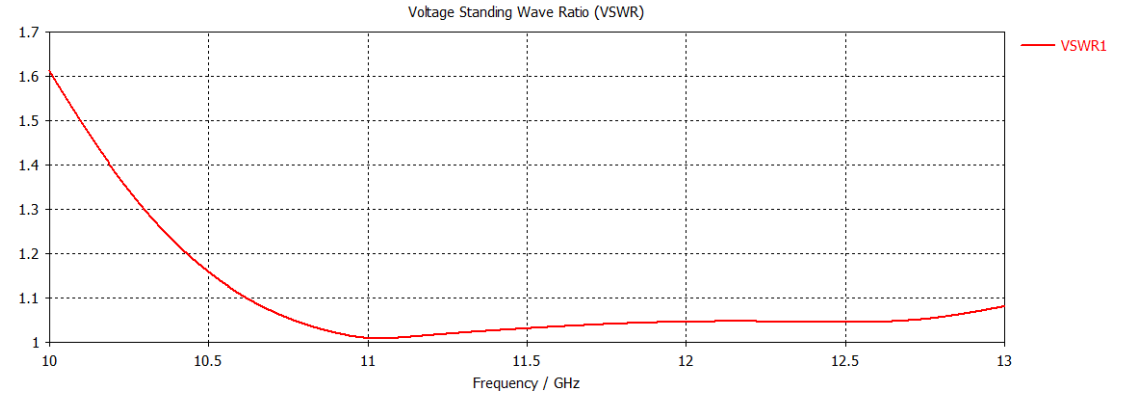

Farfield (f = 10.7 GHz)

F23

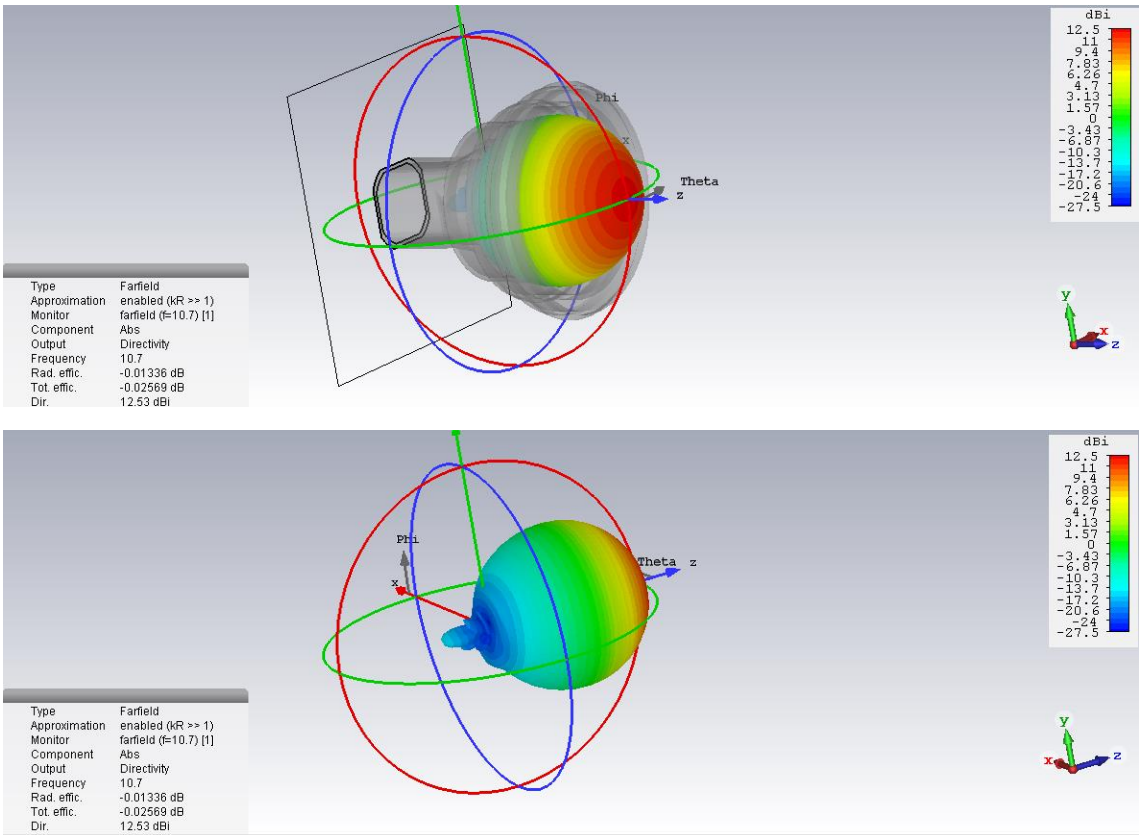

F30

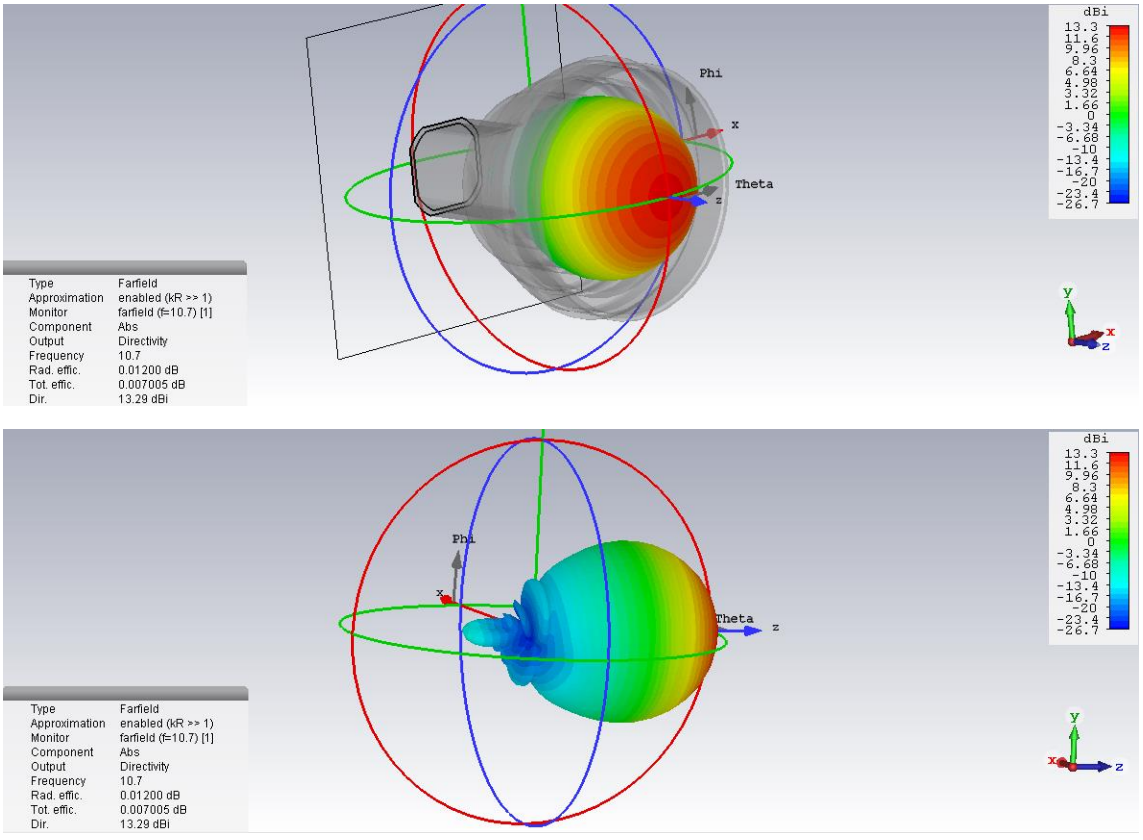

Farfield (f = 11.7 GHz)

F23

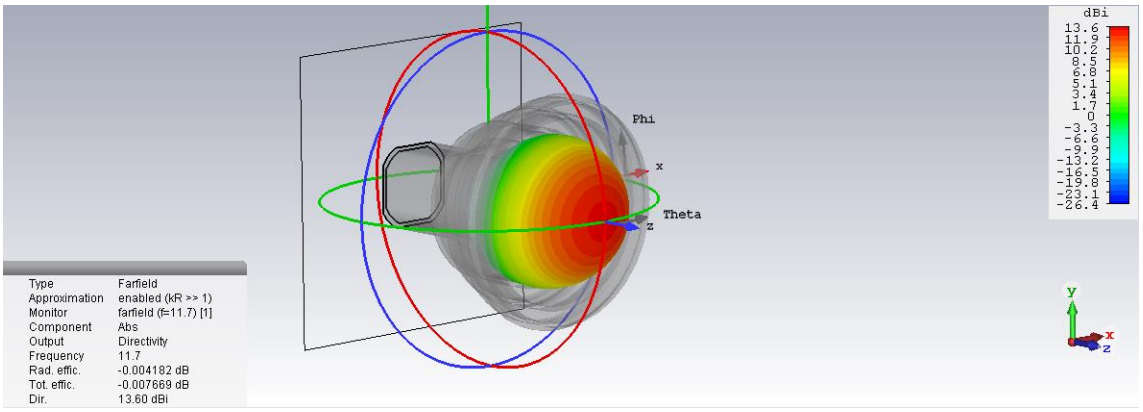

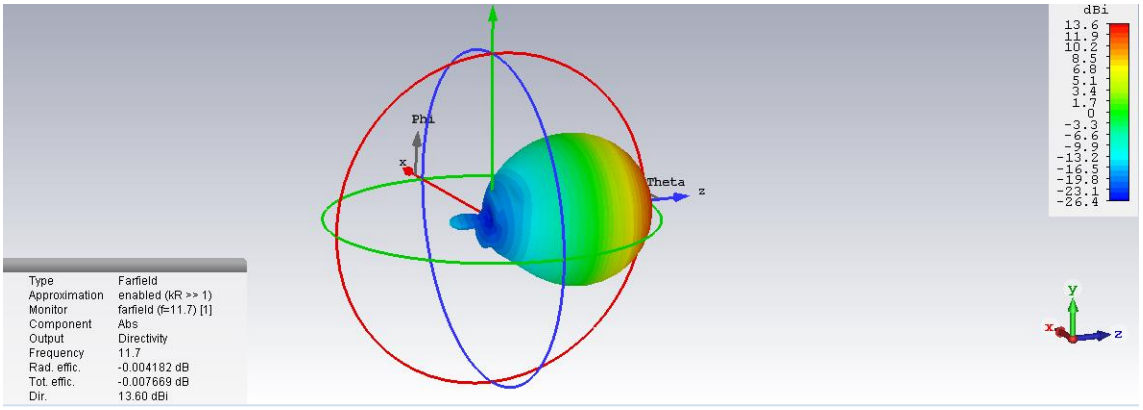

F30

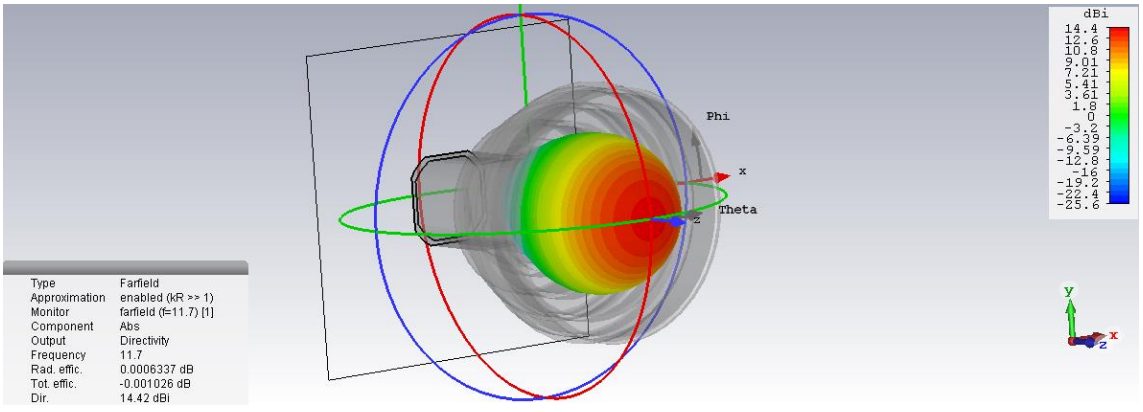

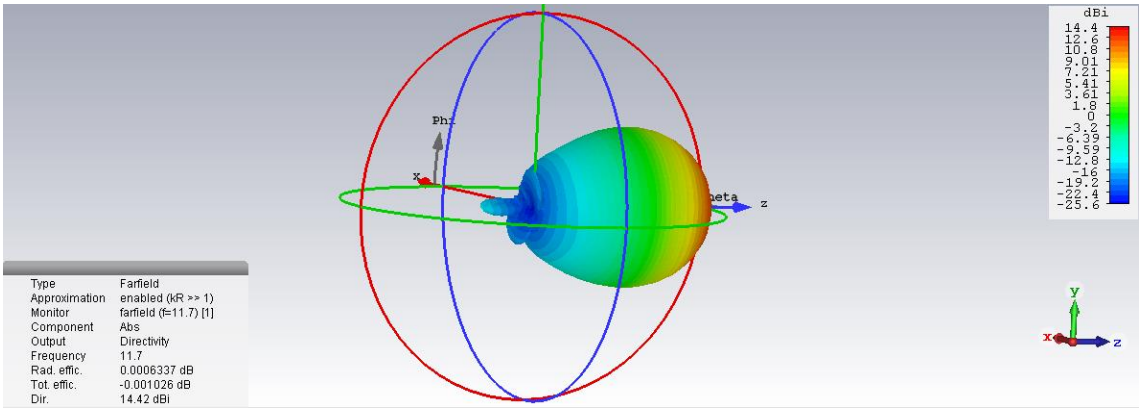

De seguida determinou-se como varia L_p / R_h em função de S com base na tabela 1 e verificou-se que a distribuição segue a linha de tendência descrita por uma função polinomial de 6º grau:

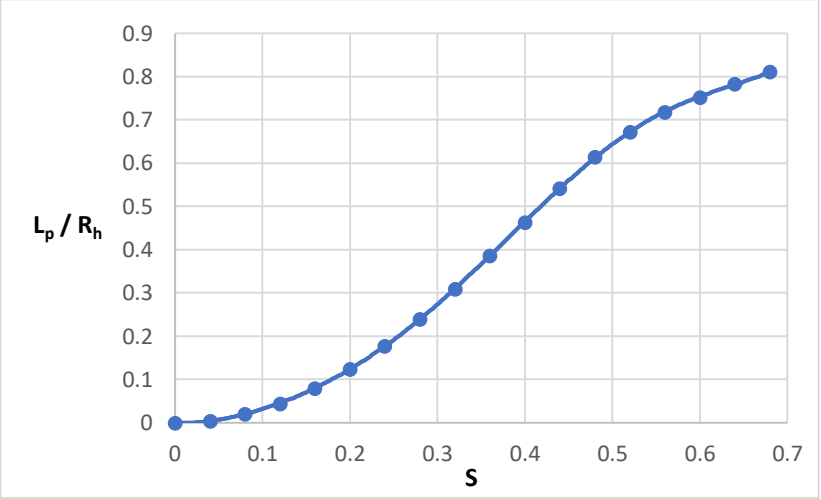

Fig. 4 – Representação gráfica dos dados da tabela 1.

$$L_p / R_h = 79.826*S^6 - 138.16*S^5 + 80.164*S^4 - 21.138*S^3 + 5.5796*S^2 - 0.0984*S + 0.0003$$
$$R^2 = 1$$

Resta saber os valores a utilizar (as medidas das antenas foram retiradas das imagens esquemáticas das antenas, fornecidas pela empresa Famaval e visualmente, através do software CST. Estão apresentadas em mm).

Tab. 2 – Dimensões dos diferentes parâmetros das antenas (em mm).

Antena	H_L /(mm)	a_0 /(mm)	a /(mm)	R_h /(mm)	y /(mm)
F23	32,19	9,11	23,92	57,23	5,239
F30	38,78	9,11	23,92	67,05	4,412

Convém relembrar que $y = R_h - L\left(\frac{a}{a-a_0}\right)$.

Resultados

Os cálculos efetuados são apresentados para as frequências de $\mathbf{f_1 = 10,7\ GHz}$ e $\mathbf{f_2 = 11,7\ GHz}$, devido à relação entre a frequência e o comprimento de onda $\boldsymbol{\lambda}$. Como $\boldsymbol{\lambda = c/f}$, onde c = velocidade da luz = $3*10^8$ m/s, temos que $\boldsymbol{\lambda_1 = 28,04\ cm}$ e $\boldsymbol{\lambda_2 = 25,64\ cm}$. Dessa forma, todas as grandezas vão ser apresentadas para cada uma das frequências (f_1 e f_2).

Determinação do Centro de Fase (L_p)

Conseguimos calcular S através da fórmula $S = a^2/(2\lambda R_h)$ e L_p / R_h dos dados.

f_1 = 10,7 GHz

Antena	R_h /(mm)	S	L_p / R_h	L_p /(mm)
F23	57,23	0,178291	0,098996	5,666
F30	67,05	0,152187	0,072761	4,878

f_2 = 11,7 GHz

Antena	R_h /(mm)	S	L_p / R_h	L_p /(mm)
F23	57,23	0,194954	0,117830	6,743
F30	67,05	0,166410	0,086567	5,804

Determinação do Ponto de Maior Intensidade de Campo Elétrico (z_0)

f_1 = 10,7 GHz

Antena	a /(mm)	R_h /(mm)	w_0 /(mm)	z /(mm)	z_0 /(mm)
F23	23,92	57,23	12,670	10,160	4,922
F30	23,92	67,05	13,311	9,112	4,700

f_2 = 11,7 GHz

Antena	a /(mm)	R_h /(mm)	w_0 /(mm)	z /(mm)	z_0 /(mm)
F23	23,92	57,23	12,244	11,740	6,502
F30	23,92	67,05	12,966	10,612	6,200

Determinação do offset entre o centro de fase (L_p) e o ponto de maior intensidade de campo elétrico (z_0)

Para confirmar que os valores obtidos são coerentes, efetuou-se o cálculo do centro de fase de duas formas independentes. O primeiro pelo método descrito na subsecção I. O outro na subsecção presente (pela determinação do offset $\boldsymbol{\Delta_{pc} = z_0 - L_p}$).

Antena	f1	f2
	Δ_{pc} /(mm)	Δ_{pc} /(mm)
F23	- 0,744	- 0,242
F30	- 0,179	+ 0,396

Podemos observar que em nenhum dos casos temos que o centro de fase é exatamente no mesmo ponto onde ocorre a máxima intensidade de campo elétrico, no entanto, é bastante perto, sendo aceitável usar o mesmo ponto.

Conclusão

O ponto de maior intensidade e o centro de fase estão reunidos na tabela seguinte.

Antena	f_1 = 10,7 GHz		f_2 = 11,7 GHz	
	z_0 /(mm)	z_{pc} /(mm)	z_0 /(mm)	z_{pc} /(mm)
F23	4,922	5,666	6,502	6,743
F30	4,700	4,878	6,200	5,804

Em geral, é vantajoso colocar o ponto de centro de fase das antenas de alimentação no focus de refletores parabólicos para minimizar as perdas relacionadas com o "reflector aperture phase error loss" [3].

Referências

[1] Goldsmith, P. F.: Quasioptical Systems: Gaussian beam quasioptical propagation and applications, IEEE Press, Piscataway, NJ, 1998.
[2] https://en.wikipedia.org/wiki/Phase_center.
[3] Milligan, T. A.: Modern Antenna Design, IEEE Press, Hoboken, NJ, 2005.